CIVIL ENGINEERING STUDIES

STRUCTURAL RESEARCH SERIES NO. 317

PRIVATE COMMUNICATION
NOT FOR PUBLICATION

METALLURGICAL STUDIES OF FATIGUE DAMAGE IN MARAGING STEEL

by
ROBERT W. HINTON
and
W. H. BRUCKNER

A REPORT OF AN INVESTIGATION CONDUCTED
by
THE DEPARTMENTS OF MINING, METALLURGY, AND PETROLEUM ENGINEERING
and
CIVIL ENGINEERING

UNIVERSITY OF ILLINOIS
URBANA, ILLINOIS
FEBRUARY 1967

METALLURGICAL STUDIES OF FATIGUE DAMAGE IN MARAGING STEEL

by

R. W. Hinton

and

W. H. Bruckner

University of Illinois

Urbana, Illinois

February, 1967

ABSTRACT

The fatigue damage of a high strength 12% nickel maraging steel was observed to entail a change in axial stress range and a change in the substructure resulting from cyclic deformation at a constant strain range. Axial tests in low cycle fatigue and longer cycle fatigue were performed on samples of solution treated and on aged 12% nickel maraging steel at constant testing temperatures ranging from $32^{o}F$ to $415^{o}F$. The substructure of untested samples and samples tested in static deformation was also observed by means of thin film electron microscopy. The change in stress range due to fatigue was resolved into two components of stress which were found to be different functions of the number of applied cycles of fatigue. A dislocation model based on the ordering of dislocation tangles was proposed and this model was supported by an activiation energy which was determined for the cyclic softening of 12% nickel maraging steel. Cyclic hardening was related to hardening by the generation of point defects from the observations made in this investigation as related to a previous investigation of LiF. Predictions of fatigue life based on the same amount of cyclic hardening at failure duplicated the experimental fatigue lives within 20% from 40 to 20,000 cycles.

ACKNOWLEDGMENT

This investigation was conducted as a doctoral research study under the direction of Professor Walter H. Bruckner of the Department of Mining, Metallurgy and Petroleum Engineering, University of Illinois, headed by the late Dr. Thomas A. Read. The study was supported in part by an investigation of the fatigue behavior of high-strength steels conducted under the general direction of Professor W. H. Munse as a part of the research program of the Civil Engineering Department of which Professor N. M. Newmark is head and sponsored by the Bureau of Ships, Department of the Navy (Contract NObs 94232, Project Serial No. SF 020-01-05; Task 729-0). The material investigated was made available by United States Steel Corporation, through Dr. S. T. Rolfe.

Appreciation is expressed to the Central Electron Microscopy Laboratory of the University of Illinois of which Dr. B. Vincent Hall is head and to Mr. Page and Mrs. Stayton, members of his staff. Appreciation is also expressed to Messrs. Ray and Kirby of the machine shop of the Department of Civil Engineering.

TABLE OF CONTENTS

TABLE OF CONTENTS (Continued)

LIST OF TABLES

LIST OF FIGURES

LIST OF FIGURES (Continued)

LIST OF FIGURES (Continued)

1. INTRODUCTION

Fatigue is defined as the failure of metals and alloys due to the application of a repeatedly applied stress. The magnitude of this repetitive stress is usually well below the static fracture stress of that metal or alloy. One of the most thorough investigators of fatigue, Gough,[1] has shown that fatigue is associated with plastic strain. He observed that cyclic deformation caused slip in some of the grains along the same crystallographic planes and directions that were observed for slip in these same metals and alloys which were statically deformed. Gough observed that grain orientation with respect to the direction of stress was important in determining whether slip occurred within the grain. Most of Gough's observations were made on the surface of the sample and this is true of a majority of observations made to date. Also, most metals and alloys were tested in either reversed bending or bending caused by a rotating beam loaded as a cantilever. The maximum fiber stress is on the surface in this type of test and most of the fatigue failures are located on or near the surface. Many investigators confirm the observations of Gough concerning the slip traces and some[2] have shown that certain slip traces develop into fatigue cracks. Additional structural changes on the surface of a sample subjected to bending were observed by Forsyth[3] who showed that some of the metal was extruded and that other areas of the metal were intruded where slip bands were located. Wood[4] showed that fatigue cracks initiated at these intrusions and extrusions when soft metals were subjected to relatively small stresses in fatigue. Most of the observations of fatigue damage were

made for relatively large plastic strains or for very soft metals and alloys. When the applied stress is in the nominal elastic range, fatigue failure occurs after a large number of cycles. The structural changes in Wood's fatigue samples were not obvious and in fact, the plastic strain was probably localized about a few regions in which the heterogeneity of the metal or surface condition of the sample caused a stress concentration.

The observation of the change in substructure of a metal due to fatigue is now possible by the use of the electron microscope and thin metal foil preparations. Segall and Partridge[5] observed that the substructure in aluminum after fatigue was similar to the substructure formed by static deformation. This is a significant observation because the strain range of the static test was large compared to the strain range applied to a sample to produce a fatigue failure after 10^5 to 10^6 cycles. Segall and Partridge found a high density of dislocation loops in the aluminum samples that were cyclically strained to produce a fatigue failure. These dislocation loops were similar to those caused by vacancy condensations observed in quenched aluminum samples. This is a good indication that vacancies are produced by the repetitive application of a small plastic strain. The relatively high production of point defects in fatigue samples compared to cold-worked samples has been indicated indirectly by the measurement[6] of stored energy which was released from fatigued samples of copper compared to cold-worked samples of copper. The generation of vacancies by static deformation and fatigue has been observed by Davidge et al[7]

in sodium chloride subjected to compressive strains. Cyclic softening of work hardened copper observed by Polakowski and Palchoudhuri[8] indicates that point defects generated during the fatigue process permit some dislocations to climb out of the piled up dislocations on the slip planes. Another indication that vacancies are generated during fatigue is the observation made by Broom[9] that age hardened aluminum alloys in the optimum aged condition can be overaged during fatigue at a temperature well below the aging temperature. Forsyth[10] actually observed by transmission electron microscopy bands of large precipitates along slip planes in an aluminum alloy which were caused by overaging during fatigue. However, fatigue failures have been recorded by McCammon and Rosenberg[11] for samples subjected to fatigue at a temperature of 4°K, where vacancy mobility is negligible even under the influence of a dislocation motion indicating that point defects are not solely responsible for fatigue failure.

Freudenthal and Dolan[12] divided fatigue damage into three stages. The first stage occurs only when the applied fatigue stress is great enough to cause plastic strain. This first stage occurs for the bulk sample in a low cycle fatigue test, but it only occurs for samples tested at a low stress range at heterogeneous areas where soft regions or stress raisers are present in the fatigue sample. Regardless of the volume of the material affected this primary stage requires 10^3 to 10^4 cycles for completion. The second stage extends from the end of the strain hardening or softening (first stage) to the formation of a

visible crack. The third stage involves crack propagation to cause fatigue failure. The percent of the total fatigue life that each stage represents depends on the applied stress relative to the static yield stress and on the metal or alloy being tested. Fatigue damage that cannot be annealed out has been observed to occur at lives as low as 10% of the failure life.[12,13,14] According to theory[15] both vacancies and interstitials should be produced by the fatigue process and these point defects should be greatly reduced by annealing. The ineffectiveness of annealing in eliminating fatigue damage indicates that vacancies do not contribute directly to fatigue failure. However, vacancies may accelerate fatigue damage by permitting processes normally controlled by diffusion, such as dislocation climb or overaging, to occur during fatigue at much lower temperatures than expected.

Coffin[16] has evaluated the modern types of fatigue tests involving controlled cyclic strain. His choice of a fatigue test using a constant strain was illustrated by the extensive results that he subsequently obtained from axial fatigue tests. The strain was controlled in Coffin's tests by the use of a diameter gauge. Support for Coffin's[17,18] choice of a constant strain test was evident in the work of Manson et al[19] and of Tuler and Morrow[20] which was performed on the same type of fatigue sample using a diameter gauge in order to control the constant strain range. Yao and Munse[21] have reported the results of many investigators of the low cycle fatigue (the nominal plastic strain range applied during the test can be measured experimentally) in a review of this literature.

Coffin[22] has experimentally determined that the life of a fatigue sample subjected to a constant plastic strain range is a function of the inverse of that strain range. Manson[19] observed a similar relationship to that observed by Coffin for high strength steels and Morrow[23] has written a relationship between both the elastic and plastic strain and the fatigue life of the sample. Most of the investigators[16-23] who have used the axially stressed fatigue sample with the strain range controlled by a diameter gauge have measured the true stress during the application of repetitive stress cycles at a constant strain range. In general, these investigators found that severely cold-worked metals softened with successively applied cycles at a constant strain. The same investigators found that annealed metals cyclically hardened. Most pure metals would reach a saturation stress after a number of cycles were applied and then the only observed change in stress range was from the decrease in load due to crack propagation near the number of cycles necessary for failure. Engineering alloys of a high strength compared to the pure metals had a more complex change in stress range as observed by Manson[19] and Radziminski[24] during the application of constant strain cycles. High strength alloys such as iron and titanium base alloys undergo a crystalline phase transformation during their heat treatment. Some of the commercial alloys consist of at least two ductile metal phases. Both the phase transformation and presence of more than one ductile phase may contribute to the more complex cyclic softening and hardening observed in these alloys. Unfortunately, few observations of the change

in the metal substructure accompany the fatigue tests of these more complex alloys.

The literature on fatigue that was reviewed for low cycle fatigue tests indicates that most of the data for fatigue behavior and substructure were determined independently. Therefore, few direct correlations between fatigue and substructure exist in the literature. The substructure studies of Forsyth[3] and Segall[5] reported previously were made from thin sheets of metal either bonded to a bending device or bent as a cantilever. Only the strain could be controlled in this type of test, assuming of course, that the bond was very efficient. The stress range could not be measured at all on these thin metal sheets which were bonded to a bending jig. Feltner[25] tested in axial fatigue thin foils of aluminum (5 mils thick) from a zero stress to some maximum tensile stress. The same subgrain development due to fatigue was observed by Feltner[25] as was described for the bending fatigue of foils except that vacancy clusters in his zero to tension test were not evident. Pratt[26] observed the substructure change due to fatigue in copper samples which were mechanically tested in fully reversed torsion and found that the saturation stress, $\sigma_{sat.}$, was related to the subgrain size, c.s., by, $\sigma_{sat.} = \frac{1}{c.s.}$, in the substructure of copper. Most investigators have found that the saturation stress, $\sigma_{sat.}$, was related to the subgrain size, c.s., by $\sigma_{sat.} = \sqrt{\frac{1}{c.s.}}$ for metals tested in fatigue at total strains involving some nominal plastic strains. Keh and Weissmann[27] have observed that the subgrain size due to large tensile strains or other static deformations

such as rolling was related to the flow stress, σ_f , by the same relationship previously given for fatigue, $\sigma_f \propto 1/\sqrt{c.s.}$. Pratt,[26] who has observed the change in substructure due to fatigue of pure copper in the annealed condition, showed that the subgrain size would adjust to the saturation stress even if the saturation stress was changed during the test in fatigue. The cold-worked or extensively prestrained samples of pure aluminum undergo cyclic softening and the annealed samples undergo cyclic hardening during fatigue and both approach a similar saturation stress range as shown by Coffin.[17,18]

The brief summary of the observations of the mechanical and substructural changes due to fatigue damage should be related to the fatigue mechanisms which have been proposed in the past. Some of these fatigue mechanisms are now described briefly in the chronological order of their development. Orowan[28] was one of the first to describe a fatigue mechanism in terms of the heterogeneity of the metal. He pictured the fatigue process as a total amount of plastic strain or a total summation of the area on a slip plane that dislocations would sweep out with the application of repetitive stresses. Orowan also showed that fatigue failure was associated with some minimum value of plastic strain. Although the role of plastic straining associated with fatigue implies that dislocations are involved in the process, Machlin[29] was one of the first to formulate a theory of fatigue in terms of dislocations. Machlin's previous work concerned with the theory of creep[30] provided additional information about dislocation climb and rate processes that contributed to

his fatigue theory. His assumption that the failure was caused by microcracks that grew across slip planes in order to join one another and cause the fatigue failure may not be applicable to alloys of high strength. Microcracks at an early fraction of the fatigue life have been observed for soft metals but they may not exist in high strength alloys until a number of cycles of fatigue are applied which represent a large fraction of the number of cycles needed for fatigue failure. The relationship derived by Machlin[29] between fatigue life, N, and the experimental fatigue parameters is:

$$\text{Log } N = \text{Log}\left(\frac{2\pi W h M}{kT}\right) + \left(\frac{\Delta F_g}{2.3kT}\right) - \frac{(q' V X f \sigma_m)}{2.3kT} \qquad \text{(Equation \#1)}$$

σ_m - is constant across the cross-section of the specimen so that it applies to tests involving axial type loading in which σ_m applies for stresses above the endurance limit.

ΔF_g - Free energy of activation involved in the generation of a dislocation.

M - Amount of crack growth per source.

q' - Product of the stress concentration factor and the constant between τ and σ .

W - Frequency of cycles of stress application.

V - Atomic volume.

X - Ratio of distance between atoms in slip direction and inner planar spacing of slip planes X = 3/2 for face-centered cubic (fcc) and body-centered cubic (bcc) lattices.

f - Experimental fraction (.374) from creep analysis.[30]

τ - Shear stress in a polycrystalline sample.

k,h,T - Represent Boltzmann's constant, Plank's constant and the absolute temperature.

When Machlin's equation is abbreviated by letting $N_o = (\frac{2\pi WhM}{kT})$ and $V\tau = q'VXf\sigma_m$ then:

$$N = N_o \exp\left(\frac{\Delta F_g - V\tau}{kT}\right) \qquad \text{(Equation \#2)}$$

The intrusions and extrusions observed on fatigue samples of very soft metals has given Wood[4] support for a failure mechanism based on a failure due to the change in topography of the sample. Dislocation models for the formation of intrusions and extrusions are proposed by Hull and Cottrell[31] and by Mott.[32]

Keh and Weissmann[27] have reviewed the relationship between the flow stress and the dislocation density, ρ produced by static deformation of metals with a bcc crystal structure. Keh and Weissmann[27] reported that the relationship between the flow stress and the dislocation density, $\sigma_f \propto \alpha Gb\sqrt{\rho}$, was obeyed if the dislocation density of the tangles are used rather than the density of the dislocations within the subgrains. Li[33,34] has proposed that dislocation tangles create long range stresses which reach other dislocations located within the subgrain. The long range stresses have a range of effectiveness which is reduced in size as the dislocation tangles approach equilibrium positions leading to simple tilt or twist boundaries of subgrains. As an example Li[35] calculated the repulsive force, f , on a dislocation within the subgrain produced by a cross grid of screw dislocations to be:

$$f = \frac{Gb^2}{h} \cos\varphi \cos(2\psi - \varphi) \qquad \text{(Equation \#3)}$$

G - is the shear modulus

h - is the average distance between dislocations in the tangled regions

φ - is the angle between two parallel sets of screw dislocations in the boundary

$(2\overset{\psi}{}_{\psi-\varphi})$ - are the angles between the screw dislocation in the matrix and the dislocations in the boundary

f - the repulsive force

b - Burgers' vector

Keh[27] uses the expression given above with the optimum conditions of $\varphi = 70.5°$ in order to reduce it to the form, $\sigma_f = 0.17 G b \sqrt{\rho}$, which was observed experimentally for the numerous metals with a bcc crystal structure. The most important part of this theory is that the long range stresses decrease in size as the dislocation tangles approach equilibrium positions or more nearly perfect tilt and twist configurations in the subgrain boundaries. The stress field of a perfect tilt boundary is only effective to a distance of about h from the subgrain boundary. This short range stress became a very insignificant part of the resistance to flow since the average subgrain diameters may be ten to one-hundred times the distance of h.

2. STATEMENT OF THE PROBLEM

Pure metals, such as copper and aluminum, were usually used to investigate the relationships between the changes in substructure and fatigue. The purpose of the present investigation was to study the fatigue damage in a ferrous alloy which had undergone a phase transformation prior to fatigue. The changes in substructure and the changes in stress range due to fatigue in the bulk sample were to be correlated. The alloy chosen for investigation was a maraging steel.

3. MATERIAL USED: A DESCRIPTION OF MARAGING STEEL

Maraging steel which contained 12% nickel and 5% chromium but no cobalt was chosen for this investigation of fatigue damage. The substructure and aging response of this steel is almost identical to that of the 18% Ni - 9% Co maraging steel. However, the yield strength was lower for this 12% nickel maraging steel than the yield strength of maraging steels of higher nickel contents. A series of reports by Rolfe et al[36] described the mechanical properties of this 12% nickel maraging steel. The plate of one inch thickness used in this investigation was hot rolled from a fifteen ton, vacuum melted ingot. The composition of this heat is found in Table 1 and was obtained from the producer, United States Steel Corporation.* The mechanical properties and aging responses for this 12% nickel maraging steel are reported in Table 2 and were obtained from the producer. This 12% nickel maraging steel was under development for commercial use at the time of this investigation. During the course of this investigation the 12% nickel maraging steel was successfully thinned for observation under the electron microscope after most mechanical and thermal treatments. The martensitic substructure was clearly observed within the thin metal foils and the changes in substructure after fatigue was also clearly observed for the solution treated steel.

The ability to successfully thin the 12% nickel maraging steel for clear observations with the electron microscope may have been due to the vacuum melting process used

*The information was obtained from M. W. Lightner in a letter dated June 11, 1965.

to make this particular heat of 12% nickel maraging steel. Maraging steel processed by standard air melting techniques would probably have more inclusions and be more heterogeneous in the microstructure than the vacuum melted steel. A high inclusion content or high degree of heterogeneity of the metal matrix would greatly interfere with the uniformity of the electrolytic thinning process. The high degree of clarity with which the substructure of this 12% nickel maraging steel was observed in this investigation for samples after various mechanical treatments was due in part to the excellence of the thin films. However, the clarity of the substructure was mostly due to the absence of internal twinning in the martensite of the maraging steel when compared to the extensive internal twinning within the martensitic phase of iron-carbon and higher nickel-iron alloys than those of maraging steel. The phase transformation in the 12% nickel steel which occurs during quenching consists of the diffusionless transition of the austenitic phase of a fcc crystal structure to a martensitic phase of a bcc crystal structure.

Phase transformations or changes in crystal structure which can be observed in the iron-carbon alloys are also present in the alloys containing iron-chromium-nickel. When plain carbon steel is heated above 1330°F a fcc crystal structure is stable and this phase is called austenite. Below the eutectoid temperature (1330°F) the austenitic phase transforms to a bcc phase called ferrite. A distorted bcc crystal structure or body centered tetragonal (bct) phase called martensite is formed by a diffusionless phase transformation, a martensitic transformation, if the austenitic phase is rapidly cooled or quenched. The produc-

tion of this martensitic phase is favored by high carbon contents and rapid rates of cooling from the austenitic phase. The distortion of the bcc phase was described by Bain[37] who showed that carbon in certain interstitial sites in the bcc crystal lattice produced a bct crystal lattice. This model was supported by the increase in c/a ratio of the tetragonal lattice with the increase in carbon content. Wechsler, Lieberman and Read[38] proposed a model for the martensitic transformation which accounted for the lattice distortion and rotation. The theory of Wechsler *et al*[38] explains the internal twinning which was observed in the martensite of alloys of iron-nickel-carbon and iron-nickel[39] in which the nickel is greater than about 28 weight percent. Internal twins in martensite were observed by Dash and Otte[40] in an alloy of 18% Cr - 12% Ni by weight which were similar to the twins in the martensite of 18% Cr - 8% Ni. Dash and Otte[40] did not observe internal twins in the martensite of an alloy containing 5% Cr plus 20% Ni or an alloy containing 10% Cr and 15% Ni. Owen and Liu[41] observed a distorted bcc phase (α_2) by means of x-ray diffraction in iron-nickel alloys containing up to 27% by weight nickel when these alloys were quenched from the austenitic phase. Alloys of higher nickel content than 27% by weight contained retained austenite because the temperature for the beginning of the martensitic transformation was below room temperature. The work of Jones and Pumphrey[42] on iron-nickel alloys in the same range of composition verified the results of Owen and Liu.[41] In a more recent paper Gilbert and Owen[43] suggested that the diffusionless phase transformation of austenite to the bcc

phase during the quenching of iron-nickel and iron-chromium alloys was a massive transformation. Borgers and Burgers[44] have proposed a model for the fcc to bcc transformation and for the reverse transformation. When the martensitic phase is heated to a temperature that is high enough for austenitic stability, the reverse transformation (bcc to fcc) does occur. The substructure and true stress-true strain relationship for reverted austenite in an alloy of iron-nickel (33.5%) was described by Krauss,[45] who found that the reverted austenite contained a high density of dislocations ($10^{11}/cm^2$) and this density was about a factor of ten greater than the dislocation density in the retained austenite for the same alloy. The yield strength of the reverted austenite was about twice the yield strength of the retained austenite.

Maraging steels are iron base alloys of nickel and cobalt (18% Ni - 9% Co) and of nickel and chromium (12% Ni - 5% Cr). Maraging steels undergo a diffusionless transformation when they are cooled from the austenitic phase and the transformation product is a bcc phase similar to the one observed by Dash and Otte[40] for the iron-base alloy of 20% Ni - 5% Cr and of 15% Ni - 10% Cr. The martensitic phase in maraging steel consists of long parallel platelets which are not internally twinned, but contain a high density of dislocations due to the transformation. When alloying elements such as molybdenum, aluminum and cobalt are added to the base composition of maraging steels, precipitation hardening occurs in the martensitic phase upon subsequent aging. This process is also called age hardening and from this the term maraging steel is derived.

Decker et al[46] reported the effects of alloying elements in maraging steels on their mechanical properties and found that molybdenum, titanium, aluminum and cobalt were the main contributors to the extra static strength obtained by the precipitation hardening treatment. Reisdorf et al[47] have studied the mechanism of strengthening in maraging steels (18% Ni - 9% Co) and have concluded that precipitation of Ni_3Mo and $Ni_3(Al, Ti)$ was primarily responsible for precipitation hardening. Reisdorf et al[47] found that Ni_3Mo precipitated along dislocations in the martensite forming rods of precipitates with a density similar to the original dislocation density of the martensite. The precipitation of Ni_3Mo pinned most of the dislocations in the martensite and the pinning process would be responsible for a large increase in the yield strength. Precipitates of $Ni_3(Al, Ti)$ were concentrated in small spherical areas between the rod-shaped precipitates which would further contribute to the strength of the aged steel. The contribution of cobalt to the extra strength due to precipitation hardening was significant, but no definite evidence of the mechanism of cobalt strengthening was presented. It has been suggested that an ordered cobalt phase contributed to the strengthening, but evidence to substantiate this conjecture has not been given to date.

4. DESCRIPTION OF EXPERIMENTAL PROGRAM

4.1. Heat Treatment

All the samples that were used for this investigation were taken from a one inch thick plate of 12% nickel maraging steel which had been solution treated for one hour at 1500°F and water quenched after it had been hot rolled by the manufacturer. Precipitation hardening of the test samples was done after they were machined and rough polished to their final shape. Optimum mechanical properties were obtained from the samples after holding them at 900°F for a period of 16 hours and then final polishing them. This optimum heat treatment involving a temperature of 900°F for a period of 16 hours does not produce reverted austenite. Reverted austenite of as much as 3% by volume was produced at martensitic boundaries by holding the solution treated 12% nickel maraging steel samples at 920°F for a period of 16 hours. A Lindberg furnace was used for all of the heat treatments and this furnace had a cyclic fluctuation in temperature that was less than $\pm$ 15°F for each heat treatment. The effect of the heat treatment was recorded by measuring the hardness of the heat treated samples.

4.2. Test Sample Preparation

The axial fatigue sample of the type drawn in Fig. 1 was used in this investigation and is similar to the samples used by Yao[48] and Radziminski.[24] The direction of applied stress is parallel to the main rolling direction of the plate. The same sample geometry was used for the tensile tests except that the minimum diameter was 0.55 inch instead of the 0.45 inch for the fatigue sample. The hour-glass

shape of this sample was made with a taper radius of one inch. If only nominal elastic strains were involved in the fatigue test this taper radius would result in an elastic stress concentration at the minimum diameter near the surface of the sample of a few percent. However, the fatigue tests conducted in this investigation involved nominal plastic strains from 0.001 to 0.170 inch/inch in which the axial stress is more uniform across the cross section of the minimum diameter. All the test samples were polished in the tapered region in the following successive order with abrasive cloths marked grit number 180, 240, 320 and finally with crocus cloth. The longitudinal polishing was done by rotating the test sample about its longitudinal axis and polishing the surface in a circular manner with the abrasive cloths mounted on the stem of a drill (3500 rpm) or a high speed motor (1750 rpm). Test samples which were aged were again polished with crocus cloth. The minimum diameter was measured with a traveling microscope at numerous positions around the long axis of the sample. The standard deviation of each diameter was less than $\pm$ 0.003 inch and this measurement was in good agreement when compared with the size of the diameter obtained by using a micrometer caliper.

4.3. Special Equipment

4.3.1. Fatigue Equipment. Tests in fatigue were conducted on the 50,000 pounds Illinois type fatigue machine that is drawn in Fig. 2. The pull-heads which were especially designed by Yao[48] were rebuilt of a high strength low alloy steel (HY-80) in order to withstand the load that was required to test the 12% nickel maraging steel. When the

machine was run continuously, the constant maximum load was applied by an eccentric which resulted in a large range of strain rates. An automatic control of the load permitted a linear rate of loading of the sample near the end point of each reversal in the cycle. Moreover, the total strain range and the mean value of the strain were controlled by this automatic device.

The load applied to the sample in the fatigue machine was measured by strain gauges on the weighbar arranged as a full Wheatstone bridge. The output of this bridge was read on an SR-4 strain indicator or displayed on a Mosely X-Y recorder. The minimum diameter of the fatigue sample was measured by using a diameter gauge with a sensitivity for strain of a sample with a 0.45 inches diameter of 0.0025 inch/inch. The good sensitivity of this diameter gauge was obtained even though the jaw pressure of the diameter gauge was small relative to other sensitive diameter gauges. In order to insure that the diameter gauge was in a stable position for the duration of the test, the jaws of the diameter gauge were made of a 1/8 inch diameter copper-silver brazing rod which was contoured to fit a large area at the minimum diameter when the sample was in compression. This jaw configuration also minimized wear and cyclic creep of the sample at the jaw during the fatigue test. The geometry of the diameter gauge and position of the four Metalfilm C12-121 strain gauges on the diameter gauge is shown in Fig. 3. The strain gauges were connected as a full Wheatstone bridge and the output of this bridge was linear for the diameter changes measured in this investigation. The strain gauges that were used were self-compensating

for temperature. The constant of proportionality between the diameter change and the output of the strain gauges was 44,300 ± 500 microinches per inch for a diameter change of one inch. The dial gauge on the SR-4 strain indicator could be read at a glance to ± 2 microinches per inch which is equivalent to an error in the true strain of a 0.45 inch diameter of about ± 0.001 inch/inch.

4.3.2. Heating and Cooling Fatigue Samples. Fatigue tests that were conducted at room temperature resulted in a mean temperature of 98°F ± 5°F and the temperature was measured at the minimum diameter of the sample for all samples that failed in the range of 60 to 400 cycles. One sample each of the solution treated and of the aged steel was tested in fatigue at temperatures above room temperature and one sample of each solution treated and of the aged steel was tested in fatigue below room temperature. Heating and cooling coils of a similar geometry were placed on the samples in order to produce the desired constant temperature. The coils were wound on either side of the minimum diameter toward the pin connections for a distance of 1¼ inches. The heating coils were wires of a high electrical resistance that were covered with thin fiberglass sleeves and the cooling coils were small copper tubes. Liquid nitrogen was forced under pressure through the copper tubes in order to cast the sample in a block of ice that held the temperature of the metal at the minimum diameter to 32°F during fatigue. Thermocouples were placed against the metal surface at the minimum diameter and the thermocouples were covered with multilayers of fiberglass tape in order to record the temperature at the minimum

diameter. Additional thermocouples were placed near the heat source or heat sink in order to aid in producing a symmetrical flow of heat into or out of the minimum diameter. The strain gauges on the diameter gauges were not heated or cooled by more than a few degrees from room temperature because of their relatively large distance from the coils. The mean temperature was maintained well within $\pm$ 10°F at the minimum diameter for these specially heated or cooled samples that were tested in fatigue.

4.4. Procedures

4.4.1. Fatigue Tests. The minimum and maximum diameter corresponding to the desired true strain range for each particular fatigue test was calculated. The diameter size was converted to diameter gauge readings where the initial diameter of the corresponding fatigue sample was equivalent to a mean strain of zero. The values of the minimum and maximum diameters that were converted to SR-4 indicator readings were maintained during each cycle of fatigue. As the applied load approached the maximum strain its value was recorded from the SR-4 indicator measuring the load. At this maximum strain the load was reversed and applied in the opposite sense until the minimum strain was approached at which point the load was again measured and reversed. True stress at the maximum and minimum strain for each cycle was obtained in this manner until failure occurred. For samples that did not fail after 100 cycles intermittent cycles were subsequently applied before the stress was measured for an additional group of three to five cycles. The maximum and minimum strains were approached by using the device which produced

a linear rate of loading. Although the rate of pull-head motion was constant when this loading device was used, the strain rate was still not the same at different strains because of the different amount and rate of necking at these different strains. The difference in the strain rate caused by necking of the sample did not change the stress range by an amount that could be measured in this investigation because the strain rate sensitivity as defined by Dieter[49] was only 0.018 for the 12% nickel maraging steel in the solution treated condition. This low sensitivity means that the measured strain rates which were different by a factor of 660 would only cause a difference in the yield strength at small strains of 14 ksi or about 10% of the yield strength, and the difference is even smaller when the strength is compared at higher strains. When duplicate samples were tested in fatigue at the same strain range, the stress range that was measured for identical cycles agreed within 3 ksi to 4 ksi. For the first 80% of the applied cycles for failure the reproducibility in stress range for identical cycles was better than 98%. Duplicate tests were not obtained for the last 20% of the life because only one sample at each strain range was tested to failure. The rest of the samples which were tested at that strain range were tested to 80% of the previously determined service life. Therefore, the reproducibility was only obtained for the first 80% of the fatigue life of the sample.

For samples tested in fatigue that had lives greater than a few thousand cycles no change in stress range from the initial stress range was observed. These samples were

tested in fatigue by continuous cycling of the eccentric load after the first 20 to 30 cycles were applied with the device which produced a constant rate of loading and the stress range was measured at each reversal in stress. The fatigue life of a sample was defined in this investigation as the number of cycles needed for a load decrease that permitted the pull-head assembly to open far enough to shut off a microswitch. This amount of extra pull-head movement usually occurred when the fatigue crack propagated across at least one-half of the cross section of the fatigue sample. This amount of fatigue crack propagation corresponded by a few cycles with the first significant decrease in load that was observed in tension.

4.4.2. Tensile Tests. True stress-true strain relationships for both the solution treated and the aged steels were determined by measuring the load and the diameter of the sample for every 500 pounds change in load after the yielding and until failure occurred. The true stress was corrected for necking by using the Bridgman[50] correction. The Bridgman[50] correction was measured for different strains of the 12% nickel maraging steel in both the solution treated and the aged condition and the results are shown in Fig. 4. The true stress-true strain diagrams were reproduced within 3 ksi to 4 ksi for duplicate samples of the solution treated and the aged samples. The true fracture strain of duplicate samples agreed within a few percent and the fracture strain was symmetrical about the rolling direction or long axis of the fatigue samples.

4.4.3. Hardness Tests. The extent of precipitation hardening was indicated by the Rockwell "C" or Diamond Pyramid

Hardness (DPH) of the sample after heat treatment. The hardness of cross sections taken from fatigue samples was obtained after the 0.015 inch thick cross sections which were cut from the minimum diameter were mechanically polished to a 3/0 emery finish and then electropolished. All of the DPH values were obtained from an indentation made with either one kilogram load or a 100 gram load. The depth of this indentation was less than 0.001 inch and the thickness of the polished sample was always greater than the 0.006 inch required to insure that the hardness was not influenced by the supporting stage.

4.5. Electron Microscopy

4.5.1. Procedure for Thin Films. The change in the substructure of the 12% nickel maraging steel due to heat treatment and fatigue was directly observed with an electron microscope in thin metal foils which were processed from the bulk sample. All the observations were made with a RCA electron microscope, model EMU-3C, operated at 100Kv. The thickness of the thin metal foils was approximately 2000 Å (2×10^{-5} cm) thick and the thin films were produced by the following procedure. After the sample had been heat treated or deformed in static tension, or tested in fatigue to a certain fraction of the number of cycles needed for failure, samples were cut out of the bulk with a water cooled microsaw. The cross section of the fatigue sample was cut at the minimum diameter of the sample and the saw cut was perpendicular to the direction of axial stress. The saw cut sections were about 0.015 inch thick and were rough polished in steel blocks that had recesses machined in them of 0.015, 0.012, 0.010, 0.008 and 0.006 inch

depths for each block. The depth of deformation that was caused by this type of polishing was shown by Szirmae[51] to be less than a few thousandths of an inch. The 0.006 inch sections were then electropolished in a 10% perchloric-acetic acid bath cooled by an ice bath to about 17°C. The electrolyte was stirred vigorously during the electropolishing operation in order to cool the sample. Bollmann's[52] technique for thinning was used with the edge of the sample protected by a conducting mask. When the sample was thinned to a thickness of 0.001 to 0.002 inch the entire disk was cut into small sections that would contain a 0.01 inch square section. Each small section was then placed between two small stainless steel washers with an outside diameter of 0.138 inch and an inside diameter of 0.06 inch. The small section contained in between the washers was thinned in the 10% perchloric-acetic acid bath until a small hole appeared. The small sample was then washed from the stainless steel washers with water and absolute ethyl alcohol for observation with the electron microscope. The small sections were catalogued according to their position in the cross section of the fatigue sample.

The substructure was more evident for solution treated samples which were tested in fatigue when the dislocations were decorated by partial precipitation hardening before thinning at which time the samples were at least 0.006 inch thick. Also fewer dislocations were lost when the metal foil became extremely thin because of the decoration. Most of the fatigue samples were observed in both the as-fatigued and the decorated condition. The selected area for electron

diffraction was a triangular area of 0.6 microns on a side.

4.5.2. Analysis of Substructure. The average dislocation density, ρ , observed in the thin films of the 12% nickel maraging steel was estimated by using the expression:[53]

$$\rho = (n_1/L_1 + n_2/L_2) \, 1/t \qquad \text{(Equation \#4)}$$

in which n_1 and n_2 are the number of intersections made by dislocation lines with two normal sets of grid lines and L_1 and L_2 are the respective lengths of the grid lines. The foil thickness, t, was not determined for each area of interest but was taken as 2000 Å based on the experience of Keh and Weissmann[27] which was in good agreement with the values of the thickness determined in this investigation. This assumption for the thickness and the possibility that not all dislocations in the undecorated condition were observed at a given orientation should be kept in mind when the dislocation densities are considered. Assuming an average diameter per particle for the rod-shaped precipitates a volume fraction of the precipitate phase was obtained by determining the area density of particles from the equation just cited[53] for the orthogonal line analysis of dislocations.

The average subgrain size, c.s., was determined by a line analysis, L/n, where L is the length of a line placed in a random orientation and n is the number of intersections with low angle boundaries that intersect this line.

A good measurement of the spacing between dislocations in the boundary between two subgrains or the cell wall was obtained from the decorated samples. The spacing of dislo-

cations in the cell wall was not as accurate for the undecorated samples because the strain fields overlapped and obscured individual dislocations located in the wall but the position of dislocations was well ordered in the fatigue samples. The line of known length, L, was placed perpendicular to the dislocations in the cell wall and the number of individual dislocations, n_1, along it were counted for many cell walls. The dislocation density of the cell wall was obtained by squaring (n_1/L_1). Another average dislocation density in the cell wall was calculated from the rotation of the reciprocal lattice about the [111] as observed by electron diffraction. The spacing, h, between dislocations in the cell wall of a tilt boundary was related to the tilt angle, θ, by the expression given by Sleeswyk:[54]

$$\theta = \frac{b}{h} \qquad \text{(Equation \#5)}$$

in which $\underline{b}$ is the magnitude of the Burgers' vector. The tilt angle, θ, was approximately equal to the rotation of two adjacent subgrains about a 111 type direction for the 12% nickel maraging steel. The average dislocation density in the cell wall from this lineal analysis was equal to $(1/h)$ in which the cell wall was one dislocation in width. The density of dislocations in the cell walls of samples tested to large plastic strains in which dislocation tangles were observed was determined by the orthogonal line analysis given by Equation #4 and resulted in an area density of dislocations.

5. PRESENTATION AND ANALYSIS OF RESULTS

5.1. Results of Fatigue of Solution Treated 12% Nickel Maraging Steel at Room Temperature

5.1.1. The Fatigue Life of 12% Nickel Maraging Steel in the Solution Treated Condition. The fatigue diagram for the number of cycles to failure or life, N_f, of the sample and the constant true strain range, $\Delta\epsilon_t$, maintained during each cycle is shown in Fig. 5. A mean strain of zero was maintained for the duration of each test. The fatigue life is also plotted versus the nominal true plastic strain range, $\Delta\epsilon_p$, based on the plastic strain range for the first cycle and is shown in Fig. 5. The nominal plastic strain range was obtained from the total strain range which was measured by subtracting the nominal elastic strain range, $\Delta\epsilon_e$, so that $\Delta\epsilon_p = \Delta\epsilon_t - \Delta\epsilon_e$. The nominal elastic strain range is equal to the measured true stress range, σ_r, divided by the elastic modulus of the material, E. The relationship between plastic strain and fatigue life for the nickel maraging steel in the solution treated condition can be approximated by $N_f \propto (\frac{\Delta\epsilon_p}{2})^{-1.1}$. The total strain as a function of fatigue life as shown in Fig. 5 can be approximated by Morrow's equation:[23]

$$\Delta\epsilon_t/2 = \sigma'_f/E \ (2N_f)^b + \epsilon_f \ (2N_f)^c \qquad \text{(Equation \#6)}$$

The coefficients and exponents of Morrow's equation[23] which were obtained for the relationship shown in Fig. 5 indicated that the fatigue diagram for the solution treated 12% nickel maraging steel was similar to fatigue of many other metals and alloys.

Only one sample at each constant strain range was tested in fatigue to failure. Any additional samples tested in fatigue were subjected to a predetermined percentage of the number of cycles needed for failure as predicted by the fatigue diagram in Fig. 5. These additional samples tested in fatigue but not to failure were sectioned for transmission electron microscopy in order to observe the change in substructure due to fatigue.

5.1.2. The Change in Stress Range for Each Applied Cycle of Fatigue. The change in true stress range for each applied cycle was divided into two components and each component was found to be a different function of the total number of applied cycles. The true stress range, σ_r , was obtained by adding the true tensile stress at the maximum strain to the true compressive stress at the minimum strain. A true stress range was obtained for each applied cycle for tests in fatigue conducted at constant total strain ranges of 18%, 7%, 2.6% 1.3%, 1% and 0.8%.

The stress range was first divided into two components for the tests conducted at a 2.6% and a 7% total strain range. The true stress range that was measured for each cycle applied at a 2.6% and at a 7% strain range is shown in Fig. 6. A duplicate test performed to 80% of the predicted life at a strain range of 7% is also shown in Fig. 6. Cyclic softening was observed for the first part of the test which was similar to the tests conducted at a smaller constant range of strain. The extra stress range due to cyclic hardening was more evident after a large fraction of the cycles needed for fatigue failure were applied as shown in Fig. 6.

The true stress range for each applied cycle for the tests with constant strain ranges of 1.3%, 1% and 0.8% is shown in Fig. 7. Excessive softening occurred within the first twenty cycles and then a nearly constant true stress range was observed during the latter part of the test. This constant true stress range observed in the latter part of the test is frequently referred to as a "saturation stress."[26] The term "saturation stress"[26] will not be used in this investigation because each of the two components of the true stress range as determined for the solution treated steel did not have a constant stress range over a number of applied cycles of fatigue.

When a strain range of 18% was maintained for each applied cycle, the change in stress range with each cycle did not deviate more than a few percent from the stress range measured for the first application of tension and compression, the first cycle, as shown in Fig. 8. The change in the stress range with an increasing number of applied cycles of fatigue is analyzed in terms of cyclic softening and cyclic hardening in the next section in which nominal plastic strain ranges from 0.17 to 0.001 inch/inch were used for the tests in fatigue conducted at total strain ranges of 18% to 0.8%.

5.1.3. Analysis of the Change in Stress Range by the Resolution of a Cyclic Softening and a Cyclic Hardening Component of Stress. When the change in stress range, σ_r, which was measured for each applied cycle was divided by the initial stress range measured for the first cycle, σ_o, the fractional change in stress range due to cyclic softening, $\frac{\sigma_s}{\sigma_o} = \frac{\sigma_o - \sigma_r}{\sigma_o}$, was the same for idential cycles for the first ten to twenty cycles for all the strain ranges

(18% to 0.8%) maintained during fatigue. A curve drawn to fit this cyclic softening shown in Fig. 8 is described by the equation:

$$N = N_o \exp \left(\frac{k' \sigma_s}{\sigma_o} \right) \qquad \text{(Equation \#7)}$$

for which N is the number of applied cycles up to and including the cycle in which the change in stress range was measured and N_o was the number of applied cycles before softening or a change from σ_o began. The value of N_o was unity ($N_o = 1$) for all the solution treated samples which were always tested in the as-quenched condition involving all the strain ranges which were tested. The change in stress range due to cyclic hardening, σ_H, was obtained by assuming that cyclic softening continued according to:

$$\sigma_s = \sigma_o / k' \ln N/N_o \qquad \text{(Equation \#8)}$$

until the sample failed in fatigue. Both the initial stress range and the stress range at a particular cycle were determined experimentally to give the measured change in stress range, $\sigma_o - \sigma_r$. The difference between the experimental change in stress range, $\sigma_o - \sigma_r$, and the calculated change in stress range, σ_s(calculated), was equal to σ_H. The relationship between σ_H and the number of applied cycles, N, shown in Fig. 9 was approximately:

$$\sigma_H = C \, N/N_o \qquad \text{(Equation \#9)}$$

The constant, C, was different for each strain range, but when the constant, C, was plotted versus the initial plastic strain range as shown in Fig. 10, the constant, C, was equal

to $(8\Delta\epsilon_{pi})$. The change in stress range due to cyclic hardening was approximately related to the number of applied cycles by the relationship:

$$\sigma_H = 8\Delta\epsilon_{pi} (N/N_o) \qquad \text{(Equation \#10)}$$

The plastic strain changes during a test in fatigue conducted at a constant total strain range if the stress range changes. The plastic strain for each applied cycle is equal to $\Delta\epsilon_{pi} + \frac{\sigma_s - \sigma_H}{E}$ where E is the modulus of elasticity of the steel and for small strains the approximation, $(\sigma_s - \sigma_H)/E \doteq \ln (1 + \sigma_s - \sigma_H/E)$ is accurate. The change in stress range is a function of the total number of applied cycles, Equation #8, and the equation for the change in stress range due to cyclic hardening is:

$$\sigma_H = 8 (\Delta\epsilon_{pi} + \frac{\sigma_o}{E_k} \ln N/N_o)N/N_o \div (1+8N/EN) \qquad \text{(Equation \#11)}$$

The calculated values for the fractional change in stress range, $\sigma_r/\sigma_o = \frac{\sigma_o - \sigma_s + \sigma_H}{\sigma_o}$, are plotted as solid lines in Fig. 8. The curves for cyclic softening and hardening were initially fitted "by eye" because of the small scatter and large number of experimental points. An analysis of regression variance as outlined by Bartee[55] was performed to insure that fitted curves for change in stress range for the tests in fatigue conducted at 2.6% and 7% total strains were within a 90% confidence limit for the number of applied cycles representing 80% of the fatigue life, N . A decrease in tensile loads near the number of cycles needed for failure prevented the measurement of the stress range. The constant stress range that was recorded for the number

of cycles in the last half of fatigue at a strain range of 1% to 0.8% and the small change in the stress range measured for the first half of the life of a sample subjected to 18% strain range was approximately fitted by a balance of cyclic softening and hardening that was assumed to occur simultaneously for the duration of fatigue.

5.1.4. The Change in Substructure of Solution Treated 12% Nickel Maraging Steel Caused by Fatigue. Subgrains were developed in the martensitic platelets of the samples tested in fatigue which were similar to the subgrains and other substructures developed in pure metals which were tested in fatigue or by static deformation. All of the samples of the solution treated 12% nickel maraging steel were water quenched to room temperature and tested in fatigue in the as-quenched condition. The austenitic phase developed by the solution treatment transformed to a martensitic structure upon quenching in water to room temperature. The prior austenite grain size was ASTM No. 8-9 which is equivalent to an average grain diameter of about 20 microns (0.02mm). The martensitic platelets consisted of narrow blades that frequently extended across the entire diameter of the prior austenite grain. The platelets in the as-quenched steel shown in Fig. 11 observed in a thin section taken from the bulk sample had a high density of dislocations ($4 \times 10^{10}/cm^2$). The dislocations in this solution treated and quenched steel were generated by the martensitic transformation and these dislocations were uniformly dispersed. No cell structure was indicated in many thin sections observed in the as-quenched condition. The average martensitic platelet width was

0.7μ (microns) or approximately 1/20 of its length. A twin orientation was always observed between two parallel martensitic platelets. This twin orientation is shown in the [111] selected area diffraction pattern shown in Fig. 12. The twin planes or boundaries between the platelets fit the $(112)_{\alpha}$ type with the reservation that as much as a 5° rotation of the plane perpendicular to the electron beam would produce a similar diffraction pattern. Internal twinning in the martensitic platelets was not observed except for a small area observed a few times which contained three to five bands that appeared to be internal twins. It was pointed out in the description of 12% nickel maraging steel that the absence of internal twinning makes this martensitic structure different from iron alloys containing either a high carbon content or a higher nickel content than about 27% nickel in which internal twinning in the platelets of martensite is extensive. The misfit caused by the transformation of austenite (fcc) to martensite (bcc) is accommodated in this 12% nickel maraging steel by a high dislocation density. The vacancy concentration in the martensitic phase is also expected to be high because of the rapid cooling and diffusionless phase transformation during the quench. Vacancy clusters were not evident in the as-quenched steel as shown in Fig. 11.

The change in substructure due to static deformation is presented for true tensile strains between 50% and 70% in order to compare the change in substructure in the maraging steel caused by fatigue. The substructure developed by extensive plastic flow of at least 50% true strain is

shown in Fig. 13 in which dislocations are piled up along the length of the platelets of martensite and subgrains are formed. The martensitic platelets were frequently bent indicating extensive plastic flow. The boundaries between platelets were still evident and each boundary followed the bend contours of the two adjoining martensitic platelets. The average subgrain size within the martensitic platelets was about 0.2μ (microns). A typical electron diffraction pattern which was produced by a selected area in a statically deformed platelet which was oriented with its [111] parallel to the electron beam is shown in Fig. 14. The five or six diffraction spots rotated about the [111] represent the number of subgrains or the number of parts of subgrains which were in a selected area of $0.16\,\mu^2$. Five or six subgrains between $0.1\,\mu$ and $0.3\,\mu$ in diameter would fit into this area of $0.16\,\mu^2$ and would be expected to give a sufficient intensity for an electron diffraction pattern which is in agreement with the observed subgrain size. The average angle of rotation about the [111] between adjacent diffraction spots is 2° to 3° if the 5° twin related spots are not counted. The accuracy of this measurement of angular rotation of an electron spot about the length of the electron beam is not appreciably affected by the 5° rotation of the Ewald sphere[56] (for all practical purpose the Ewald sphere is a plane for electrons accelerated by 100 K_V) perpendicular to the length of the electron beam. The measurement of the average rotation of the spot about the length of the electron beam should be accurate to within a few tenths of a degree. The linear density of dislocations in the cell wall, $\sqrt{\rho_w}$,

was calculated from the average rotation of 2.5° of adjacent diffraction spots from the relationship determined by Sleeswyk,[54] $\theta=b/h$, in which $\sqrt{\rho_w} = 1/h$ was $(1.7\pm0.4)\times10^6$/cm. The density of dislocations within the subgrain boundary which was calculated from the rotation of diffraction spots about the 111 direction was in agreement with the observed density of dislocations of $(1.2\pm0.5)\times10^6$/cm indicating that the subgrains were joined by nearly pure tilt boundaries. Dislocations within the subgrains were decreased from $4 \times 10^{10}/cm^2$ in the as-quenched condition to about $2 \times 10^{10}/cm^2$ in the statically deformed steel. The measurements of substructure for the solution treated 12% nickel maraging steel are listed in Table 3. The standard deviations listed for each value represents the deviation between areas from the center of the tensile sample to areas near the surface of the sample. No difference in substructure was evident for thin foils made from any part of the cross section of the test samples either tested as a static tensile test or in axial fatigue. At least five different areas were chosen for each sample from which the measurements were made and the average of these measurements are listed in Table 3.

Measurements of substructure were made in the decorated and as-tested condition of a representative number of thin foils from solution treated samples tested in fatigue to a certain fraction of their fatigue life, N_f , and the results are listed in Table 3. The decoration of dislocations in the fatigue samples was done by a partial age hardening treatment. The heat treatment used for decoration consisted of holding the tested samples at 880°F until partial aging

was indicated by an increase in hardness which required from 3 to 17 hours for the various samples. This decoration treatment did not change the appearance of the substructure but it did pin dislocations that could have slipped out of thin foils if they had not been pinned by the decoration. Decoration also reduced the strain field around dislocations in the subgrain boundaries. Measurements of dislocation densities within the subgrains and of the subgrain size are considered more accurate in the decorated condition. The observed linear densities of dislocations in the subgrain boundaries agreed with those calculated from electron diffraction patterns for densities on the order of 10^6/cm. A cell wall density on the order of 10^5/cm was not calculated from the electron diffraction patterns because the angle of rotation (0.4°) of adjacent subgrains about the [111] did not separate the diffraction spots enough for an accurate measurement.

The density of dislocations within the subgrain was decreased by both static deformation and by fatigue from the as-quenched dislocation density. Many of the dislocations which were in the as-quenched substructure were probably swept into the position which formed tilt boundaries of a low angle. The subgrain size listed in Table 3 decreased with increasing strain for samples tested in fatigue. The relationship between cell size and the nominal plastic strain range for the samples tested in fatigue is shown in Fig. 15 in which

$$\text{c.s.} = 0.19 \left(\Delta\epsilon_p / 2 \right)^{-0.18} \text{ microns} \qquad \text{(Equation \#12)}$$

for $0.01 < \frac{\Delta\epsilon_p}{2} < 0.6$. When the extra nominal plastic strain

due to cyclic softening is added to the initial plastic strain, $\Delta\epsilon_{p_i}$, for the sample tested at $\Delta\epsilon_t = 1.06\%$ (0.001 $\sim \Delta\epsilon_{p_i}$), this point approaches the curve drawn to fit the other points shown in Fig. 15. The cell size of the tensile test of $\epsilon_t = 0.6 \pm 0.1$ fits the curve for the cell size of the fatigue samples. The size of subgrains in the solution treated 12% nickel maraging steel produced by cyclic deformation was dependent on the nominal plastic strain range after most of the cyclic softening had taken place.

The density of dislocations observed in the well ordered subgrain boundaries increased as the plastic strain range increased for the tests in fatigue. The densities of dislocations in the cell wall of the subgrains produced by fatigue at total strain ranges of 18% to 7% were nearly the same as the static test in which a strain between 50% to 70% was produced. Even though the density of dislocations within the subgrain boundaries were of the same order of magnitude for the statically deformed samples and for the fatigue samples, the dislocations were usually in regular positions within the subgrain boundaries of fatigue samples compared to the tangles of dislocations not in a regular array which were observed in the subgrain boundaries of statically deformed samples. Fatigue involving lower total strain ranges of 2.6% and 1.06% produced a smaller density of dislocations in the cell walls which was on the order of 10^5/cm contained within very well ordered subgrain boundaries. The density of dislocations within the subgrains listed in Table 3 were decreased by fatigue compared to the density of dislocations within the subgrains of the untested samples and the statically deformed sample.

The substructure produced by fatigue is shown in Figs. 16, 17, and 18. The subgrains also appear to contain point defects in the samples tested at a constant total strain range of 1.06% which is shown in Fig. 16. The effect of decoration can be seen by comparing the undecorated substructure in Fig. 16 and with the decorated substructure in Fig. 17. The usual appearance of subboundaries in an undecorated sample tested in fatigue at a constant strain range of 7% is shown in Fig. 18. The martensitic boundaries were not obvious because the subgrains included the boundaries in their formation but the original boundaries were present after fatigue and could be identified by the twin relationship discussed previously.

5.2. Results of Fatigue of Aged 12% Nickel Maraging Steel at Room Temperature

The fatigue diagram and the relationship for cyclic softening and cyclic hardening of the aged samples tested in fatigue were similar to the data for the solution treated samples tested in fatigue, but the change in substructure due to fatigue was not observed because of the high density of precipitate particles in the substructure. Except for the extra nominal elastic strain due to the higher yield strength of the aged samples compared to the solution treated samples, the fatigue diagram for the aged samples shown in Fig. 19 is similar to the fatigue diagram of the solution treated samples. This fatigue diagram for the aged samples could be approximated by:

$$N_f = \gamma \, (\Delta\epsilon_p/2)^{-1.5} \qquad \text{(Equation \#13)}$$

in which γ is the value of N_f when $\Delta\epsilon_p/2 = 1$. Only one sample was tested in fatigue to failure for each strain range. Additional tests in fatigue were stopped at a predetermined percentage of the fatigue life in order to observe the substructure.

The stress range was determined for each cycle conducted at a constant total strain range with a mean strain of zero. The stress range measured at each cycle for strain ranges of 2.6% and 7% are shown in Figs. 20 and 21. A duplicate test for the sample tested at a 2.6% strain range in fatigue up to 80% of the number of cycles needed for the fatigue life is also shown in Fig. 20. The measured stress range for identical cycles of the duplicate test was in agreement within 1½% of the total stress range for identical cycles. The change in stress range was resolved into a cyclic softening and cyclic hardening component of stress and the relationship was identical to that for the solution treated samples. The change in stress range due to cyclic softening, σ_s, was described by Equation #7. The remaining component of the change in stress range was due to cyclic hardening according to the equation:

$$\sigma_H = 8(\Delta\epsilon_{pi} + \sigma_s/E) N/N_o \div (1 + 8N/EN_o) \quad \text{(Equation \#14)}$$

The fractional change in stress range, σ_r/σ_o, and the fitted curves of $\frac{\sigma_o-\sigma_s+\sigma_H}{\sigma_o}$ (calculated) are plotted in Fig. 22. The form of the cyclic softening equation and the cyclic hardening equation is identical for the solution treated and for the aged samples but the values of k' and N_o are significantly different. When the solution treated samples were tested in fatigue, it was determined that $k' = 22 \pm 2$

and $N_o = 1$ for all fatigue tests conducted at room temperature. When the aged samples were tested in fatigue, $k' = 45 \pm 2$ and N_o was larger than one and was not the same for the tests conducted at room temperature for strain ranges of 2.6% and 7%. The values of N_o for the aged samples are plotted as shown in Fig. 23 for corresponding fatigue lives and for the plastic strains maintained during the tests in fatigue. The approximate relationship:

$$N_o \cong (0.09/\Delta\epsilon_p) + 1 \qquad \text{(Equation \#15)}$$

is indicated by the limited number of tests at room temperature.

The substructure developed by fatigue of the aged 12% nickel maraging steel was expected to be similar to the substructure developed by the fatigue of the solution treated samples because of the similarity in cyclic softening and cyclic hardening during fatigue. Although excellent thin films were made of the fatigue samples, a change in the substructure was not observed in the aged samples tested in fatigue. The high density of precipitate particles in the aged samples was considered responsible for either the absence of substructure due to fatigue or if a substructure was developed by fatigue the high density of precipitates did not permit the observation of that substructure. The rod-shaped precipitate particles were thought to nucleate along dislocations produced from the martensitic transformation as described by Reisdorf.[47] A typical view of the aged 12% nickel maraging steel is shown in Fig. 24 in which the orientation and density of these rod-shaped precipitates ($3 \times 10^{10}/cm^2$) in the substructure are similar to the

orientation and density of dislocations within the martensitic platelets of the as-quenched steel. Two types of precipitates were formed by the age hardening treatment and these are shown in Fig. 24. The rod-shaped particles constituted a volume fraction of about 0.01 and the small spherical precipitate particles located between the rod-shaped particles constituted a volume fraction of about 0.04. The streaks which were observed in the <110> of electron diffraction patterns of a selected area of the aged samples with the [100] parallel to the electron beam as shown in Fig. 25 indicates that the precipitates cause a directional strain in the <110> . Qualitatively the streaks were not changed when the aged samples were tested in fatigue.

No change in the stress range for a change in the substructure of as much as 3% by volume of reverted austenite was observed for overaged samples tested in fatigue at constant total strain ranges of 2.6% and 0.8%. The reverted austenitic phase outlined the martensite boundaries when the samples were overaged by holding them at a temperature of 920°F for 16 hours. The samples containing reverted austenite were then tested in fatigue to failure at constant total strain ranges of 2.6% and 0.8%. The fatigue life of each test is plotted in the fatigue diagram shown in Fig. 19 along with the results of the optimumly aged samples that did not contain any reverted austenite. The stress range for each cycle applied at a constant total strain range of 2.6% shown in Fig. 20 is for one sample with 3% reverted austenite tested to failure and for another sample without a reverted austenitic phase tested to 80% of the fatigue life. No difference in the stress range was

observed for identical cycles of the sample containing a small amount of reverted austenite and the sample without reverted austenite. The substructure which contained reverted austenite shown in Fig. 24 was tested in fatigue at a strain range of 0.8% and failed after 3,000 cycles. The yield strength of reverted austenite was apparently greater than that of the aged martensitic matrix because the substructure of the reverted austenite was not changed from the untested aged samples. The high strength of the reverted austenite may be partly due to the dislocation density of the reverted austenite which was on the order of $10^{10}/cm^2$ and partly due to the small grain size of the reverted austenite. The grain size of reverted austenite was so small that a polycrystalline type of diffraction pattern was always obtained for a selected area which contained a single strip of reverted austenite. Although the areas between precipitate particles in the aged martensitic matrix were too distorted to observe the substructure, no additional dislocations were observed in the phase of reverted austenite which was deformed to near the fracture strain by large static deformations.

5.3. The Activation Energy of Cyclic Softening of the 12% Nickel Maraging Steel

The relationship between the number of applied cycles and the change in stress range, Equation #7, which was determined at room temperature applied for tests in fatigue conducted above and below room temperature. The value of k' was proportional to $1/T^{\circ}K$ in which $T^{\circ}K$ is the absolute temperature of the sample during the test for both

the solution treated and the aged samples. The value of N_o at temperatures other than room temperature was still equal to one cycle for the solution treated samples tested in fatigue but the relationship, Equation #15, observed at room temperature for the aged samples tested in fatigue was not indicated by the tests in fatigue conducted at 32°F in which N_o was 13.5 cycles or at 415°F in which N_o was six cycles. The results of the fractional change in stress range for each cycle of fatigue applied at a constant temperature for each test is shown in Fig. 22. The value of the slope of each curve in Fig. 22 is k' which is independent of the value of N_o for that curve. The values of k' are plotted versus the corresponding value of in Fig. 26 in which the slope of each curve for the solution treated and the aged steel is assumed equal to the activation energy, Q, of cyclic softening divided by the gas constant, R. The activation energy for cyclic softening was - 32 $\pm$ 2 kcal./gm. atom for the cyclic softening of the aged steel and + 32 $\pm$ 2 kcal./gm. atom for the cyclic softening of the solution treated steel. From the values and signs of the activation energies which were determined for cyclic softening, it was assumed that the equation for cyclic softening due to the fatigue of the aged steel was of the form:

$$N = N_o \exp [Q_v - V(\tau-\tau_o)\ \sigma_s]/\ (RT\sigma_o) \qquad \text{(Equation \#16)}$$

In Equation #16 Q_v is the activation energy for self-diffusion which is approximately the same as the energy required for the formation of vacancies in a pure metal,

$\underline{V}$ is the activation volume, τ is the applied shear stress and τ_o is the back stress along the slip plane produced by dislocations which were tangled and formed a barrier on that slip plane. A full description of the relationship in Equation #16 is given in the discussion.

5.4. The Effect of Fatigue of the 12% Nickel Maraging Steel on the True Stress-True Strain Relationship and the Hardness

The true stress-true strain curves for the final stress range due to fatigue at one-half of the total strain range which was maintained during the fatigue test was less than the true stress at the same total strain for a tensile test. The hardness of the sample was decreased by fatigue in which the initial plastic strain range, $\Delta\epsilon_{pi}$, was at least 0.001 inch/inch. The static and dynamic relationship for the true stress and the true strain is shown in Figs. 27 and 28 in which the measured values are plotted and the relationship is corrected for necking by the Bridgman[50] correction for the 12% nickel maraging steel which is shown in Fig. 4. The value of the stress range plotted in Figs. 27 and 28 for the dynamic curve is the calculated stress range at failure for cyclic softening and cyclic hardening since the measured values of the stress range at failure were decreased by the load drop due to partial fracture. The dynamic curve extrapolates to the static fracture strain, ϵ_f, for the aged samples tested in fatigue. A true stress equal to the value of the yield strength for the solution treated steel was not significantly increased until a true strain greater

than 39% was applied during the static test as shown in Fig. 27. The exponent of strain hardening, n, for the solution treated steel tested in static tension between a true strain of 39% and true fracture strain, ϵ_f , was 0.10. The exponent of strain hardening, n', of the true stress-true strain relationship for fatigue was also 0.10 for values of strain less than 39% in which work hardening was not produced by the static test. A summary of the strain hardening exponents and the value of the stress, K, at $\epsilon_t = 1.0$ is given in Table 4. The exponent of strain hardening, n, for the aged steel is equal to 0.03 for the tensile test and is nearly 0.07 for the dynamic relationship of aged samples tested in fatigue. The most important observation of the static and dynamic curves shown in Figs. 27 and 28 is that the cyclic softening is mainly due to a decrease in the yield strength of the steel. This reduction in yield strength is related to a reduction in the extent of the long range stresses as described in the discussion.

The hardness of samples tested in fatigue was decreased and examples of this decrease in hardness are listed in Table 5. The solution treated samples softened by fatigue were heat treated by holding them at a temperature of 880°F until the optimum hardness was reached as shown in Fig. 29. The amount of time required to reach the optimum hardness is called the aging response. The aging response of samples tested in fatigue prior to the heat treatment at a temperature of 880°F is shown in Fig. 29. Aged samples that were softened by fatigue were re-aged to nearly the same optimum hardness as shown in Table 5 and Fig. 29.

The similarity in aging response and optimum hardness between solution treated and the aged samples and the samples softened by fatigue prior to heat treatment does not indicate that fatigue damage is repaired by heat treatment. The heat treatment does not remove subgrains developed by the fatigue of solution treated samples which may cause crack initiation. A similar density of dislocations was reported in Table 3 in which the undecorated samples were not heat treated after fatigue and the decorated samples were aged at a temperature of 880°F.

5.5. A Criterion for Fatigue Failure

The magnitude of the stress range increase due to cyclic hardening was approximately a constant at the fatigue life of each sample and (constant) was independent of the strain range maintained during the fatigue test for $0.001 < \Delta\epsilon_p < 0.17$. The relationships for cyclic softening and cyclic hardening which were found in this investigation were assumed to occur simultaneously for the same number of cycles and by eliminating N/N_o from both relationships cyclic hardening is a function of cyclic softening:

$$\sigma_H = 8(\Delta\epsilon_{pi}+\sigma_s/E)\exp(k'\sigma_s/\sigma_o) \div [1+8/E\exp(k'\sigma_s/\sigma_o)] \quad \text{(Equation \#17)}$$

The relationship between cyclic hardening and cyclic softening was the same for the solution treated and for the aged samples tested in fatigue except for the value of k' and the small difference in Young's modulus, E. The relationship between cyclic softening and cyclic hardening for the strain ranges used in this investigation for tests in fatigue is plotted in Fig. 30 for the solution

treated steel and for the aged steel. The values of σ_s and σ_H were calculated from the observed number of cycles, N, applied for a fatigue failure at the strain range maintained during fatigue, and each value of σ_s and σ_H is enclosed by the circle at the end of the curves which are shown in Fig. 30. The value of σ_H for the fatigue life of each sample was approximately equal to 40 ksi for the solution treated samples and equal to about 7 ksi for the aged samples as shown in Fig. 30. A predicted fatigue diagram is indicated by the dash lines in Figs. 5 and 19 in which the measured fatigue lives are plotted and a predicted fatigue diagram was calculated from the cyclic hardening equation:

$$N_f = N_o\left(1+8N_f/EN_o\right)\left(\sigma_{H\,const.}\right) - 8\left(\Delta\epsilon_{pi} + \sigma_o/kE\ln N_f/N_o\right) \quad \text{(Equation \#18)}$$

The value of N_o was equal to one cycle for the solution treated samples and Equation #15 was used for the aged samples. A negative value of $\Delta\epsilon_{pi}$ was used for the lower strain part of the fatigue diagram involving long lives and this negative value of $\Delta\epsilon_{pi}$ represented the difference between nominal elastic strain at which yielding took place ($\Delta\epsilon_{\text{yielding}} \approx 1\%$) and the nominal elastic strain range of the test in fatigue, σ_o/E, in which $\sigma_o/E \doteq \ln(1+\sigma_o/E)$ for the small elastic strains observed in this investigation.

6. DISCUSSION

6.1. Cyclic Softening and the Ordering of Dislocation Tangles

The decrease in the stress range due to cyclic softening which was mainly caused by a reduction in the yield stress was related to the rearrangement of dislocation tangles into regular arrays of subgrain boundaries with fatigue which reduced the long range stresses associated with dislocation tangles by Li.[34] Both static deformation and fatigue which involved some nominal plastic strain reduced the dislocation density within the subgrain by sweeping some of the dislocations into subgrain boundaries usually consisting of dislocation tangles. The resulting dislocation density within the subgrain appeared to be slightly lower than for the statically deformed sample as shown in Table 3. The matrix density was higher when the fatigue samples were observed after heating for decoration, which indicated that some dislocations may have escaped during the preparation and observation of the thin foil. Also the decorated matrix may have included some dislocations that were partially stuck in the subgrain boundaries in the undecorated condition. There was a striking difference between the statically deformed samples and the samples tested in fatigue when both types of samples were observed in the undecorated condition. This difference consisted of the excellent order of the subgrain boundaries in the fatigue samples compared to the tangled dislocations at the subgrain boundaries of the statically deformed samples.

Li[35] has shown that long range stresses produced by dislocation tangles would exert a slip force on dislocations within the matrix. The strength of the long range stress produced by the tangled dislocations is proportional to $1/h$ in which $\underline{h}$ is the average distance between dislocations or $1/h = \sqrt{\rho_w}$. The size of the long range stress field produced by dislocation tangles decreased with increasing ordering of the tangled dislocations into regular arrays such as tilt and twist boundaries. Only a short range stress field was presented by a perfectly ordered boundary. The strength of the short range stress field varied from zero to some maximum value and back to zero for a dislocation located respectively at a distance of about $\underline{h}$ away from the regular boundary to about $h/2$ to a position within the subgrain boundary. This short range stress field is of little significance compared to the long range stress field for small plastic strains involved in this investigation in which the subgrain size was about 4×10^{-5} cm or 40 h. Keh related this ordering of dislocation tangles to the partial recovery of deformed samples by heat treatment below the recrystallization temperature in which the subgrains have not changed in size. Theories of work hardening or yielding such as those given by Taylor,[57] Seeger,[58] and Mott and Hirsch[59,60] relate the stress, τ , to the average dislocation density or the dislocation density of the "forest", ρ , by:

$$\tau = \alpha G b \sqrt{\rho} \qquad \text{(Equation \#19)}$$

According to Li[35] the dislocation density within the tangled

region is proportional to the strength of the long range stress field and, therefore, the yield stress. For most metals the dislocation density of the tangles is about five times the matrix density of dislocations between tangles. If the decrease in dislocation density of the matrix ($\rho_m \sim 10^{10}/cm^2$) is associated with the magnitude of the stress decrease due to cyclic softening as indicated in Table 6 except for the fatigue test at a total strain range of 1.06%, the value of α is 1.3 rather than 0.2 as it usually is for most metals. The value of α is of the correct order of magnitude when the decrease in stress range is associated with the elimination of dislocation tangles ($\rho_w \sim 10^{11}/cm^2$) by forming regular arrays of previously tangled subgrain boundaries.

Segments of a dislocation which were caught in a tangled group were probably not sessile and could move with the application of cyclic stresses. These segments may acquire a high density of jogs. Some of the jogs when moved in a non-conservative manner will produce point defects. These point defects may become attached to dislocations under the influence of these dislocations moving to and from the vicinity of the point defects. The end result is that segments of the dislocation will climb into an equilibrium position which is consistent with the rest of the dislocation in the subgrain boundary. Cyclic softening may take place very early in the fatigue test if a large number of vacancies are in the structure before deformation or a high density of forest dislocations result in the production of a large concentration of vacancies during the first cycle of fatigue. In contrast the production of

vacancies may be much lower per cycle of fatigue at the same strain for a well annealed metal or a precipitation hardened alloy in which the original "forest" of dislocations are sites for precipitate particles. The jobs on the moving dislocations from which point defects are produced occur by mutual intersection of the newly generated dislocations which provide the strain. The production of point defects for the same amount of strain is much lower for the annealed or aged alloy. This lower production of point defects per cycle of fatigue for the strain range is indicated for the aged steel in which cyclic softening did not begin until a certain number of cycles, N_o, were applied and $N_o \approx 0.09/\Delta\epsilon_p + 1$. Cyclic softening was immediate, $N_o = 1$, for the solution treated samples which were always tested in the as-transformed condition and $N_o \approx 1$ for the aged samples tested in fatigue at ranges of plastic strain, $\Delta\epsilon_p \gg 0.09$. Although the value of k' for a particular condition of the 12% nickel maraging steel was not changed by tests in fatigue at strain ranges from $0.001 < \Delta\epsilon_p < 0.17$, the value of k' was very sensitive to the temperature, T, of the sample during the test as described previously. The value of k' was proportional to 1/T and from this relationship activation energies of + 32 kcal./gm. atom and - 32 kcal./gm. atom were determined for the cyclic softening of the solution treated and the aged samples respectively tested at constant temperatures. The activation energy is associated with the energy of self-diffusion, Q_v, if it is assumed that the form of the cyclic softening equation is:

$$N = N_o \exp [Q_v - V (\tau - \tau_o)] \sigma_s / (RT\sigma_o) \qquad \text{(Equation \#16)}$$

for the aged samples tested in fatigue. The form of the equation for cyclic softening of the solution treated samples tested in fatigue in the as-transformed condition in which a sufficient number of vacancies were available after the first cycle is:

$$N = N_o \exp [-V (\tau - \tau_o)] \sigma_s / (RT\sigma_o) \qquad \text{(Equation \#20)}$$

The value of Q_v determined from the cyclic softening of the solution treated and the aged samples tested in fatigue in which $Q_v - V(\tau-\tau_o) = -32 \pm 2$ kcal./gm. atom and $-V(\tau-\tau_o) = +32 \pm 2$ kcal./gm. atom was equal to -64 ± 4 kcal./gm. atom. This value of the activation energy for cyclic softening is comparable to - 60 kcal./gm. atom[61] for the formation of vacancies in iron which was obtained from the activation energy for self-diffusion. Some support for the assumed form of the equation for cyclic softening in terms of an activation energy is given by a similar equation derived by Machlin,[29] but his dislocation model for failure in fatigue was quite different.

The change in substructure due to fatigue observed in this investigation for the solution treated samples was not observed for the aged samples because of the high density of precipitate particles even though excellent thin films were made of the aged samples tested in fatigue. It is concluded from the analogy of the relationship of cyclic softening for both the solution treated and the aged samples

that Li's[35] model of long range stresses due to dislocation tangles and the reduction of the yield stress due to the partial order of the dislocation tangles proposed for cyclic softening should also be applicable to the aged samples tested in fatigue. The "forest" of precipitate particles should remain unchanged in this iron alloy system during fatigue since reversion or overaging similar to that observed during the fatigue of age hardened aluminum alloys[10] required much more thermal activation. A large number of dislocation tangles would be expected because of the high density of dislocations required to produce the strain in the aged structure with closely spaced precipitate particles as evidenced by the high yield strength (180 ksi) of the aged steel. A partial ordering of these dislocation tangles during fatigue should result in the same order of magnitude of stress decrease as in the solution treated samples tested in fatigue.

6.2. Cyclic Hardening in Terms of Point Defects

The extra stress due to cyclic hardening, σ_H , was considered to be related to the hardening caused by the deposition of point defects during fatigue. A relationship between the extra stress due to strain hardening and the accumulation of point defects on the glide bands through which dislocations had travelled during the application of strain was found by Gilman and Johnson[62] for single crystals of LiF. Gilman[62] suggested that the extra stress due to strain hardening, $\Delta\tau$, was proportional to the density of dislocations, ρ , because the strain hardening was caused by point defects left behind by the expanding

dislocation loops. Evidence for the existence of these point defects in LiF were observed by special etching techniques. In Gilman's[62] suggestion for defect hardening of LiF the number of defects would be proportional to the area swept out by the moving loops which in turn would be proportional to the plastic strain. Gilman and Keith[63] investigated the effect of cyclic loading of LiF on the dislocation behavior and found that the density of dislocations within the glide band increased to some limiting value which was reached after 10 or more cycles and the dislocation density was not decreased by the reversed strain portion of the loading cycle. Gilman and Keith[63] suggested that fatigue failure of LiF is probably due to the formation and coalescence of point defects. The relationship for the increase in stress range due to cyclic hardening, σ_H, obtained from this present investigation, $\sigma_H = 8\Delta\epsilon_p N/N_o$, indicates that $\sigma_H \propto (\rho A)N$ in the case in which $N_o = 1$ assuming $(\rho A) \propto \Delta\epsilon_p$ for small plastic strain ranges less than 0.17. This relationship indicates that either an extra number of dislocations, $\Delta\rho \propto \Delta\sigma$, were created for each cycle of fatigue, N, or that the lattice resistance to movement of the same number of dislocations was increased by the same amount for each cycle of fatigue involving a constant range of plastic strain. A decrease in the density of dislocations not in subgrain boundaries was observed in fatigue samples and the extra stress due to cyclic hardening was not caused by the formation of additional dislocations. The contribution of point defects to cyclic hardening was expected since a high concentration of point defects in the fatigue samples of the solution

treated samples was observed by transmission electron microscopy in which the dislocation loops were observed after extensive fatigue as shown in Fig. 16. The density of dislocations responsible for the small plastic strain of a sample subjected to a number of cycles of fatigue is probably not changed much or at least the product of the dislocation density and the area swept out by these dislocations, (ρA), is a constant. The point defects which were left on the slip plane by jogs which failed to reabsorb these point defects upon a complete reversal in strain should become a permanent part of the lattice and cause an increase in the lattice resistance to flow. If a constant number of point defects become a permanent part of the lattice for each cycle of fatigue, then the extra stress caused by the defect hardening is proportional to the product $(\rho A)\,N$ and the extra stress, σ_H, is a function of $\Delta\epsilon_p N$. The aged 12% nickel samples tested in fatigue also had an increase in stress, σ_H, due to cyclic hardening according to Equation #10 in which $N_o \approx 0.09/\Delta\epsilon_p + 1$ so that at plastic strains of $\Delta\epsilon_p \gg 0.09$ the value of N_o approaches one. For plastic strains of $\Delta\epsilon_p \ll 0.09$ the relationship approaches $\sigma_H \propto (\Delta\epsilon_p)^2 N$ which is the relationship Coffin[16,17] has established for part of the low cycle fatigue curve of alloys such as mild steel, aluminum and titanium assuming a constant value of σ_H at failure. The reason for the application of a number of cycles, N_o, before cyclic softening began was related to the efficiency of the substructure in producing and associating the point defects with the dislocations which should also apply to cyclic hardening. The condition, $\sigma_H \doteq 89(\Delta\epsilon_p)^2 N$, is never reached for the aged 12%

nickel maraging steel because the extra plastic strain produced by cyclic softening, $\sigma_s/E \doteq \ln(1+\sigma_s/E)$, in Equation #11 caused fatigue failures at a value of N smaller than $\sigma_H \doteq 89(\Delta\epsilon_p)^2 N$ predicted for small strains without cyclic softening.

6.3. The Application, in General, of the Analysis of Cyclic Softening and Cyclic Hardening

The data of Tuler and Morrow[20] for cold-worked (OFHC) copper and annealed (OFHC) copper were analyzed according to the relationships determined for the 12% nickel maraging steel as shown in Appendix A. The similarity of the cyclic softening and cyclic hardening relationships for the 12% nickel maraging steel which has a bcc crystal structure and the oxygen free high conductivity (OFHC) copper which has a fcc crystal structure indicates that the low cycle fatigue of other metals and engineering alloys can be described by these relationships.

7. CONCLUSIONS

7.1. Fatigue damage in the solution treated and quenched 12% nickel maraging steel was observed to be associated with a change in the substructure resulting from the fatigue strain. The polygonized structure observed for the solution treated and quenched 12% nickel maraging steel was similar to the fatigue damage observed by others in studies of pure metals.

7.2. The change in stress range measured at the reversal of each fatigue cycle was uniquely analyzed as a decrease in stress range due to cyclic softening and an increase in stress range due to cyclic hardening. The number of applied cycles, N, was related to the decrease in stress range, σ_s , due to cyclic softening according to Equation #7. Cyclic hardening occurred simultaneously and the magnitude of the increase in stress range, σ_H , was dependent on the number of applied cycles (Equation #10). Identical relationships for cyclic softening and cyclic hardening were observed for fatigue samples of both the solution treated and the aged steels tested in fatigue at a constant total strain range that included nominal plastic strains from 0.001 to 0.170.

7.3. The number of applied cycles was eliminated from both equations (#7 and #11) to give cyclic hardening as a function of cyclic softening, (Equation #17), because cyclic softening and cyclic hardening occurred simultaneously for the 12% nickel maraging steel tested in fatigue.

7.4. Cyclic softening of cold-worked copper presented by Tuler and Morrow[20] obeyed Equation #7, which was observed for the cyclic softening of maraging steel in this

investigation. The extra stress range per cycle of fatigue presented by Tuler and Morrow[20] for annealed copper decreased with successive cycles of fatigue. The extra stress of copper tested in fatigue was associated with point defect hardening, but the relationship shown in Equation #10 was modified to include the decrease in the plastic strain with each successive cycle of the samples tested in fatigue at a constant total strain range as given by the summation in Equation #21 (Appendix A).

7.5. It is concluded that cyclic softening is due to dislocation climb as supported by the measurement of activation energies for cyclic softening. The activation energy for the cyclic softening of the solution treated steel was + 32 kcal./gm. atom. The activation energy for the cyclic softening of the aged steel was - 32 kcal./gm. atom. If the activation energy for cyclic softening is described as $Q_v - V(\tau - \tau_o)$ for the aged steel and as $-V(\tau - \tau_o)$ for the solution treated steel, then Q_v equals - 64 kcal./gm. atom or approximately the activation energy for vacancy formation in iron.[61] Additional evidence that vacancies were needed for cyclic softening was given by the number of cycles needed before softening began. For the solution treated and quenched steel softening occurred immediately ($N_o = 1$) and for the aged steel N_o was dependent upon $(\Delta\epsilon_p)^{-1}$ described by Equation #15. The dependence of N_o upon $(\Delta\epsilon_p)^{-1}$ indicated that at small plastic strains a number of cycles were needed in order to create enough vacancies to partially orient the dislocation tangles and to reduce the long range stresses associated with them by Li.[35] The same low production of point defects per

cycle of fatigue at small values of $\Delta\epsilon_p$ caused a reduction in the amount of cyclic hardening.

7.6. The increase in stress range due to cyclic hardening in the 12% nickel maraging steel was associated with point defect hardening because of the relationship, Equation #10, between the extra stress range due to cyclic hardening, σ_H, the plastic strain, $\Delta\epsilon_p$, and the number of applied cycles of fatigue, N. The relationship, Equation #10, was the same for the 12% nickel maraging steel tested in both the solution treated and the aged condition for nominal plastic strain ranges from 0.001 to 0.170. This conclusion was supported by the observations of Gilman and Johnson[62] and Gilman and Keith[63] concerning the relationship between the plastic strain, dislocation density, and extra stress due to point defects in single crystals of LiF tested by monotonic and reversed bending.

7.7. For the quenched and aged 12% nickel maraging steel no change in the substructure could be observed as resulting from fatigue strain because the high density of precipitate particles obscured any recognition of a change in the substructure.

7.8. Qualitatively the strain fields around dislocations in the solution treated steel and the strains in the <110> caused by the precipitates in the aged steel were not changed by fatigue.

7.9. The orientation and location of martensite boundaries were not changed by fatigue where plastic strains from 0.001 to 0.170 were involved. Parallel martensite platelets were usually oriented with respect to

one another by a $(112)_\alpha$ twin orientation. These twin related platelets were present in the solution treated and aged samples.

The density of dislocations observed in the subgrain boundaries of samples tested in fatigue and static tension was in good agreement with the density which was calculated from the rotation of electron diffraction spots about the [111] assuming a simple tilt boundary.

7.10. Two types of precipitates were observed in the substructure of 12% nickel maraging steel. Rod-shaped particles which had the same crystallographic orientation and nearly the same particle density as the original dislocations in the solution treated steel accounted for a volume fraction of 0.01. Spherical particles located between the rod-shaped particles were only resolved under optimum conditions and they accounted for a volume fraction of 0.04 with a density similar to that of the other type of particles.

7.11. Reverted austenite up to a volume fraction of 0.03 did not change the fatigue results from those observed for the optimumly aged steel. The reverted austenite nucleated at martensite boundaries when the 12% nickel maraging steel was overaged and the reverted austenite had a small grain size.

7.12. The aging response for the samples of solution treated steel which were tested in fatigue was about the same as for the untested samples except for the samples tested at 7% and 18% total strain ranges. The aged steel which was softened by fatigue regained its hardness after a few hours at the optimum aging temperature. The thermal

response which was observed on aging after 80% of the number of cycles needed for failure were applied does not imply that fatigue damage was nullified by heat treatment. The polygonized structure produced by fatigue was still observed in the heat treated fatigue samples and may contribute to failure upon further fatigue testing.

7.13. A prediction of the number of cycles needed for a fatigue failure was obtained by assuming that a constant value of σ_H existed at failure for fatigue lives from 40 to 20,000 cycles. The original value of σ_H at failure was obtained from fatigue samples that failed after 40 to 600 cycles in which σ_H was related to the generation of point defects by the relationship shown in Equation #10. The calculated fatigue curves agreed with the observed fatigue curves within 20% of the life for both the solution treated and the aged steels.

LIST OF REFERENCES

1. Gough, H. J. "Crystalline Structure in Relation to Failure of Metals -- Especially by Fatigue." Proceedings, American Society of Theoretical Mechanics, Vol. 33, 1933. pp. 3-114.

2. Smith, G. C. "The Initial Fatigue Crack." Proceedings, Royal Society (London), Vol. 242A, 1957. pp. 189-196.

3. Forsyth, P. J. E. "Slip Damage and Extrusion." Proceedings, Royal Society (London), Vol. 242A, 1957. pp. 198-202.

4. Wood, W. A., S. McCousland and K. R. Sargant. "Systematic Microstructural Changes Peculiar to Fatigue Deformation." Acta Metallurgica, Vol. 11, No. 7, 1963. pp. 643-652.

5. Segall, R. L. and P. G. Partridge. "Dislocation Arrangements in Aluminum Deformed in Tension or by Fatigue." Philosophical Magazine, Series 8 Vol. 4, No. 44, 1959. pp. 912-919.

6. Clarebrough, L. M., M. E. Hargreaves, G. W. West and A. K. Head. "The Energy Stored in Fatigued Metals." Proceedings, Royal Society (London), Vol. 242A, 1957. pp. 160-161.

7. Davidge, R. W., C. E. Silverstone and P. L. Pratt. "The Generation of Point Defects by Deformation and Fatigue in Alkali Halides." Philosophical Magazine, Series 8, Vol. 4, No. 44, 1959. pp. 985-987.

8. Polakowski, N. H. and A. Palchoudhuri. "Softening of Certain Cold-Worked Metals Under the Action of Fatigue Loads." Proceedings, American Society of Testing and Materials, Vol. 54, 1954. pp. 701-716.

9. Broom, T., J. H. Molineux and V. N. Whittaker. "Structural Changes During the Fatigue of Some Aluminum Alloys." The Journal of the Institute of Metals, Vol. 84, 1955-1956. pp. 357-363.

10. Forsyth, P. J. E. and C. A. Stubbington. "Some Observations on the Microstructural Damage Produced by Fatigue of an Aluminum - 7.5% Zinc - 2.5% Magnesium Alloy at Temperatures between Room Temperature and 260°C." Acta Metallurgica, Vol. 14, No.1, 1966. pp. 5-12.

11. McCammon, R. D. and H. M. Rosenberg. "The Fatigue and Ultimate Tensile Strengths of Metals Between 4.2 and 293°K." Proceedings, Royal Society (London), Vol. 242A, 1957. pp. 203-211.

12. Freudenthal, A. M. and T. J. Dolan. "The Character of Fatigue of Metals." Fourth Progress Report, Office of Naval Research, Contract NG-Ori-71, Task Order IV, Engineering Experimental Station, University of Illinois, Urbana, Illinois, February, 1948.

13. Sinclair, G. M. and T. J. Dolan. "Use of a Recrystallization Method to Study the Nature of Damage in Fatigue of Metals." Proceedings of the First U. S. National Congress of Applied Mechanics, American Society of Mechanical Engineers, 1951. pp. 647-651.

14. Thompson, N., N. Wadsworth and N. Louat. "The Origin of Fatigue Fracture in Copper." Philosophical Magazine, Series 8, Vol. 1, No. 2, 1956. pp. 113-126.

15. Read, W. T., Jr. Dislocations in Crystals. McGraw-Hill Book Co., Inc., New York, 1953. pp. 69-90.

16. Coffin, L. F., Jr. and J. F. Tavernelli. "A Compilation and Interpretation of Cyclic Strain Fatigue Tests on Metals." Transactions, American Society for Metals, Vol. 51, 1959. pp. 438-453.

17. Coffin, L. F., Jr. and J. F. Tavernelli. "The Cyclic Straining and Fatigue of Metals." Transactions, Metallurgical Society of the American Institute of Mining, Metallurgical, Petroleum Engineers, Vol. 215, 1959. pp. 794.

18. Raymond, M. H. and L. F. Coffin, Jr. "Geometric and Hysteresis Effects in Strain-Cycled Aluminum." Acta Metallurgica, Vol. 11, No. 7, 1963. pp. 801-807.

19. Smith, R. W., M. H. Hirschberg and S. S. Manson. "Fatigue Behavior of Materials Under Strain Cycling in Low and Intermediate Life Range." National Advisory Committee for Aeronautics, Technical Note D-1574, 1963.

20. Tuler, R. R. and J. Morrow. "Cyclic Dependent Stress-Strain Behavior of Metals." Theoretical and Applied Mechanics Report No. 239, University of Illinois, Urbana, Illinois, 1963.

21. Yao, J. T. P. and W. H. Munse. "Low Cycle Fatigue of Metals -- Literature Review." The Welding Journal, Research Supplement, April, 1962.

22. Tavernelli, J. F. and L. F. Coffin, Jr. "Experimental Support for the Generalized Equation Predicting Low Cycle Fatigue." Journal of Basic Engineering, Transactions, American Society for Mechanical Engineers, Series D, Vol. 84, No. 4, 1962.

23. Morrow, J. "Cyclic Plastic Strain Energy and Fatigue of Metals." Internal Friction, Damping and Cyclic Plasticity, Special Technical Publication, No. 378, American Society for Testing and Materials, 1965.

24. Radziminski, J. B. "The Effect of Plastic Prestrains on the Low Cycle Fatigue Behavior of Titanium." Ph. D. Thesis submitted to the Graduate College, University of Illinois, Urbana, Illinois, 1965.

25. Feltner, C. E. "Dislocation Arrangements in Aluminum Deformed by Repeated Tensile Stresses." Theoretical and Applied Mechanics Report No. 252, University of Illinois, Urbana, Illinois, 1962.

26. Pratt, J. E. "Dislocation Substructure in Strain Cycled Copper." Theoretical and Applied Mechanics Report No. 652, University of Illinois, Urbana, Illinois, 1965.

27. Keh, A. S. and S. Weissmann. "Deformation Substructure in Body Centered Cubic Metals." Electron Microscopy and Strength of Crystals, ed. by G. Thomas and J. Washburn, Interscience Publishers, New York, 1963. Chapter 5.

28. Orowan, E. "Theory of the Fatigue of Metals." Proceedings, Royal Society (London), Vol. 171A, 1939. pp. 79-106.

29. Machlin, E. "Dislocation Theory of Fatigue of Metals." Annual Report of National Advisory Committee for Aeronautics, Vol. 845, 1946.

30. Machlin, E. and A. Norwich. "Quantitative Treatment of the Creep of Metals by the Dislocation and Rate Process Theories." Annual Report of National Advisory Committee for Aeronautics, Vol. 845, 1946.

31. Cottrell, A. H. and D. Hull. "Extrusion and Intrusion by Cyclic Slip in Copper." Proceedings, Royal Society (London), Vol. 242A, 1957, pp. 211-213.

32. Mott, N. F. "A Theory of the Origin of Fatigue Cracks." Acta Metallurgica, Vol. 6, No. 3, 1958. pp. 195-197.

33. Li, James C. M. "The Interaction of Parallel Edge Dislocation with a Simple Tilt Dislocation Wall." Acta Metallurgica, Vol. 8, No. 4, 1960. pp. 296-311.

34. Li, James C. M. "Energy of a Crossed Grid of Screw Dislocations." Journal of Applied Physics, Vol. 32, No. 10, 1961. pp. 1873-1875.

35. Li, James C. M. Discussion to A. S. Keh's paper in Direct Observations of Lattice Defects in Crystals, ed. by J. B. Newkirk and J. H. Wernick, Interscience Publishers, New York, 1962. p. 213.

36. Rolfe, S. T., R. P. Haak and E. J. Imhof, Jr. "Low Cycle Fatigue of Experimental HY-130/150 and HY-180/210 Steels and Weldments." U. S. Steel Project Report No. 40.018-001 (32)(37), Navy Contract No. Nobs-88540, 1964.

37. Bain, E. C. "The Nature of Martensite." Mining and Metallurgy, American Institute of Mining, Metallurgy and Petroleum Engineers, Vol. 5, 1924. pp. 394-395.

38. Wechsler, M. S., D. S. Lieberman and T. A. Read. "Cubic to Orthorhombic Diffusionless Phase Change -- Experimental and Theoretical Studies of AuCd." Journal of Applied Physics, Vol. 26, 1955. p. 473.

39. Wayman, C. M. and R. L. Patterson. "Internal Twinning in Ferrous Martensites." Acta Metallurgica, Vol. 11, No. 11, 1964. pp. 1306-1311.

40. Dash, J. and H. M. Otte. "The Martensite Transformation in Stainless Steel." Acta Metallurgica, Vol. 11, No. 10, 1963. pp. 1169-1178.

41. Owen, E. A. and Y. H. Liu. "Further X-ray Studies of Equilibrium of the Iron-Nickel System." Journal of the Iron and Steel Institute, Vol. 163, 1949. pp. 132-137.

42. Jones, F. W. and W. K. Pumphrey. "Free Energy and Metastable States in the Iron-Nickel and Iron-Manganese Systems." Journal of Iron and Steel Institute, Vol. 163, 1949. pp. 121-131.

43. Gilbert, A. and W. S. Owen. "Diffusionless Phase Transformation in Iron-Nickel, Iron-Chromium, and Iron-Silicon Alloys." Acta Metallurgica, Vol. 10, No. 1, 1952. pp. 45-54.

44. Borgers, A. J. and W. G. Burgers. "Partial Dislocations on the {110} Planes in the B.C.C. Lattice and the Transition of the F.C.C. into the B.C.C. Lattice." Acta Metallurgica, Vol. 12, No. 2, 1964. pp. 255-261.

45. Krauss, G. "Fine Structure of Austenite Produced by the Reverse Martensite Transformation." Acta Metallurgica, Vol. 11, No. 6, 1963. pp. 499-509.

46. Decker, P. F., J. T. Eash and A. J. Goldman. "18% Nickel Maraging Steel." Transactions, American Society for Metals, Vol. 55, 1962. pp. 58-76.

47. Reisdorf, B. G., A. J. Birkle and P. Salmon Cox. "The Kinetics and Mechanisms of the Strengthening of Maraging Steels." U. S. Steel Project No. 89.025-02(1-11), Air Force Contract No. AF33(657-11149), Quarterly Reports, 1965.

48. Yao, J. T. P. "The Effect of Plastic Strains on the Low Cycle Fatigue Behavior of Steel." Ph. D. Thesis Submitted to the Graduate College, University of Illinois, Urbana, Illinois, 1961.

49. Dieter, G. E. Mechanical Metallurgy. McGraw-Hill Book Company, Inc., New York, 1961. p. 122.

50. Bridgman, P. W. Studies in Large Plastic Flow and Fracture. McGraw-Hill Book Company, Inc., New York, 1952. Chap. 1.

51. Szirma, A. and R. M. Fisher. "Electron Microscope Observations of Dislocations in Thin Metal Foils." Symposium on Electron Metallography, Special Technical Publication No. 262, American Society for Testing and Materials, 1960. pp. 103-106.

52. Bollmann, W. "Interference Effects in the Electron Microscopy of Thin Crystal Foils." Physics Review, Vol. 103, 1956. p. 1588.

53. Smith, C. S. and L. Guttman. "Measurement of Internal Boundaries in Three Dimensional Structures by Random Sectioning." Transactions, American Institute of Mining, Metallurgy and Petroleum Engineers, Vol. 197, 1953. pp. 81-87. (Table II, Item 4).

54. Sleeswyk, A. W. "The Tilt Angle." Acta Metallurgica, Vol. 11, No. 10, 1963. p. 1192.

55. Bartee, E. M. Statistical Methods in Engineering Experiments. Charles E. Merrill Books, Inc., Columbus, Ohio, 1966. pp. 56-59, 118-119.

56. Cullity, B. D. Elements of X-ray Diffraction. Addison-Wesley Publishing Company, Inc., Reading, Massachusetts, 1956. pp. 490-499.

57. Taylor, G. I. "The Mechanism of Plastic Deformation of Crystals -- Part I." Proceedings, Royal Society (London), Vol. A145, 1934. pp. 362-387.

58. Seeger, A. Dislocations and Mechanical Properties of Crystals, ed. by J. C. Fisher, John Wiley and Sons, Inc., New York, 1957. pp. 271-277.

59. Mott, N. F. "The Work Hardening of Metals." Transactions, Metallurgical Society of the American Institute of Metallurgical, Mining and Petroleum Engineers, Vol. 218, 1960. pp. 962-968.

60. Hirsch, P. B. "Extended Jogs in Dislocations in Face Centered Cubic Metals." Philosophical Magazine, Vol. 7, 1962. pp. 67-93.

61. Buffington, F. S., K. Hirano and M. Cohen. "Self-Diffusion in Iron." Acta Metallurgica, Vol. 9, 1961. p. 434.

62. Gilman, J. J. and W. G. Johnson. "Behavior of Individual Dislocations in Strain-Hardened LiF Crystals." Journal of Applied Physics, Vol. 31, No. 4, 1960. pp. 687-692.

63. Gilman, J. J. and R. E. Keith. "Progress Report on Dislocation Behavior in Lithium Fluoride Crystals During Cyclic Loading." Basic Mechanisms of Fatigue, Special Technical Publication No. 237, American Society for Testing Materials, 1959. pp. 3-20.

APPENDIX A

Analysis of Cyclic Softening and Cyclic Hardening of (OFHC) Copper

Tuler and Morrow[20] measured the cyclic hardening of annealed copper of the oxygen free high conductivity type (OFHC) and the cyclic softening of cold-worked copper (OFHC) and some of their results are listed in Table 7. Their results were analyzed in the same way that the 12% nickel maraging steel was analyzed for cyclic softening and cyclic hardening and are plotted in Figs. 31 and 32. The cyclic softening of the cold-worked copper could be described by Equation #7 regardless of the nominal plastic strain range used as shown in Fig. 31. The value of N_o was also a function of $(\Delta\epsilon_p)^{-1}$.

The cyclic hardening relationship was not described by Equation #7 as it was for the 12% nickel maraging steel which was determined in this investigation, but the extensive hardening of the annealed samples caused a decrease in the plastic strain range for each successive cycle of fatigue applied at a constant total strain range. If it is assumed that most of the extra stress range of the annealed copper is due to hardening by point defects, the extra stress should be related to the total amount of strain, as described previously. The increase in stress range of the copper was less for successive cycles of fatigue. This decrease in the amount of cyclic hardening with successive cycles of fatigue was probably due to the decrease in the plastic strain range because of extra stress range due to previous cyclic hardening. The cumulative amount of

extra stress due to cyclic hardening can be written as the sum of all the products of plastic strain for each cycle:

$$\sigma_H = C \sum_{i=1}^{N} (\Delta\epsilon_{po} - \Delta\epsilon_{pi}) \qquad \text{(Equation \#21)}$$

in which $\Delta\epsilon_{pi}$ is the amount of plastic strain converted to elastic strain because of the previous cyclic hardening in which $\sigma_{Hi/E} = \Delta\epsilon_{pi}$. This summation agreed with the extra stress observed for the annealed copper. The value of σ_H would be equal to a product of $C\Delta\epsilon_{po}N$ if $\Delta\epsilon_{po}$ would have remained constant during fatigue which was approximately true in the case of 12% nickel maraging steel in which σ_s and σ_H were of the same order of magnitude at corresponding cycles of fatigue. The value of $\Delta\epsilon_{po}$ was greatly decreased by cyclic hardening in the annealed copper samples because the value of σ_s for the annealed copper was very small compared to the value of σ_H at the same number of cycles of fatigue. The value of σ_s was small because the value of, σ_o, the stress range of the first cycle was small for the annealed copper when compared to the relatively large value of σ_o for the 12% nickel maraging steel.

APPENDIX B

TABLE 1

Composition of the 12% Nickel Maraging Steel Used in This Investigation*

Chemical Composition of 12Ni-5Cr-3Mo Steel from Heat No. 50169--Percent
(Check Analysis)

C	Mn	P	S	Si	Ni	Cr	Mo	Ti	Al^{+}	N^{++}	O
0.002	0.018	0.004	0.005	0.048	12.20	5.07	3.12	0.21	0.25	0.008	0.0004

$^{+}$Acid soluble
$^{++}$Kjeldahl determination

*Analysis by United States Steel Corporation

TABLE 2

The Effect of Aging Time at 900°F on the Mechanical Properties of Production Solution-Annealed 1-Inch-Thick Plate of Vacuum-Induction-Melted 12Ni-5Cr-3Mo Steel Used in This Investigation

Aging Time of 900°F,* hrs	Yield Strength (0.2% Offset), ksi	Tensile Strength, ksi	Elongation in 1 Inch, %	Reduction of Area, %	Hardness, R_C	Charpy V-Notch, ft-lb 0°F
			Longitudinal Properties			
3	165	174	16.5	69.4	41.0	85
5	166	175	16.0	68.5	41.0	80
16	180	187	16.0	67.1	43.0	68
30	179	189	16.0	65.3	42.5	61
			Transverse Properties			
3	167	174	16.0	68.2	40.5	78
5	167	176	16.0	66.9	41.0	75
16	178	185	15.0	65.7	43.0	53
30	181	190	15.0	64.1	43.5	49

*Plate samples production solution-annealed at 1500°F for 1 hour, water-quenched, laboratory aged at 900°F for the indicated times, and water quenched by United States Steel Corporation.

TABLE 3

The Densities of Dislocations and the Subgrain Sizes in 12% Nickel Maraging Steel

Condition of Sample	Dislocations within Subgrain, No./cm^2 *		Subgrain Size, Microns
	Undecorated	Decorated **	Undecorated
Solution Treated Water Quenched	4×10^{10}	3×10^{10} + (precipitates)	Platelet Width 0.7 ± 0.2
Tensile Test $50\% < \epsilon_t < 70\%$	2×10^{10}		0.21 ± 0.04
Fatigue, $\Delta\epsilon_t =$ 18% to 50% N_f	1×10^{10}	1×10^{10}	0.31 ± 0.09
Fatigue, $\Delta\epsilon_t =$ 7% to 80% N_f	low to 6×10^9	low to 8×10^9	Decorated 0.39 ± 0.07
Fatigue, $\Delta\epsilon_t =$ 2.6% to 100% N_f		5×10^9	Decorated 0.43 ± 0.09
Fatigue, $\Delta\epsilon_t =$ 1.06% to 100% N_f	low to 1×10^{10}	1×10^{10}	Decorated 0.46 ± 0.10

TABLE 3 (Continued)

Condition of Sample	Dislocations in Subgrain Boundaries, No./cm		
	Undecorated	Decorated	Undecorated°
Tensile Test to $50\% < \epsilon_t < 70\%$	$\sim 10^{11}$ tangles ▽ $(1.2 \pm 0.5) \times 10^6$		$(1.7 \pm 0.3) \times 10^6$
Fatigue, $\Delta\epsilon_t$ =18% to 50% N_f	$\sim 10^{11}$ tangles $(1.5 \pm 0.3) \times 10^6$	$(1.5 \pm 0.3) \times 10^6$	$(1.4 \pm 0.4) \times 10^6$
Fatigue, $\Delta\epsilon_t$ =7% to 80% N_f	no tangles $(1.1 \pm 0.2) \times 10^6$		Decorated $(1.4 \pm 0.3) \times 10^6$
Fatigue, $\Delta\epsilon_t$ =2.6% to 100% N_f	no tangles	$(4.5 \pm 0.5) \times 10^5$	
Fatigue, $\Delta\epsilon_t$ =1.06% to 100% N_f	no tangles $(4.6 \pm 0.6) \times 10^5$	$(4.9 \pm 0.7) \times 10^5$	

*A constant foil thickness,t, of 2000Å was assumed for the measurement of area density of dislocations.

** Decoration consisted of a heat treatment at 880°F for a number of hours.

+ Optimum age hardened at 900°F for 16 hours.

▽ An area density of dislocation tangles is given in No./cm^2.

o Determined from electron diffraction patterns.

TABLE 4

Exponents of Strain Hardening after Bridgman Correction for Necking

True Strain Range	Solution Treated n(static)*	n' (dynamic)*	K, ksi
	yielding		
0.5% to 39%	0.005		142
39% to 99%	0.100		154
Dynamic, Extrapolated to N_f Stress		0.10	154
	Aged		
	n(static)	n' (dynamic)	K, ksi
0.8% to 68%	0.029		235
Dynamic, Actual N_f Stress Used		0.068	240

*The formula, $\sigma_t = K(\epsilon_t)^n$, was used to approximate the true stress-strain curve. K is the stress at $\epsilon_t = 1$ and n equals the exponent of strain hardening.

TABLE 5

The Hardness of 12% Nickel Maraging Steel
after Different Thermal and Mechanical Treatments

Condition of Sample	Diamond Pyramid Hardness (DPH)*			
	Number of hours at 900°F			
	0	5	15	30
Solution treated, water quenched, not tested in fatigue	265**	400	430	430

Condition of Sample		Number of hours at 880°F					
		0	1	3½	4¼	12	17
Solution treated, water quenched, tested in fatigue: % strain range, $\%N_f$							
18.0%,	50%	316		239			273
7.0%,	80%	258		283			269
2.6%	100%	233			330	380	
1.0%	100%	240	333				

Aged sample softened at $2.6\%\Delta\epsilon_t 80\%N_f$	Before fatigue, 16 hours at 900°F	After fatigue, no heat treatment	Aged at 880°F 7 hours
	430	380 ± 14	430 ± 15

*A one (1) kilogram load was used for all DPH indentations except the three solution treated samples which were tested in fatigue at a strain range of 18%, 2.6%, and 1% in which indentations were made with a 100gm. load. All hardness values given above are normalized and are comparable.

**At least three measurements were made for each average value and the maximum standard deviation which was observed for any set of measurements was within ± 10 DPH except when noted next to the value.

TABLE 6

A Comparison of the Stress due to Cyclic Softening and Cyclic Hardening and the Dislocation Density in the Matrix and in the Cell Wall

% Strain Range, $\%N_f$*	Dislocations** Removed from Subgrain, $\sqrt{\rho_o - \rho_i}$	Value of σ_s, ksi	Dislocation Density in Cell Wall $\sqrt{\rho_w}$	Value of σ_H, ksi
60% Tensile Test	1.4×10^5/cm	--	3×10^5/cm ▽ 1.3×10^6/cm	30
18%, 60% N_f	1.7×10^5	38	3×10^5 ▽ 1.5×10^6	32
7%, 80% N_f	1.8×10^5	35	1.1×10^6	48
2.6%, 100% N_f	1.9×10^5	26	0.45×10^6	41
1.06%, 100% N_f	1.7×10^5	91	0.5×10^6	35

*The value of the total strain range maintained during the fatigue test and the percent of the fatigue life when the sample was cross-sectioned is given.

** ρ_o was $4 \times 10^{10}/cm^2$ for the untested sample.

▽ Tangles.

TABLE 7

The Stress Range and Strain Range from the Cyclic Data of (OFHC) Copper by Tuler and Morrow

FULLY ANNEALED SAMPLES*

Apparent $\Delta\epsilon_t$ [a]	Calculated $\Delta\epsilon_{po}$	Stress Range, ksi, at the Cycles Indicated							
		1	2	5	10	20	50	100	200
0.0206	0.0198	13.5 [b]	25.5	35.5	42.0	46.0	48.0	46.0	
(ESR) [c]		0	12.0	22.0	26.5	32.5	34.5	37.5	
0.0125	0.0119	10.0	18.5	25.5	31.5	36.0	40.0	40.5	41.0
(ESR)		0	8.5	15.5	21.5	26.0	30.0	30.5	31.0
0.0086	0.0079	9.0	14.5	20.0	24.5	29.0	33.5	35.0	35.5
(ESR)		0	5.5	11.0	15.5	20.0	24.5	26.0	26.5
0.0061	0.0057	7.0	11.5	15.5	19.0	22.5	26.5	29.0	30.0
(ESR)		0	4.5	8.5	12.0	15.5	19.5	22.0	23.0
0.0022	0.0019	5.5	7.0	8.5	10.0	11.0	13.0	14.0	16.0
(ESR)		0	1.5	3.0	4.5	5.5	7.5	8.5	10.5

TABLE 7 (Continued)

COLD WORKED SAMPLES *

Apparent $\Delta\epsilon_t$	Stable Values, $\Delta\epsilon$	Stress Range, ksi, at the Cycles Indicated							
		1	2	5	10	20	50	100	200
0.0207	0.0133	105.0	99.00	94.50	90.00	85.50			
(NSR) [d]		1.0	0.94	0.90	0.86	0.81			
0.0116	0.0053	94.5	91.50	88.00	84.00	81.00	75.00	72.00	68.50
(NSR)		1.0	0.97	0.93	0.89	0.86	0.79	0.76	0.72
0.0056	0.0001	61.0	63.50	63.50	63.50	63.50	63.00	62.50	61.50
(NSR)			1.00	1.00	1.00	1.00	0.99	0.985	0.97
0.0080	0.0018	78.0	81.00	80.00	79.00	77.00	74.00	71.00	68.00
(NSR)		1.0	1.04	1.02	1.01	0.99	0.95	0.91	0.87

		500	1000	2000	5000 (Cycles)
0.0056	cont.0.001	59.0	54.40	53.00	50.00
(NSR)		0.93	0.86	0.834	0.787

*Taken from the data of Tuler and Morrow[20] and discussed in Appendix A of this paper.
[a]Determined at the half-life of the sample.
[b]The stress for 0 to ½ cycle and ½ to 1 cycle were added together for this first cycle.
[c](ESR) is the extra stress range beyond the first cycle.
[d](NSR) is the normalized stress range based on the first cycle.

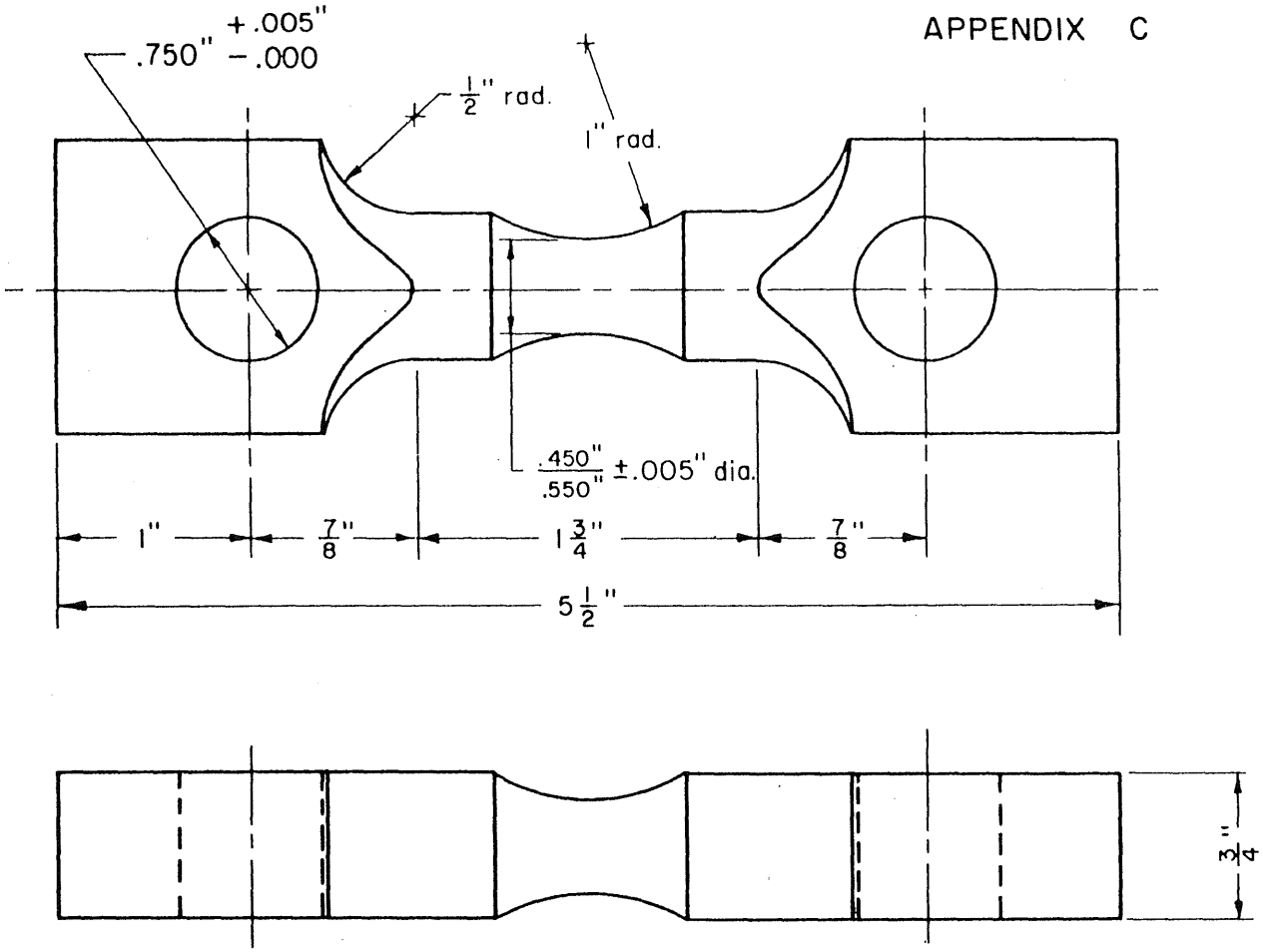

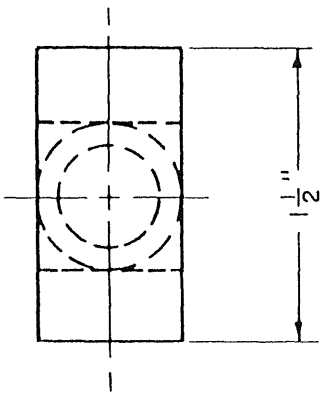

FIG. 1 DETAILS OF TEST SAMPLE

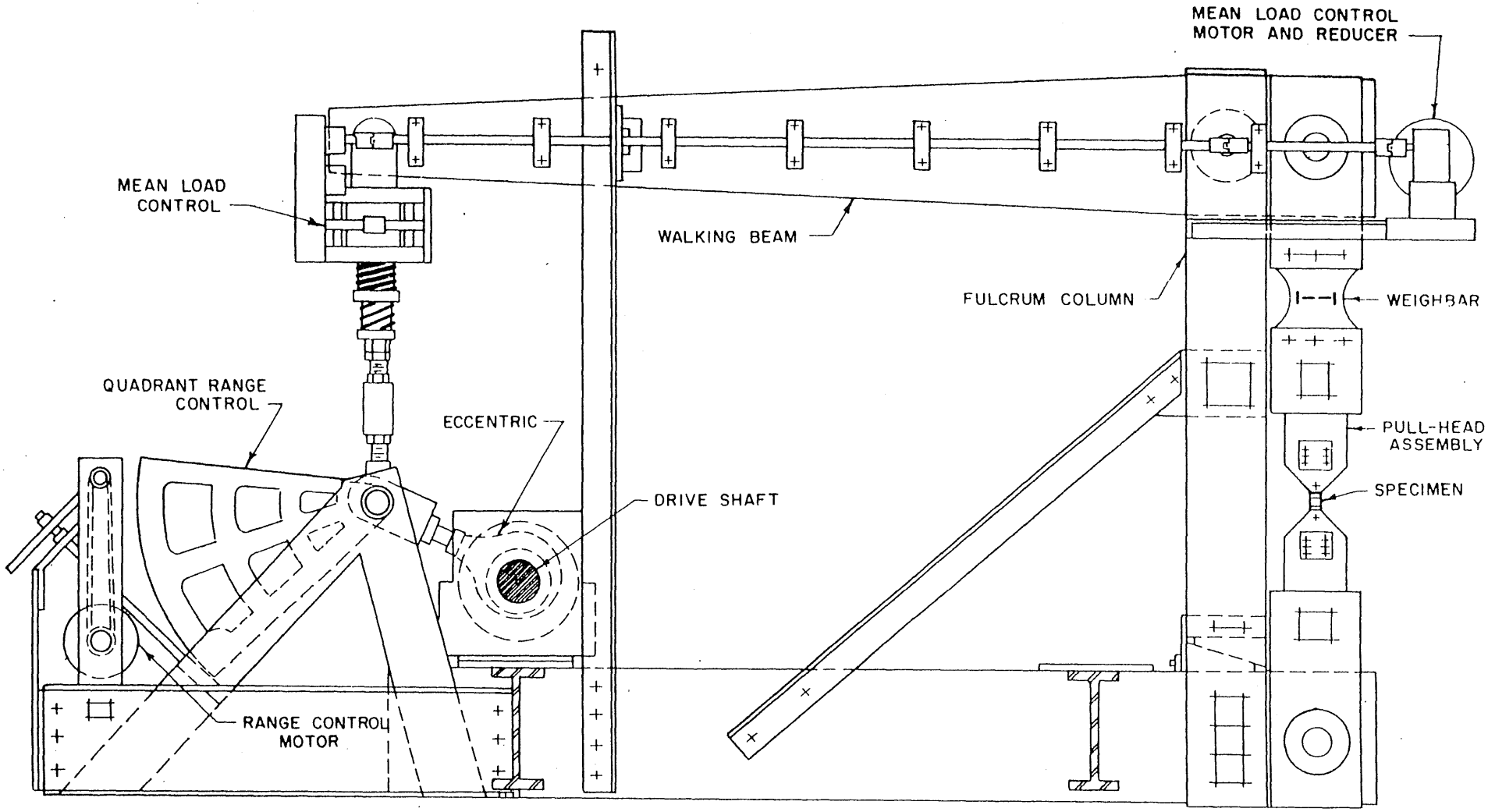

FIG. 2 50,000 LB. FATIGUE TESTING MACHINE

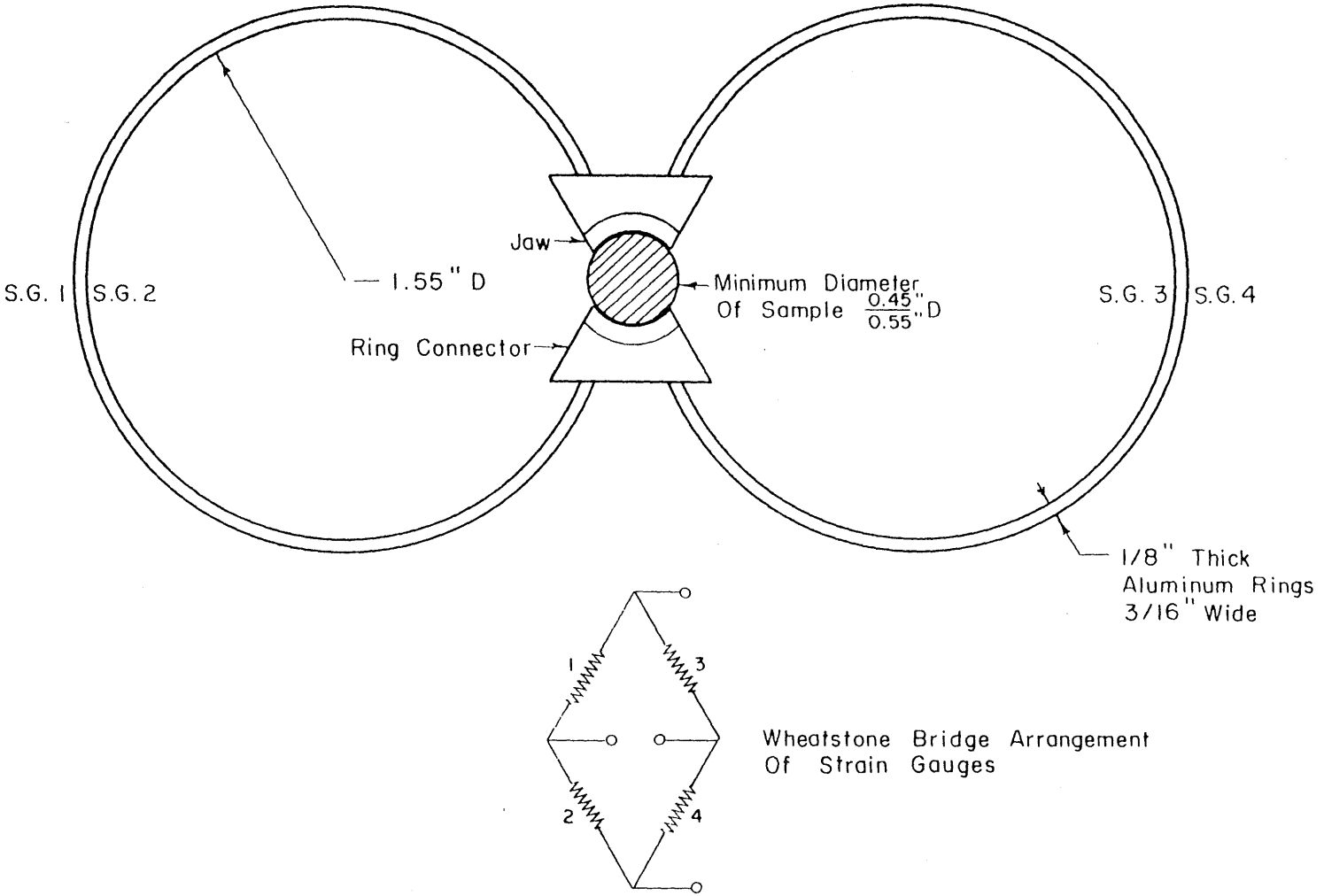

FIG. 3 SKETCH OF DIAMETER GAUGE USED TO CONTROL TRUE STRAIN.

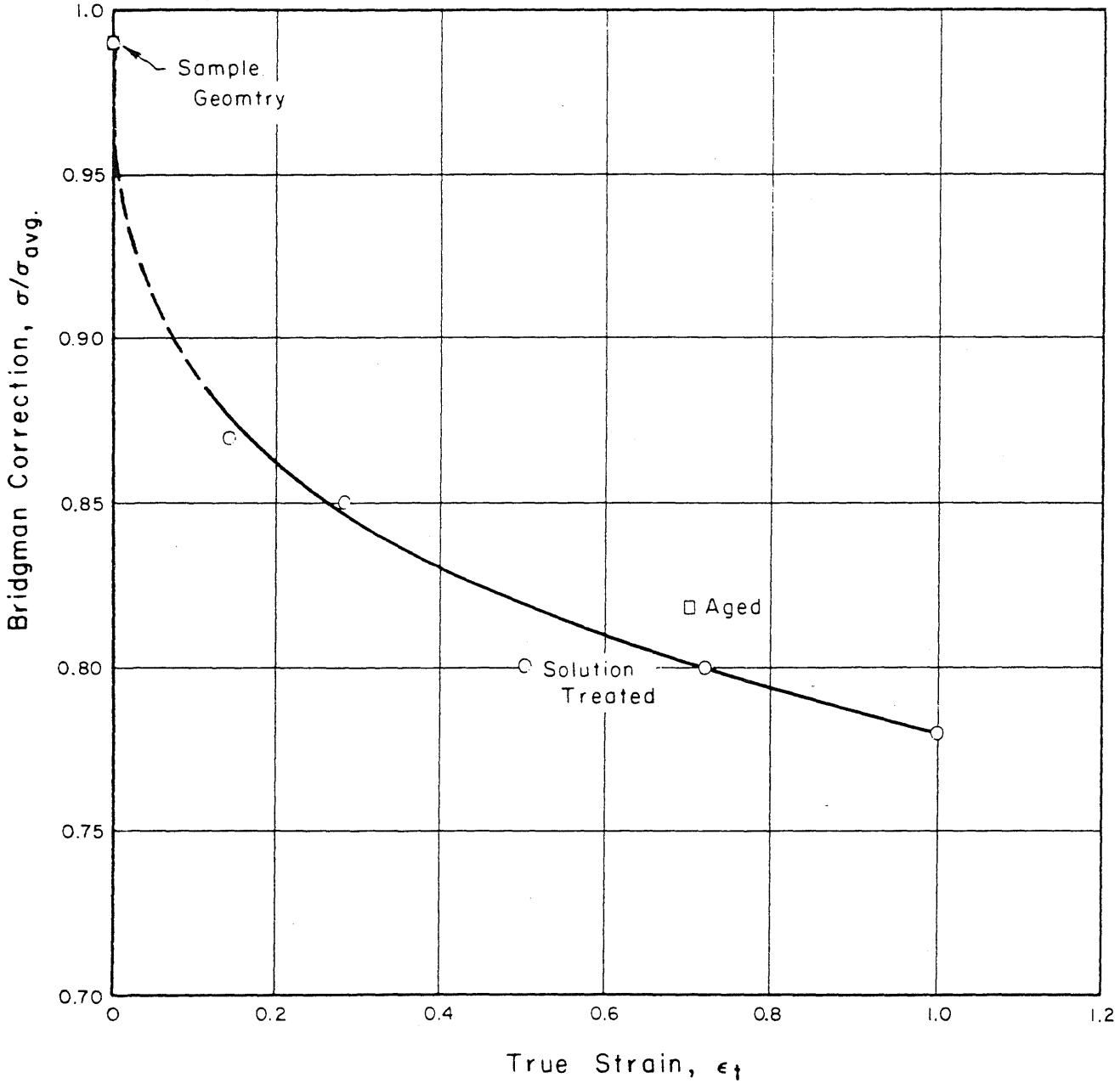

FIG. 4 BRIDGMAN CORRECTION FOR THE 12 % NICKEL MARAGING STEEL

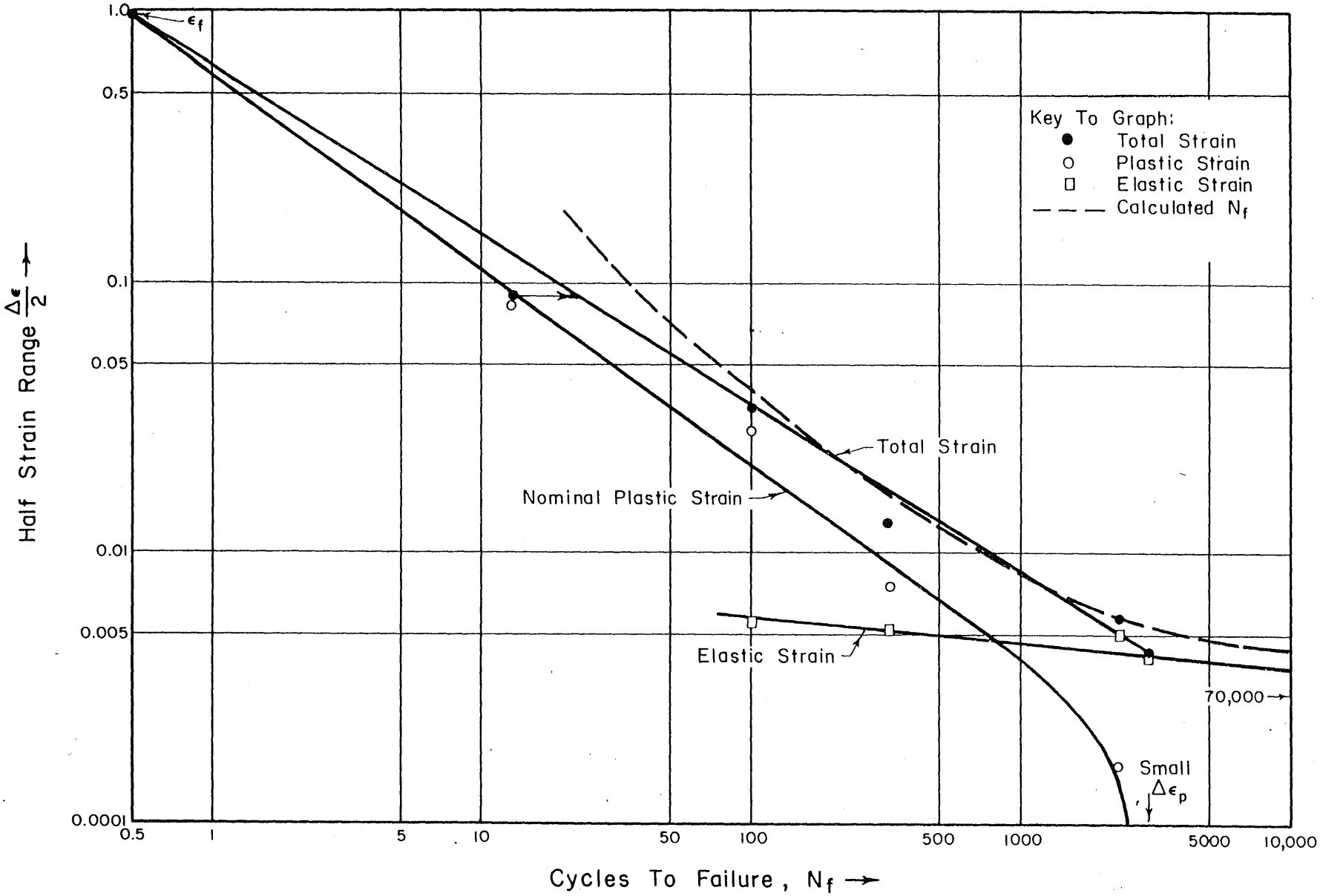

FIG. 5 AXIAL FATIGUE DIAGRAM OF THE SOLUTION TREATED 12% NICKEL MARAGING STEEL .

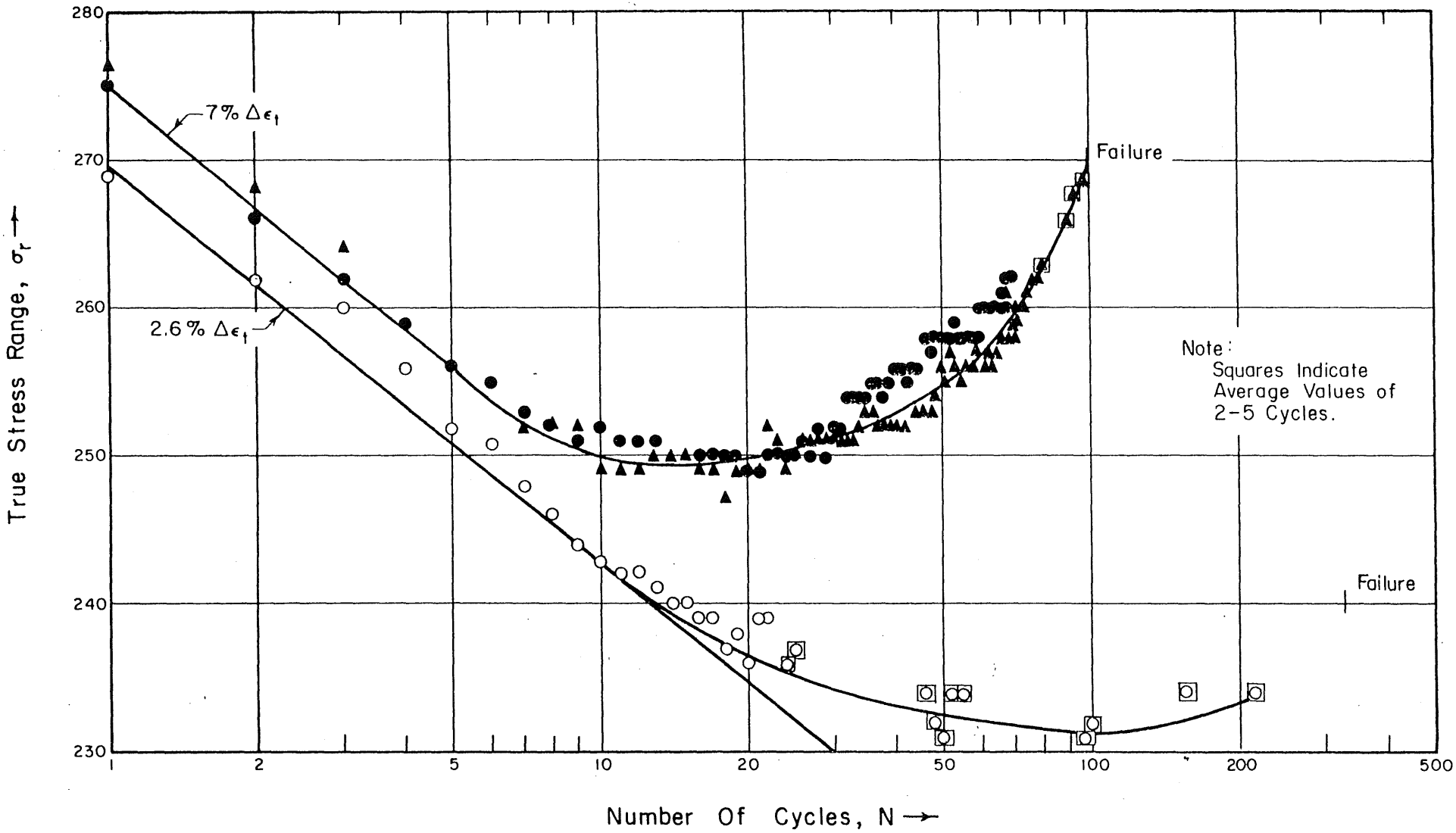

FIG. 6 THE STRESS RANGE FOR EACH CYCLE OF FATIGUE OF SOLUTION TREATED SAMPLES.

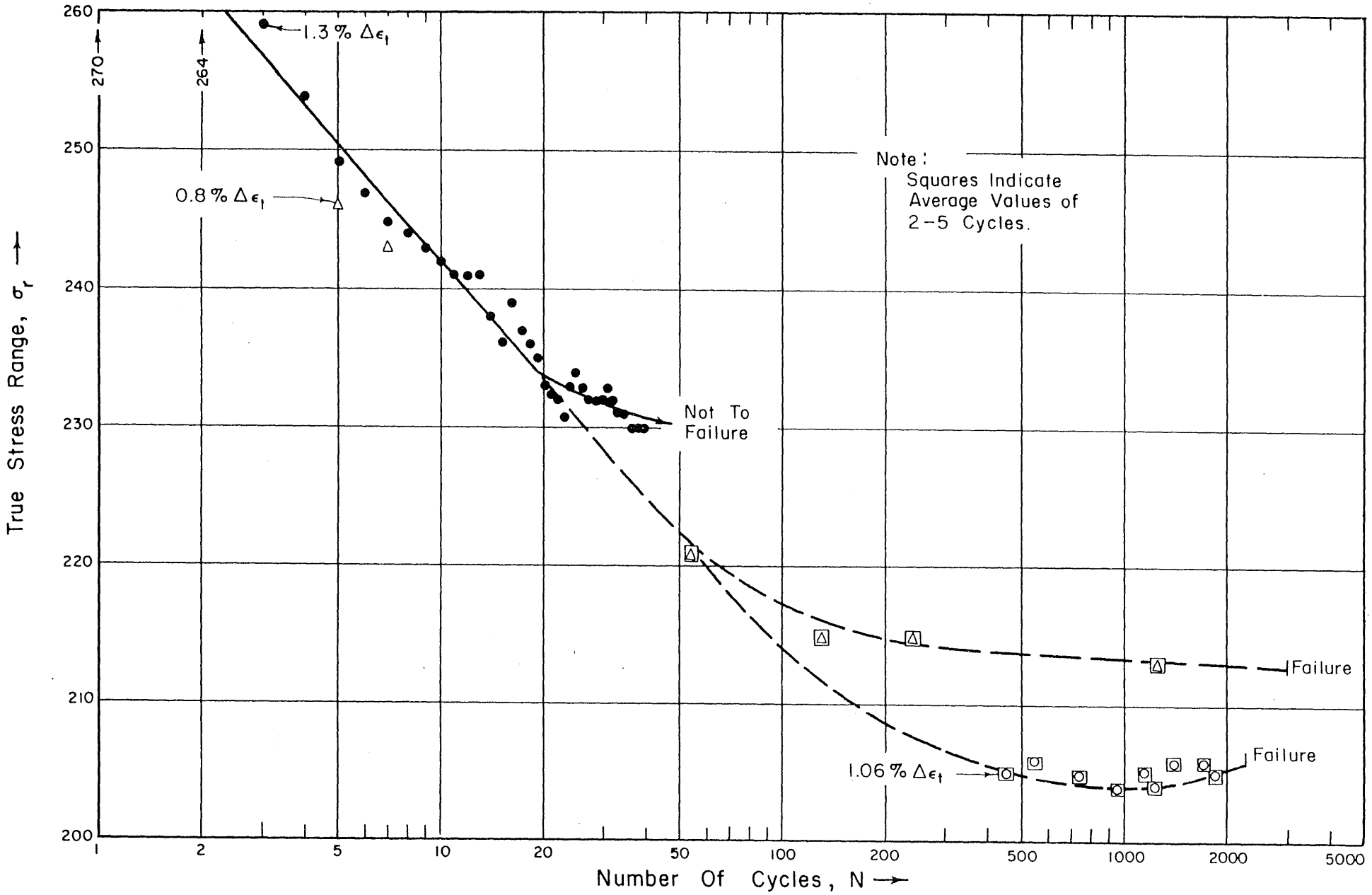

FIG. 7 THE STRESS RANGE FOR EACH CYCLE OF FATIGUE AT SMALL STRAIN RANGES.

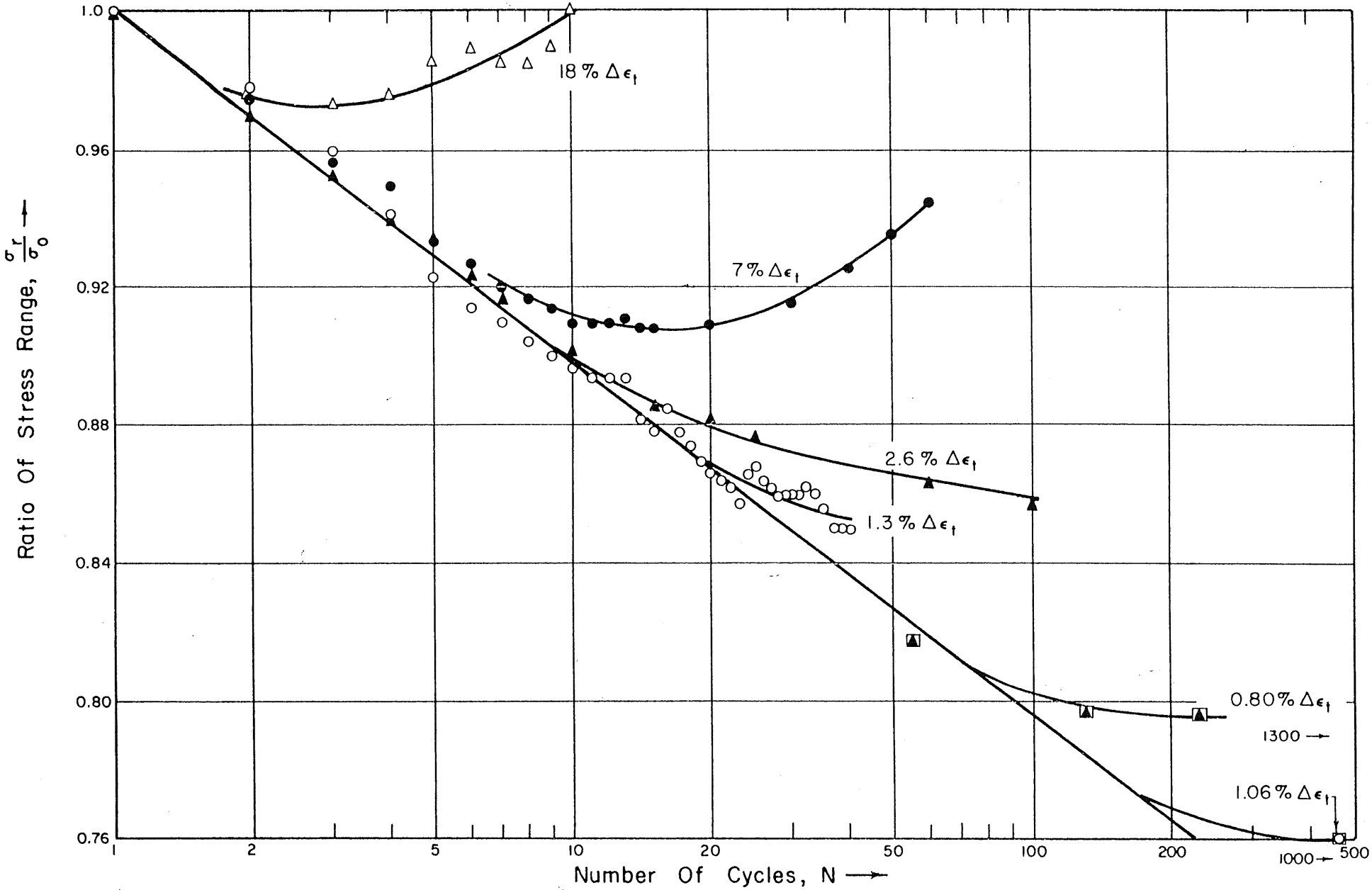

FIG. 8 THE RATIO OF THE STRESS RANGE FOR EACH CYCLE OF FATIGUE OF SOLUTION TREATED SAMPLES.

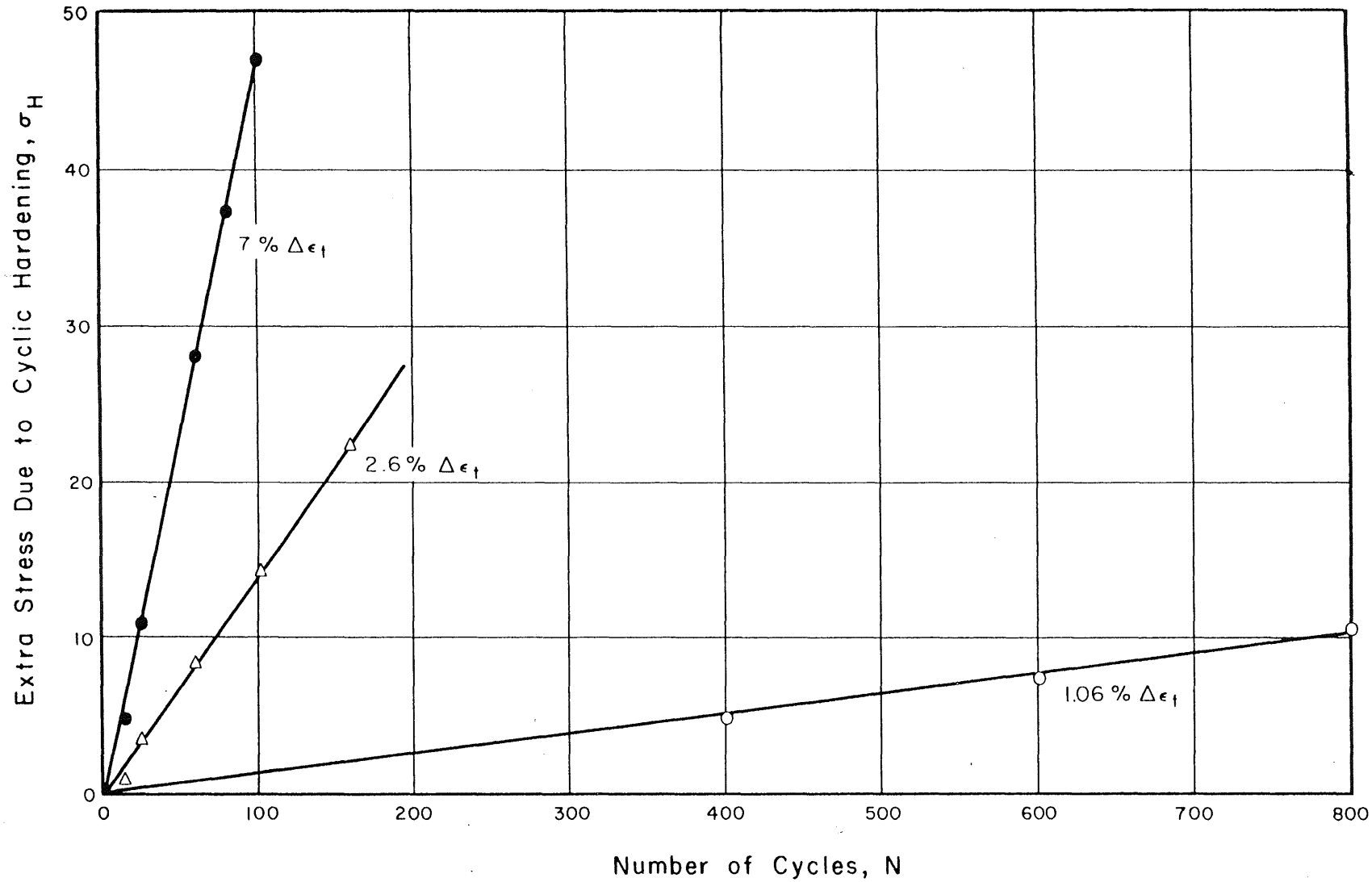

FIG. 9 THE EXTRA STRESS DUE TO CYCLIC HARDENING IN SOLUTION TREATED SAMPLES TESTED IN FATIGUE

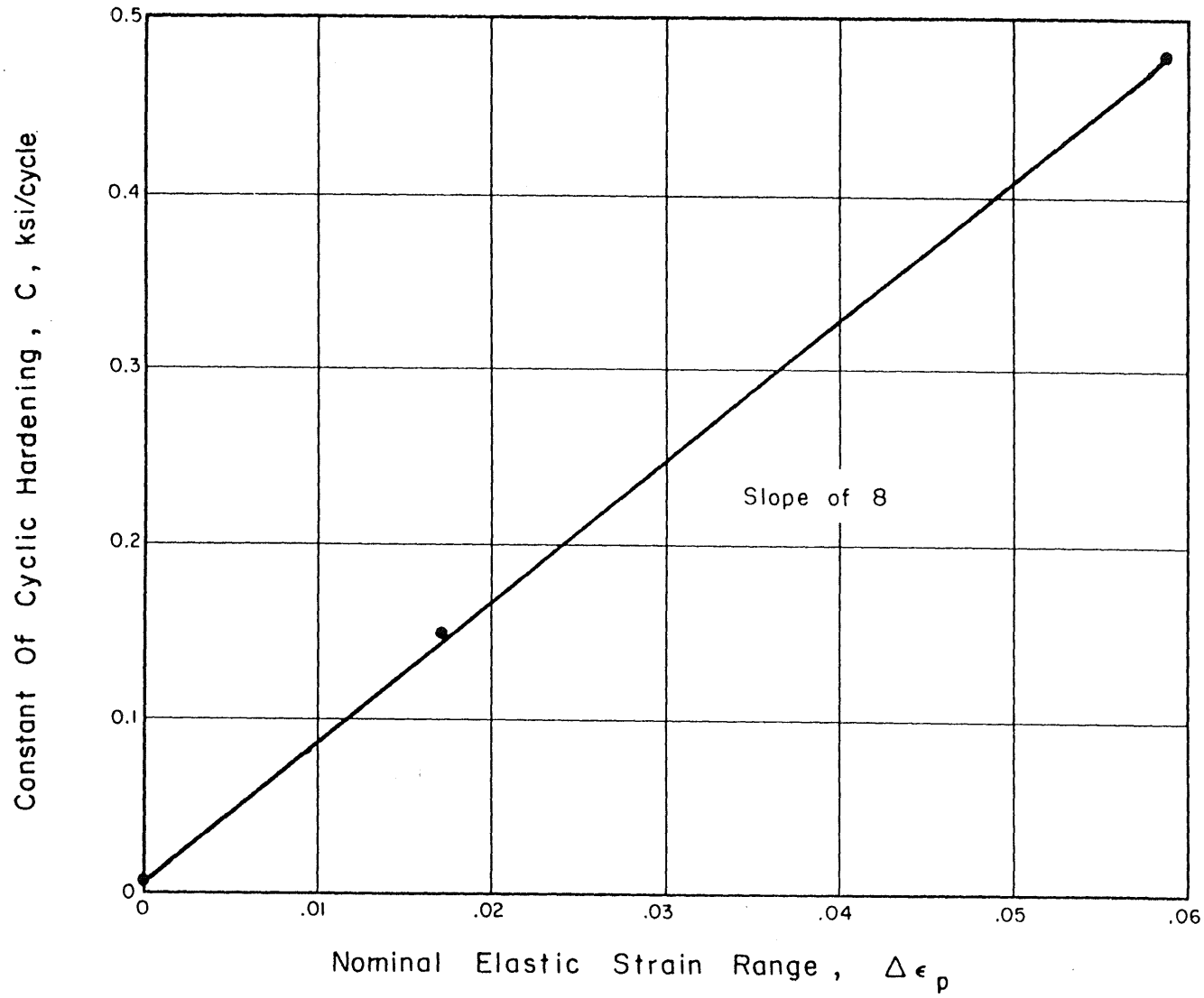

FIG. 10 THE CONSTANT OF CYCLIC HARDENING, C, VERSUS THE NOMINAL PLASTIC STRAIN.

FIG. II TRANSMISSION ELECTRON MICROGRAPH OF THE SOLUTION TREATED 12% NICKEL MARAGING STEEL

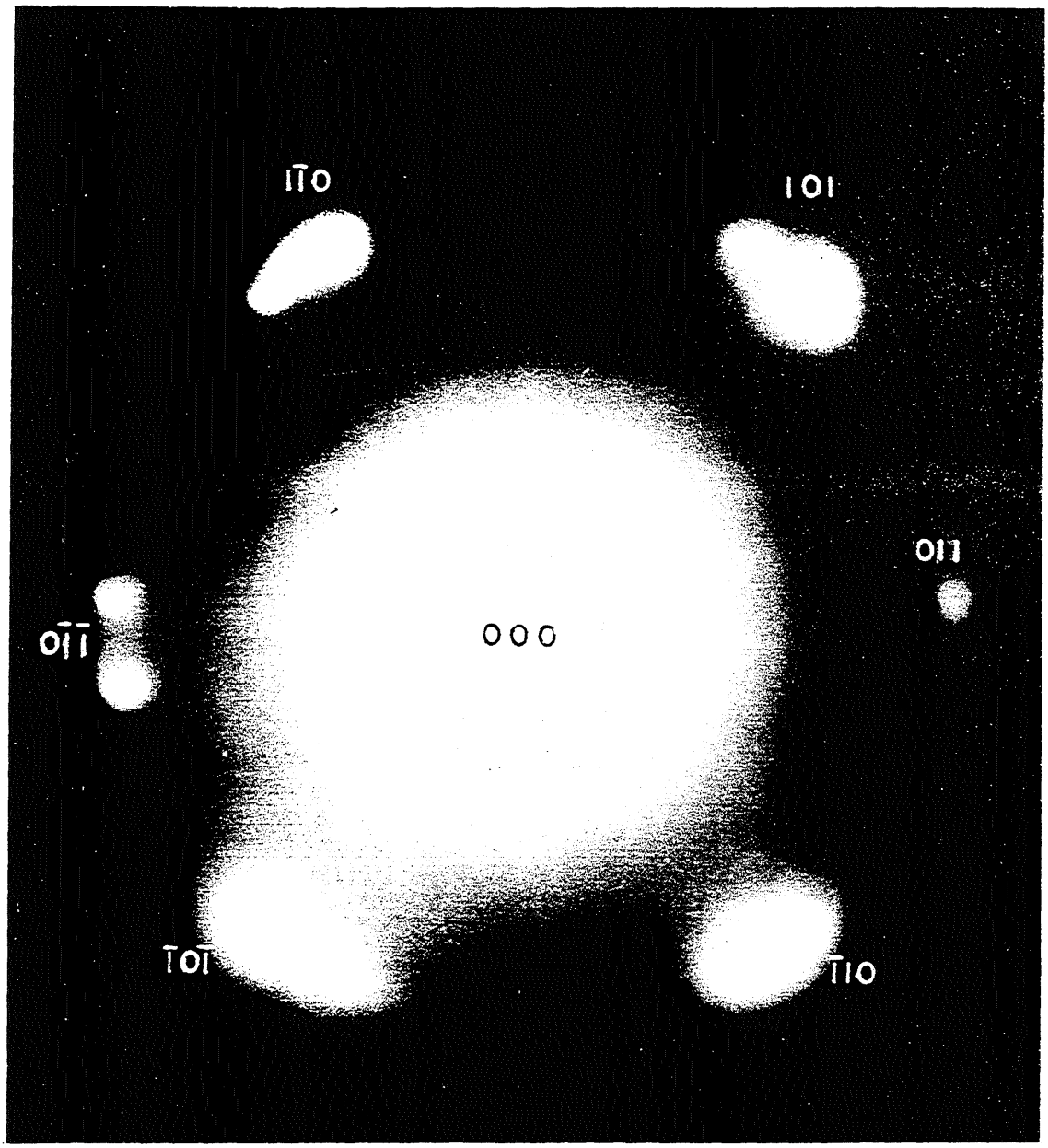

FIG. 12 TRANSMISSION ELECTRON DIFFRACTION PATTERN OF TWO MARTENSITE PLATELETS SHOWING THE TWIN ORIENTATION

FIG. 13 TRANSMISSION ELECTRON MICROGRAPH OF A SOLUTION TREATED SAMPLE AFTER A LARGE PLASTIC DEFORMATION

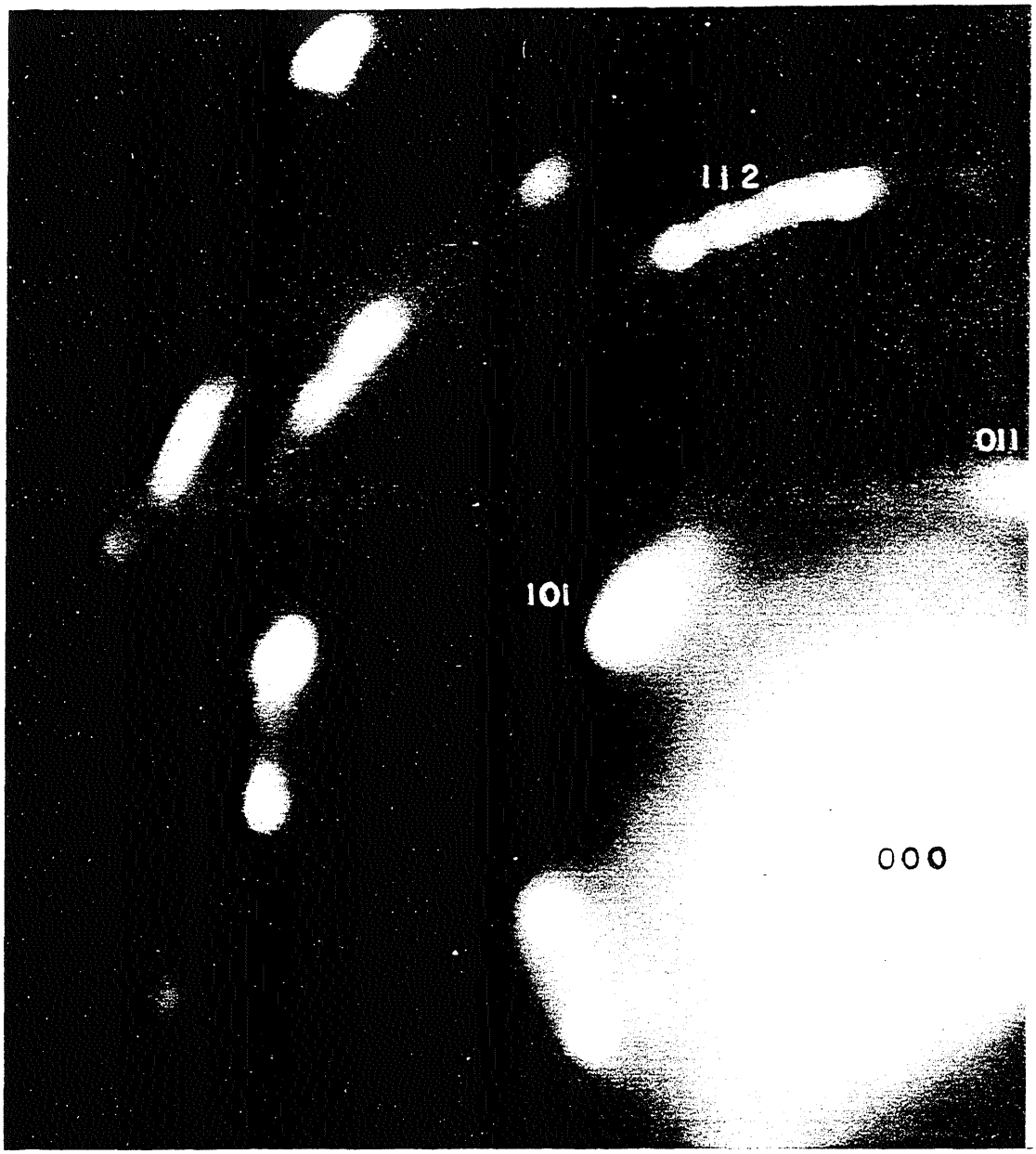

FIG. 14 TRANSMISSION ELECTRON DIFFRACTION PATTERN OF DEFORMED SAMPLE SHOWING THE ROTATION OF THE SUBGRAINS ABOUT [111]

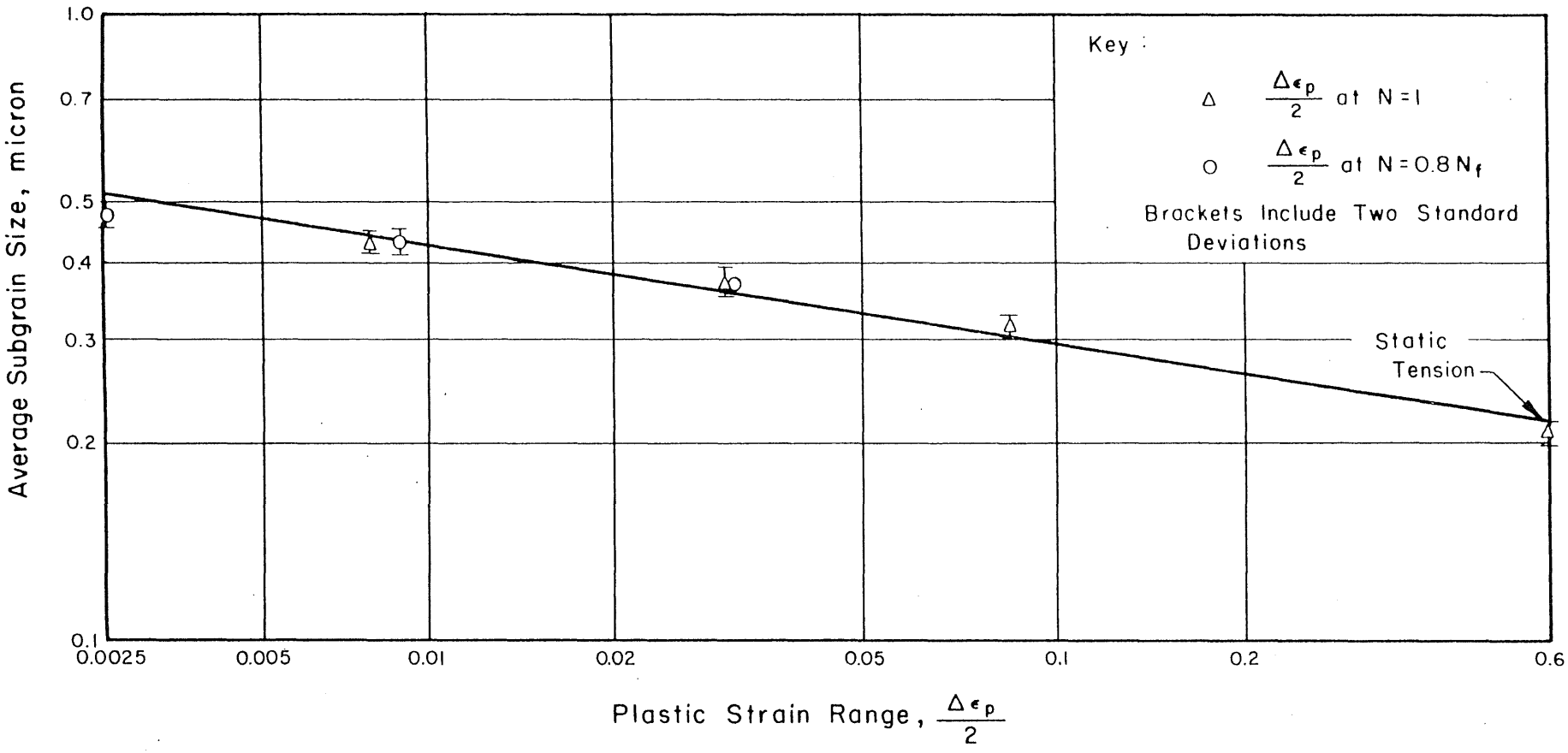

FIG. 15 SUBGRAIN SIZE OF TREATED SAMPLE VERSUS PLASTIC STRAIN

FIG. 16 TRANSMISSION ELECTRON MICROGRAPH OF A SOLUTION TREATED SAMPLE TESTED IN FATIGUE (1.06 % $\Delta\epsilon_t$)

FIG. 17 TRANSMISSION ELECTRON MICROGRAPH OF A SOLUTION TREATED SAMPLE TESTED IN FATIGUE (2.6 % $\Delta\epsilon_t$) AND DECORATED

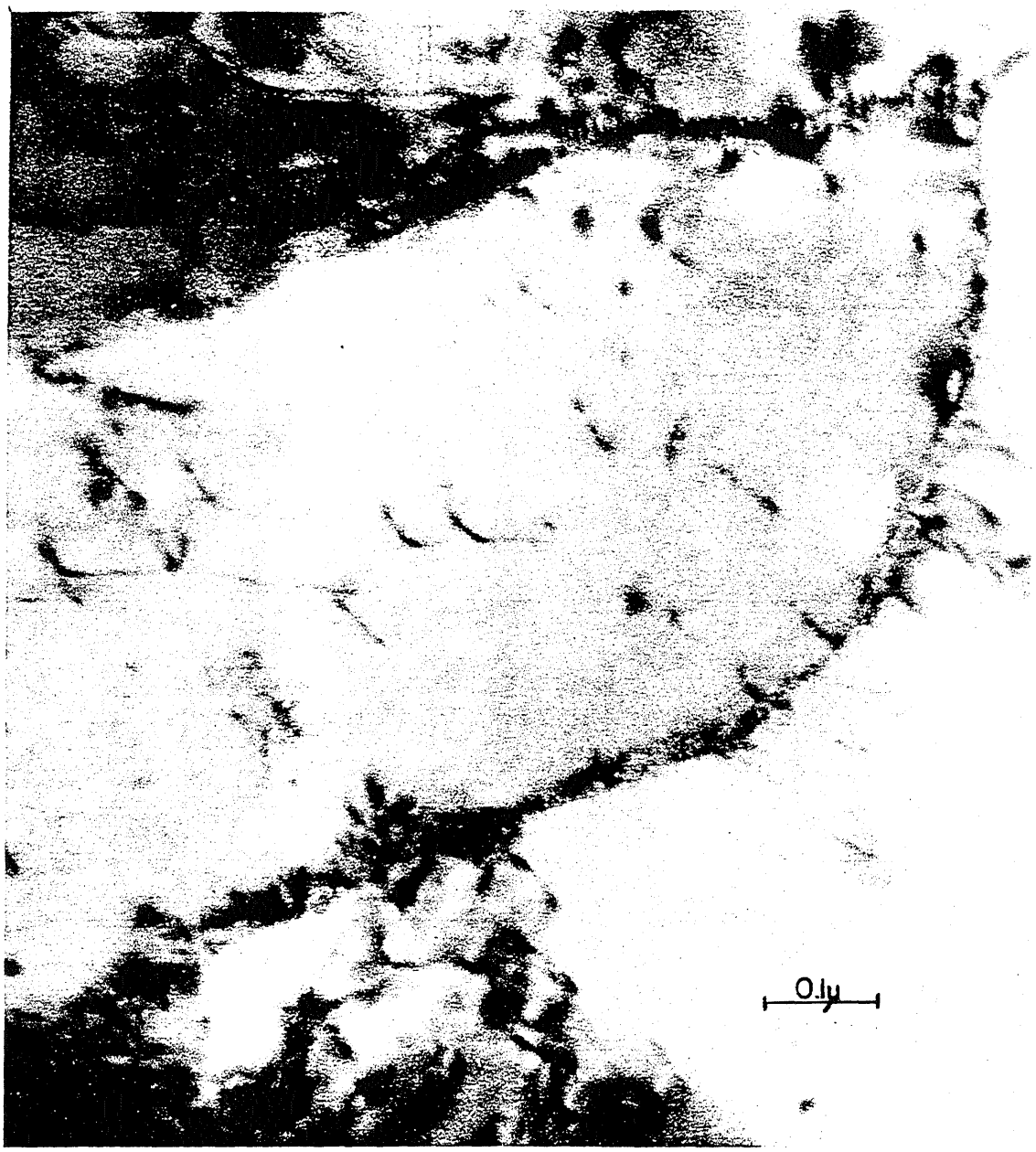

FIG. 18 TRANSMISSION ELECTRON MICROGRAPH OF A SOLUTION TREATED SAMPLE TESTED IN FATIGUE ($7\% \Delta\epsilon_t$)

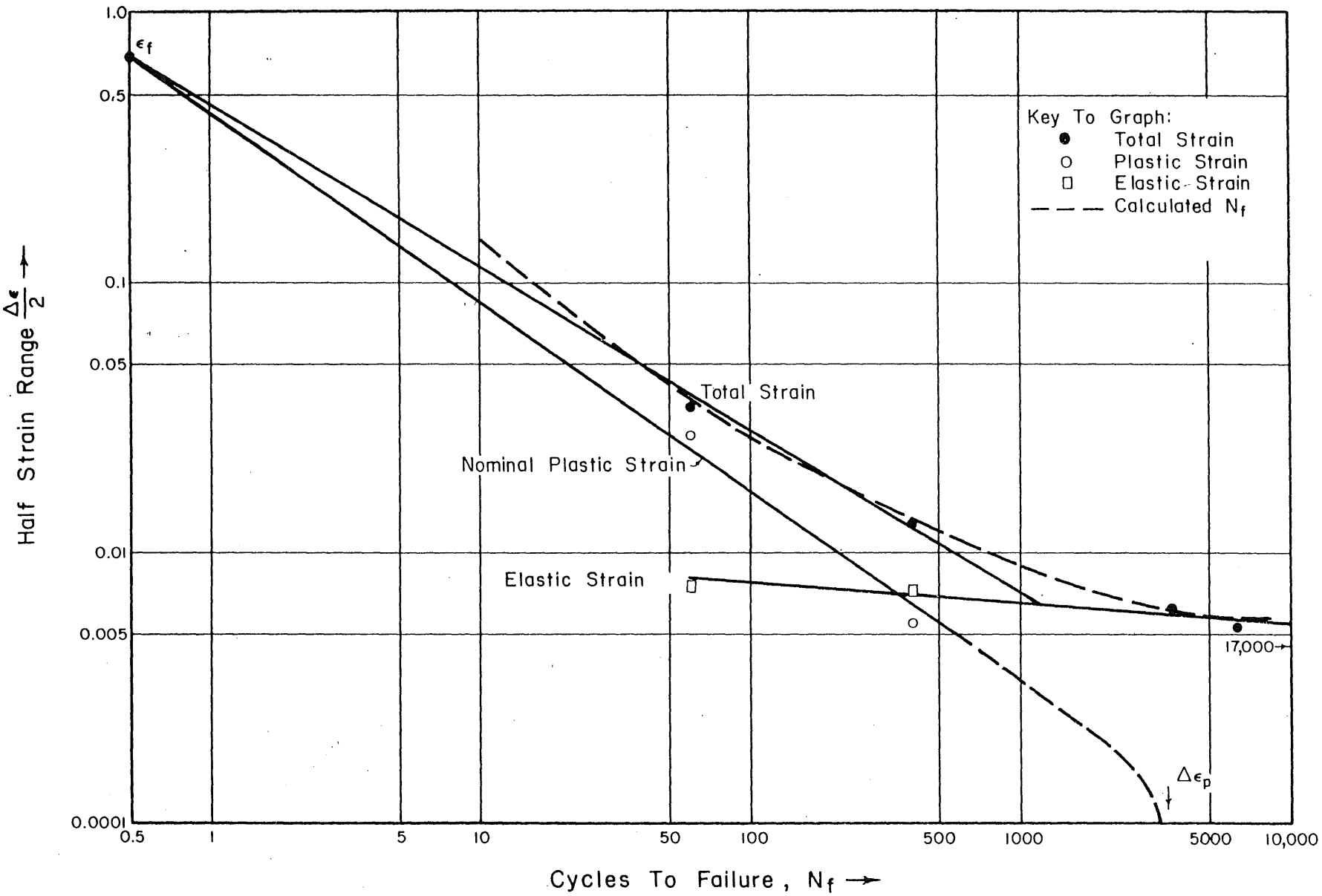

FIG. 19 AXIAL FATIGUE DIAGRAM OF THE AGED 12% NICKEL MARAGING STEEL.

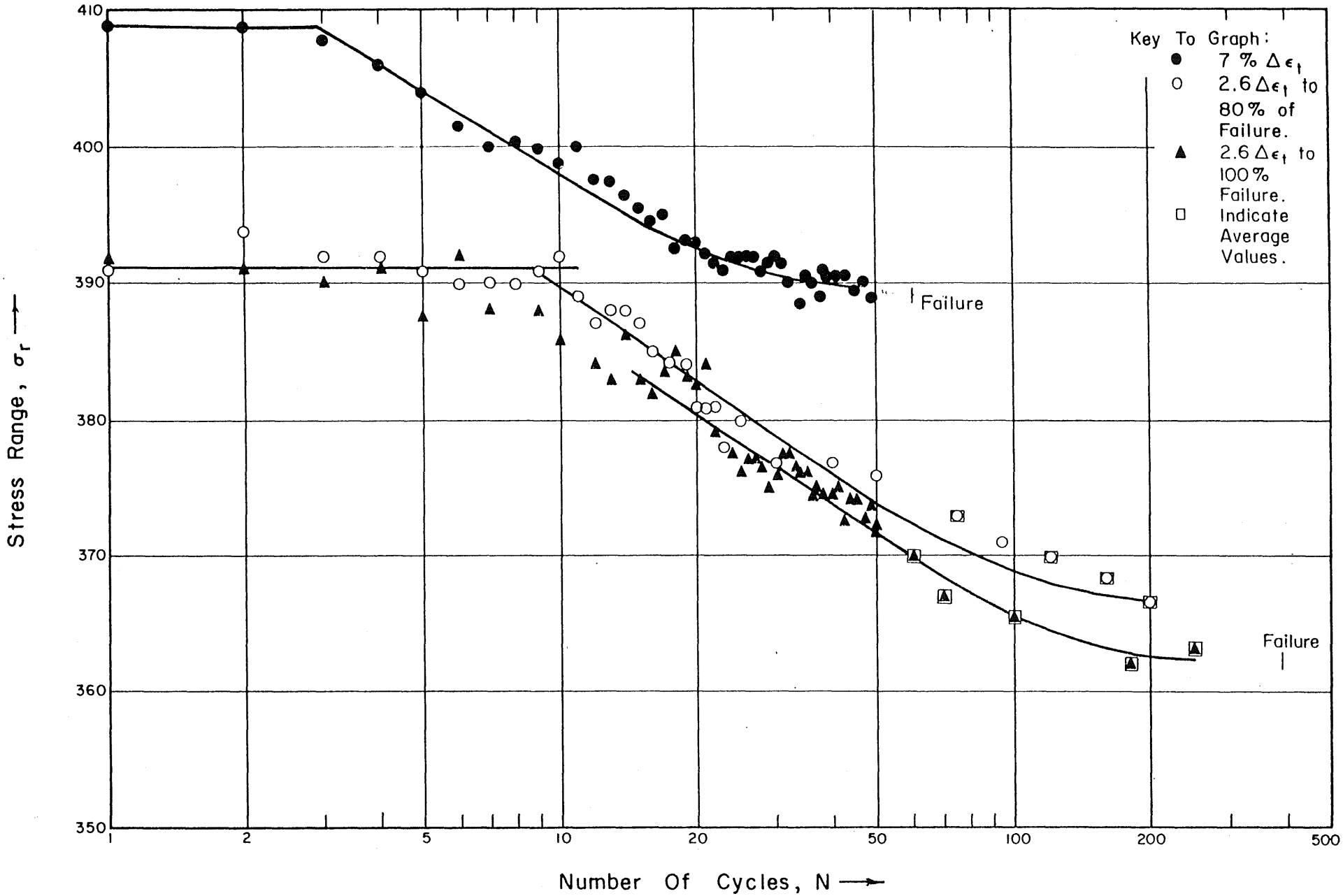

FIG. 20 THE STRESS RANGE OF THE AGED SAMPLES VERSUS THE CYCLES OF FATIGUE .

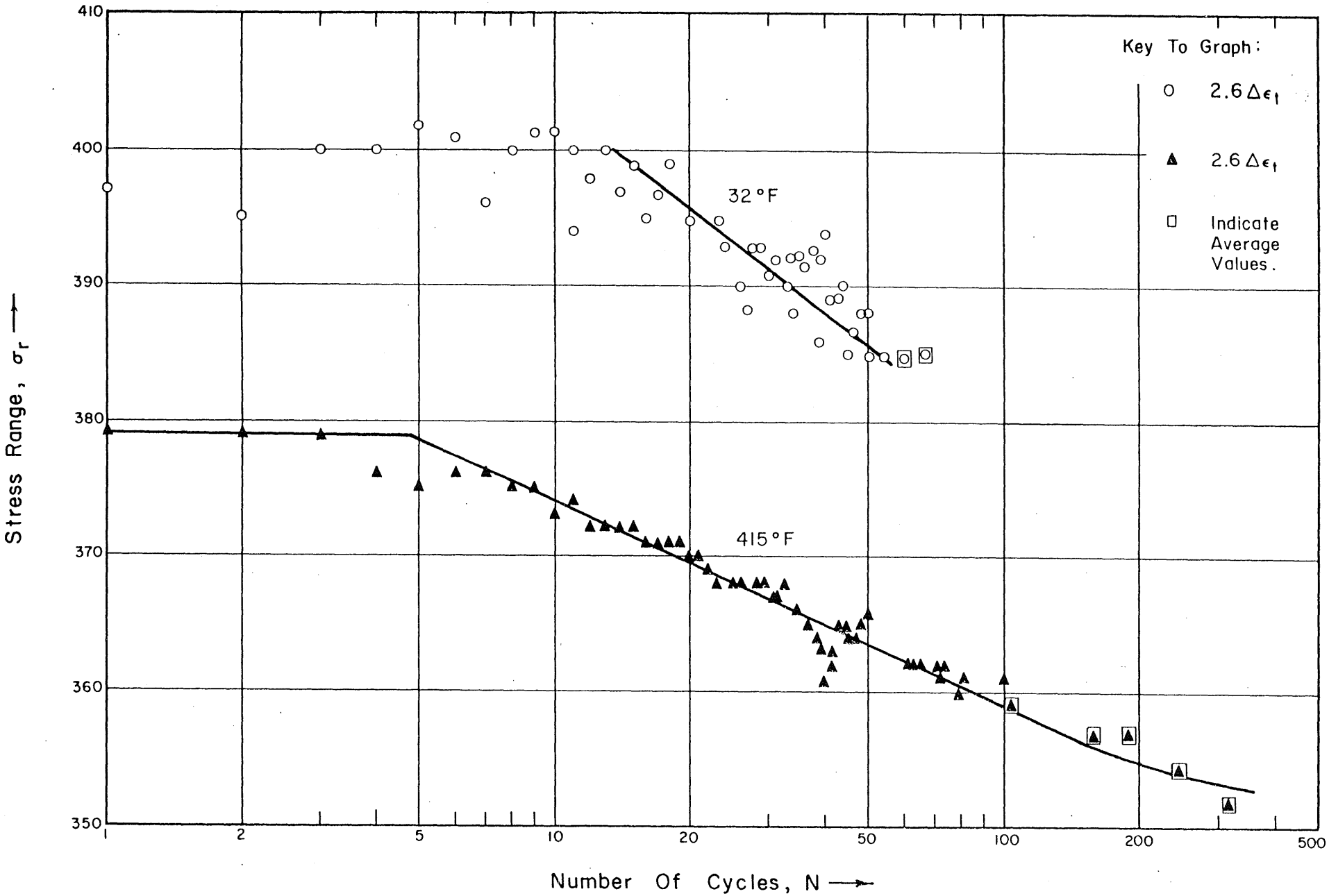

FIG. 21 THE STRESS RANGE OF AGED SAMPLES TESTED IN FATIGUE AT 32°F AND 415°F.

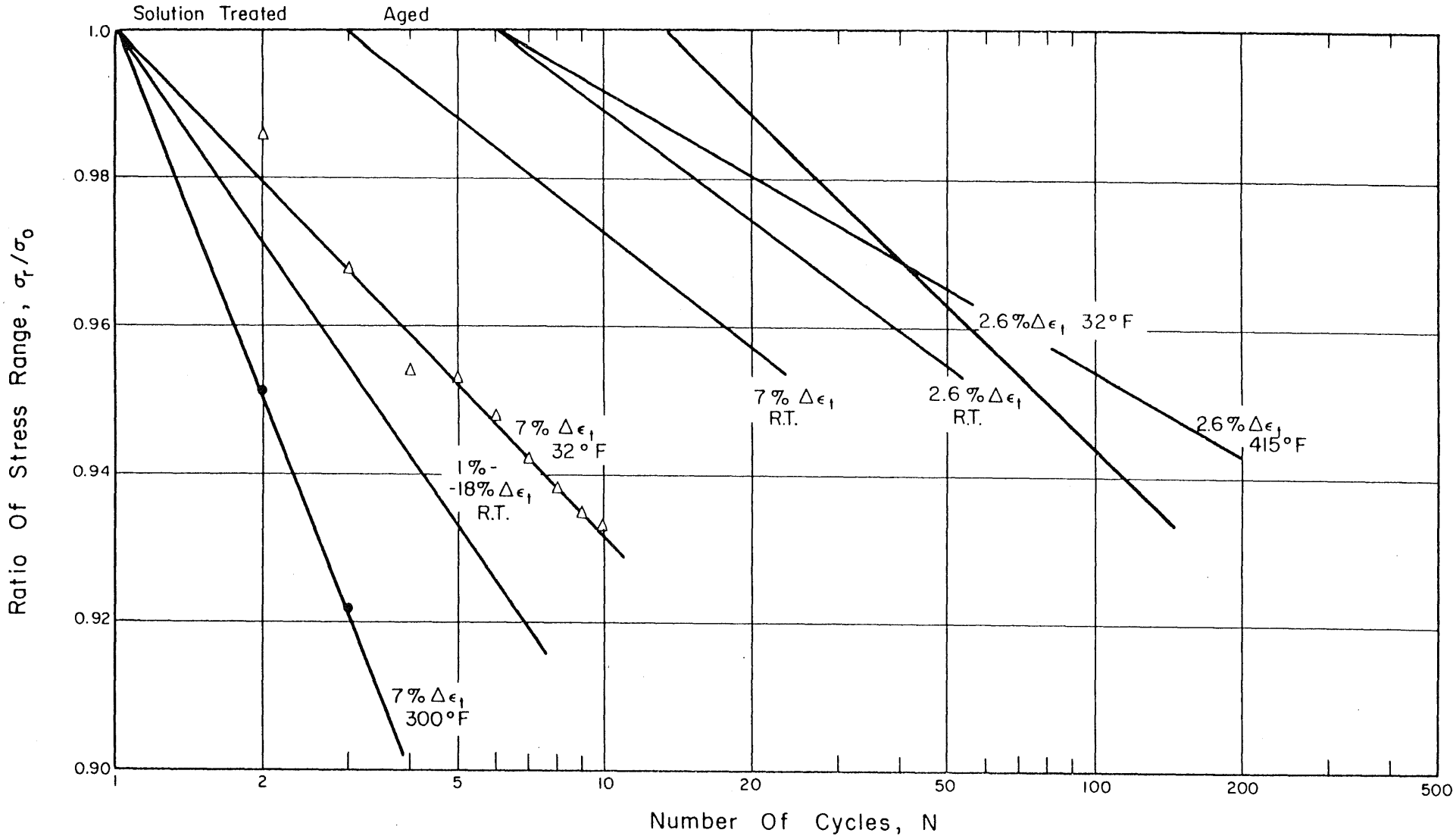

FIG. 22 RATIO OF STRESS RANGE OF STEEL SAMPLES TESTED IN FATIGUE AT DIFFERENT TEMPERATURES.

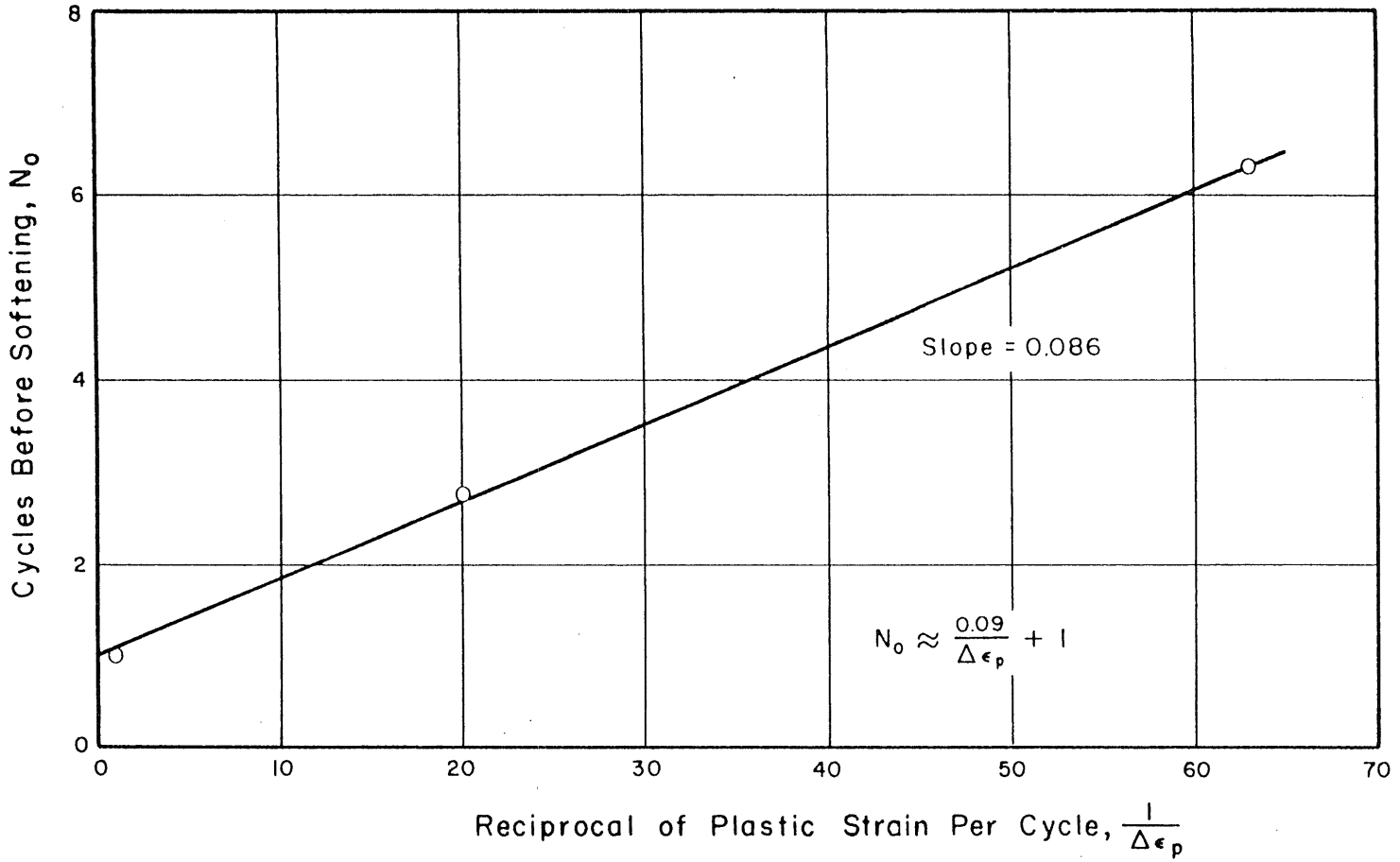

FIG.23 THE NUMBER OF CYCLES BEFORE CYCLIC SOFTENING BEGAN VERSUS PLASTIC STRAIN

FIG. 24 TRANSMISSION ELECTRON MICROGRAPH OF AN AGED SAMPLE WITH REVERTED AUSTENITE

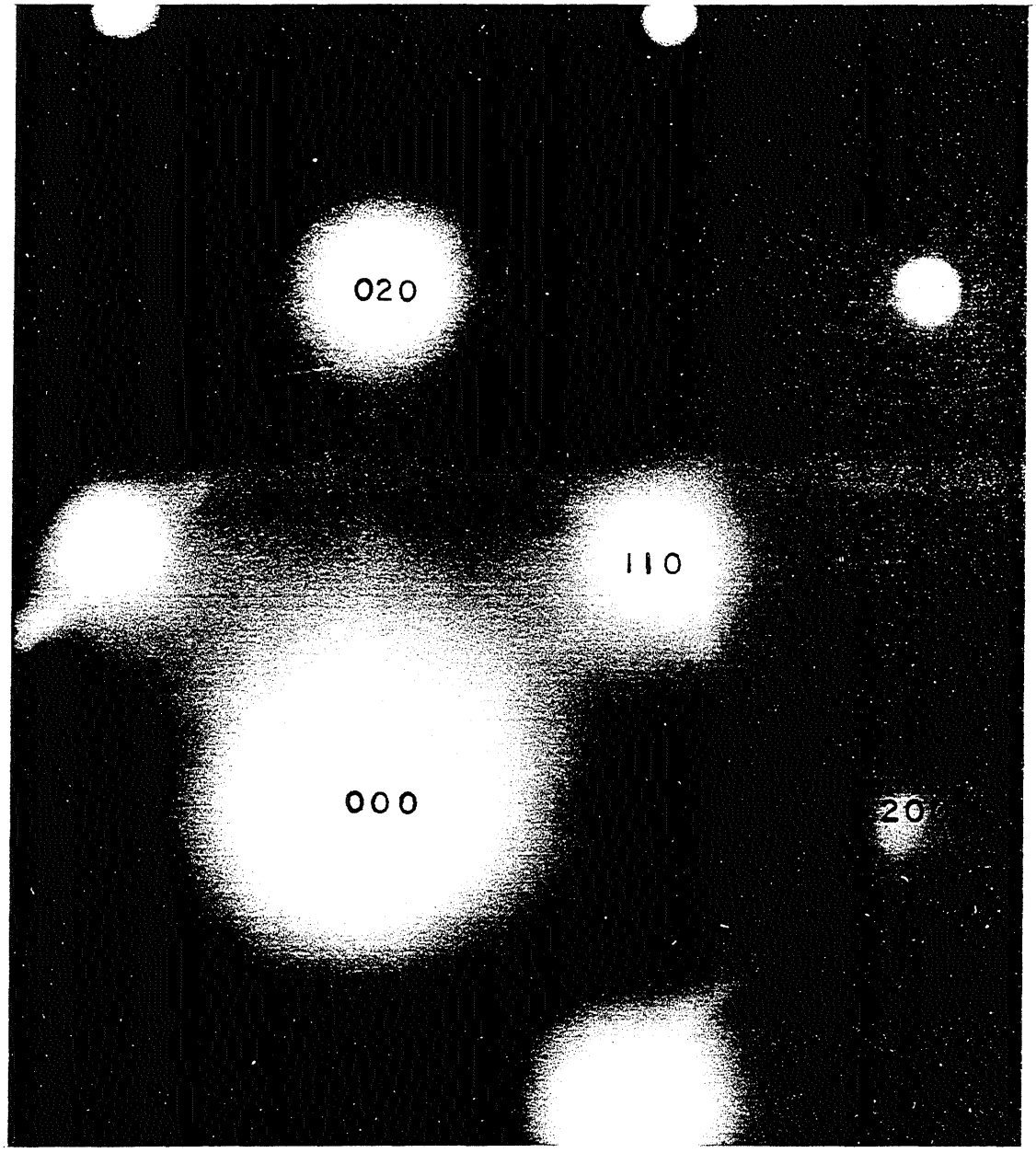

FIG. 25 TRANSMISSION ELECTRON DIFFRACTION PATTERN OF AGED SAMPLE SHOWING DIRECTIONAL STRAIN IN ⟨110⟩

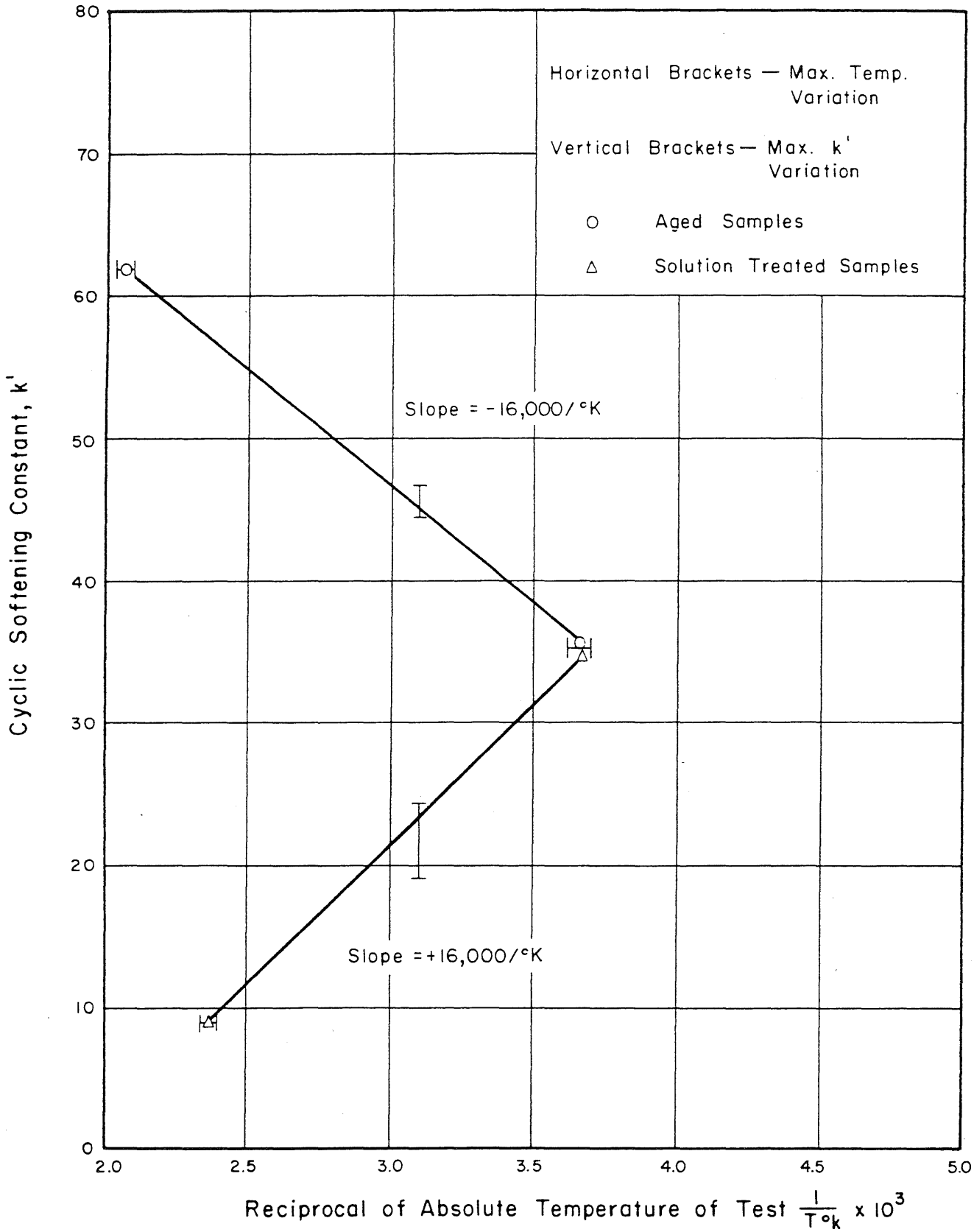

FIG. 26 THE CONSTANT OF CYCLIC SOFTENING, k', VERSUS THE (ABSOLUTE TEMPERATURE)$^{-1}$

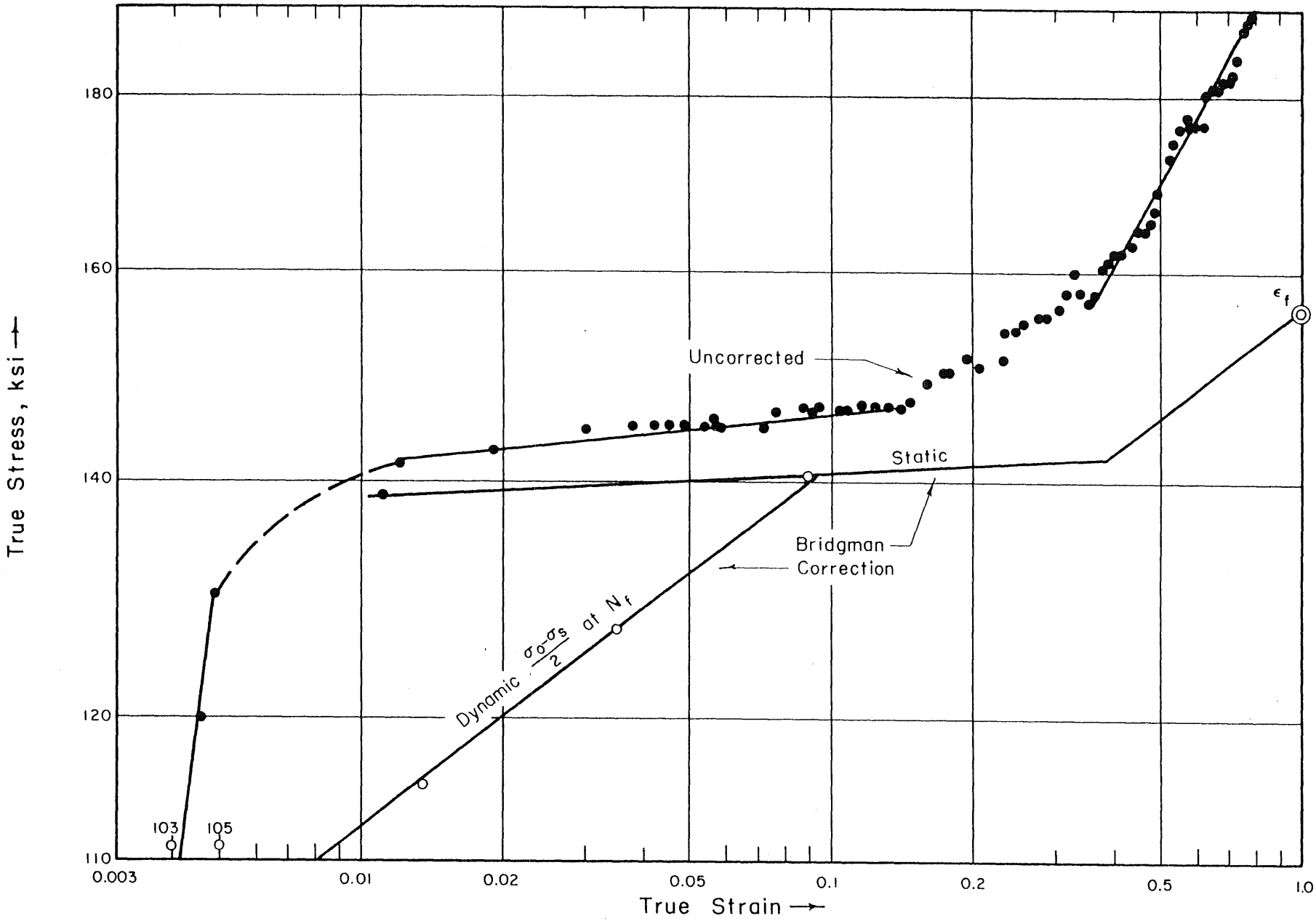

FIG. 27 TRUE STRESS – TRUE STRAIN CURVE OF SOLUTION TREATED 12% NICKEL MARAGING STEEL.

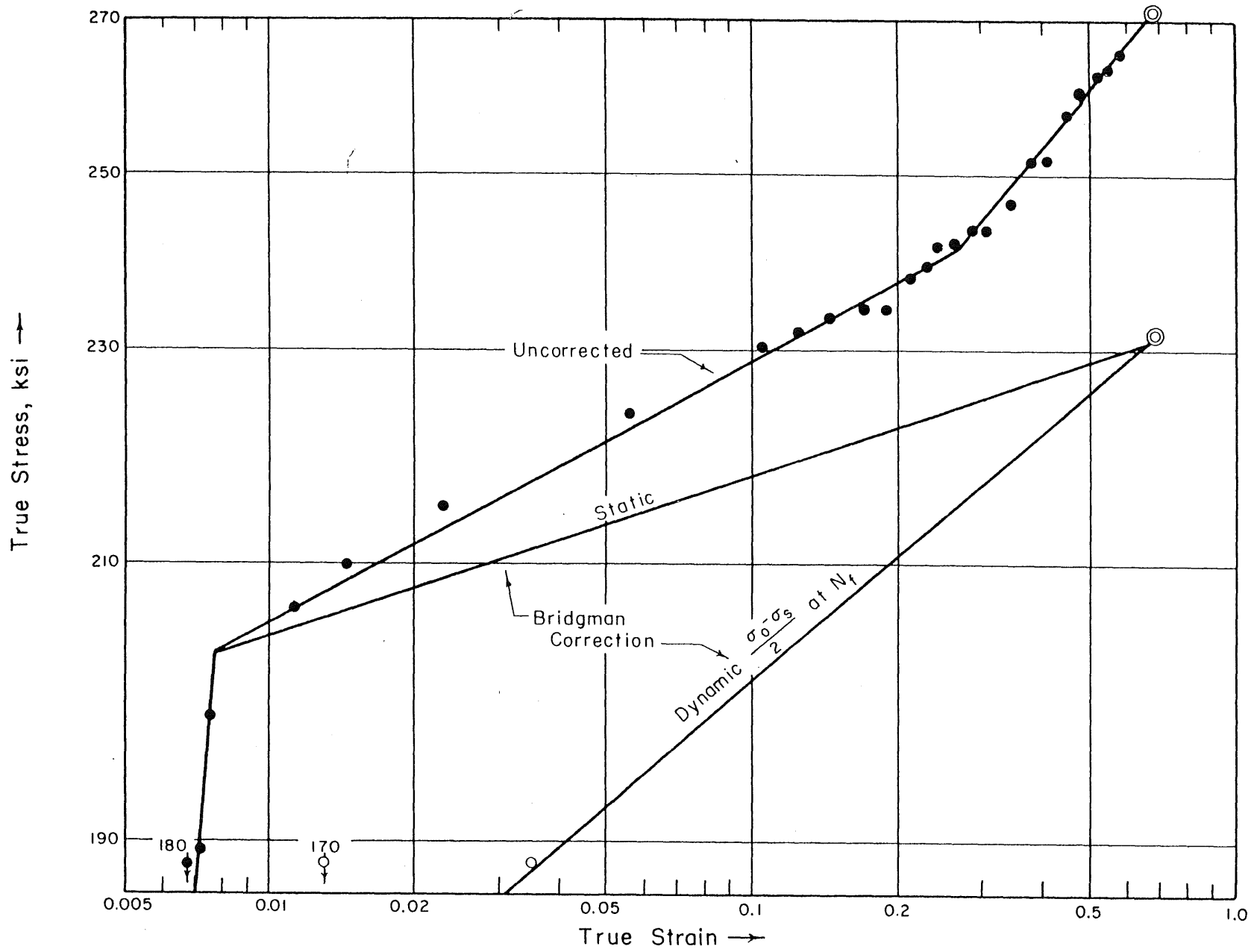

FIG. 28 TRUE STRESS – TRUE STRAIN CURVE OF AGED 12% NICKEL MARAGING STEEL.

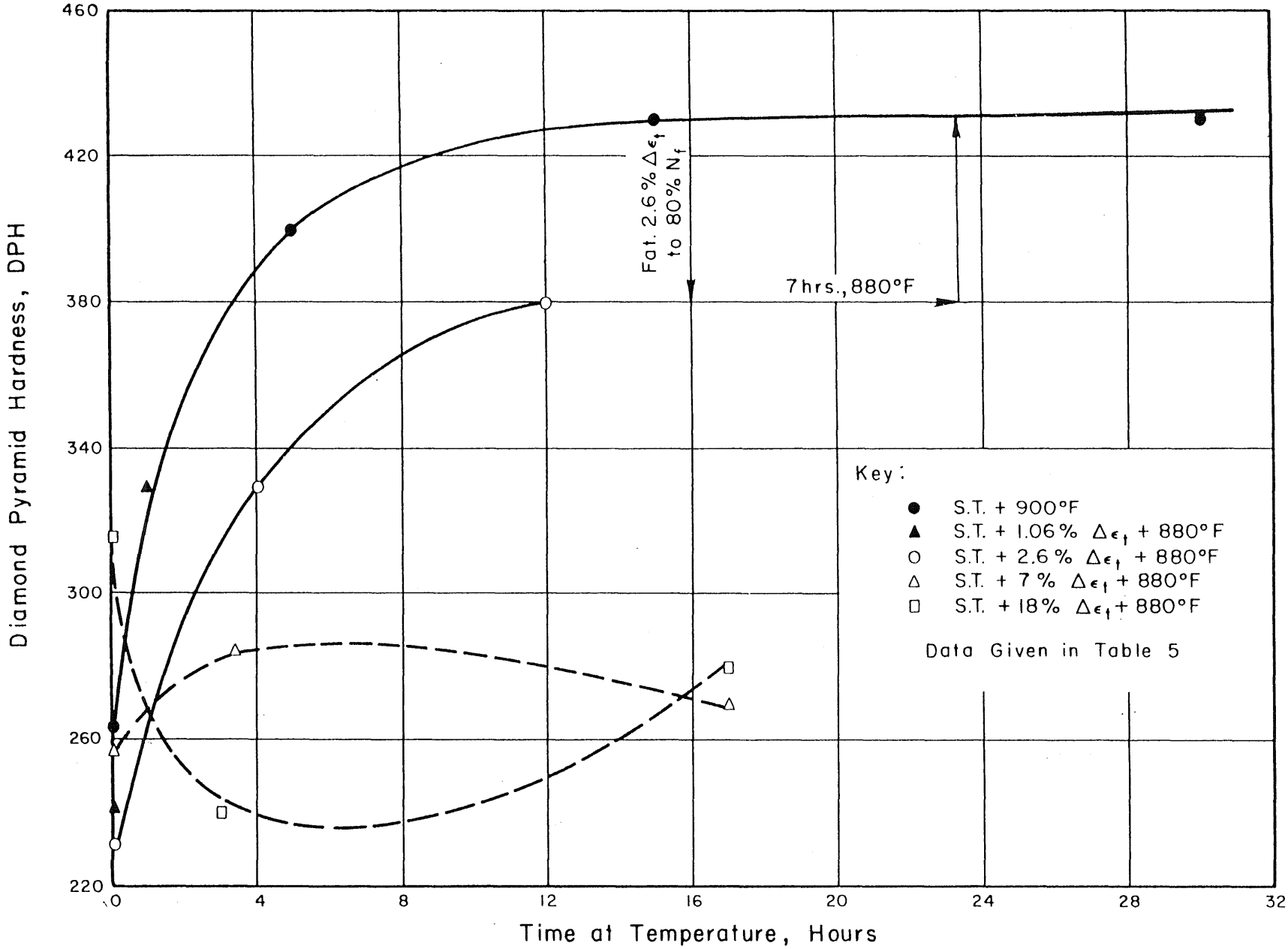

FIG. 29 THE HARDNESS OF 12% NICKEL MARAGING STEEL AFTER DIFFERENT MECHANICAL AND THERMAL TREATMENTS

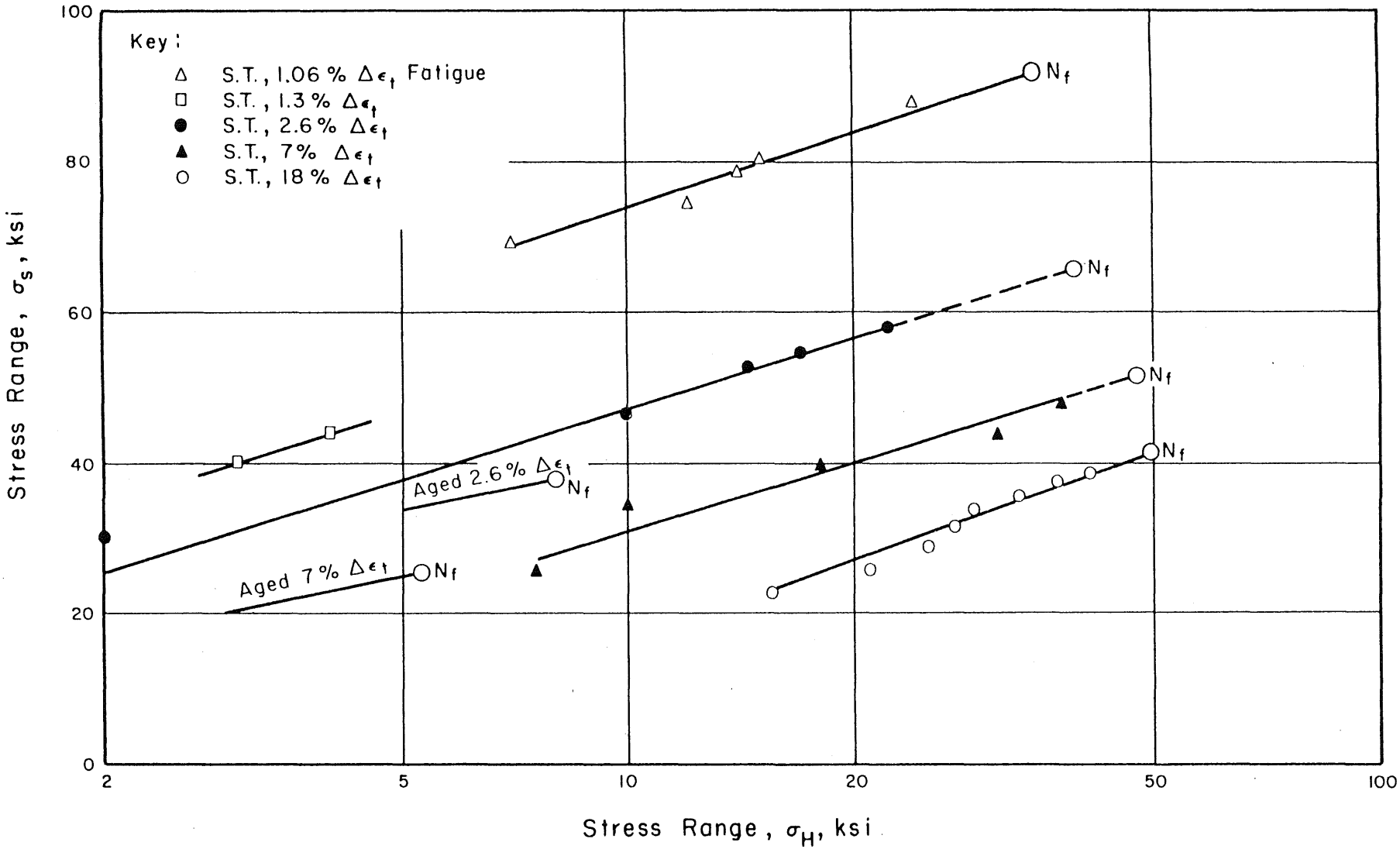

FIG. 30 CYCLIC SOFTENING VERSUS CYCLIC HARDENING FOR MARAGING STEEL

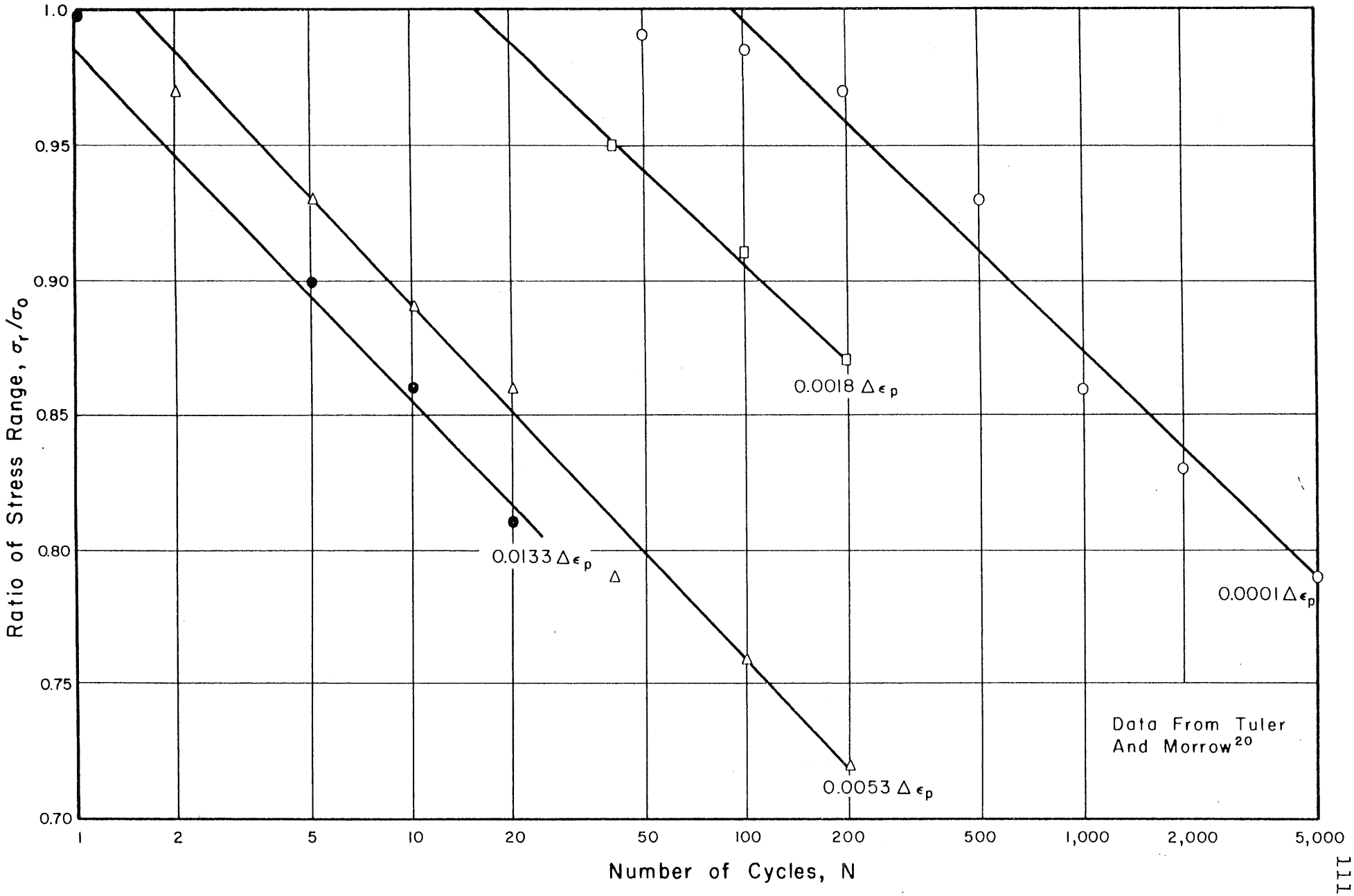

FIG. 31 CYCLIC SOFTENING OF COLD WORKED COPPER TESTED IN FATIGUE

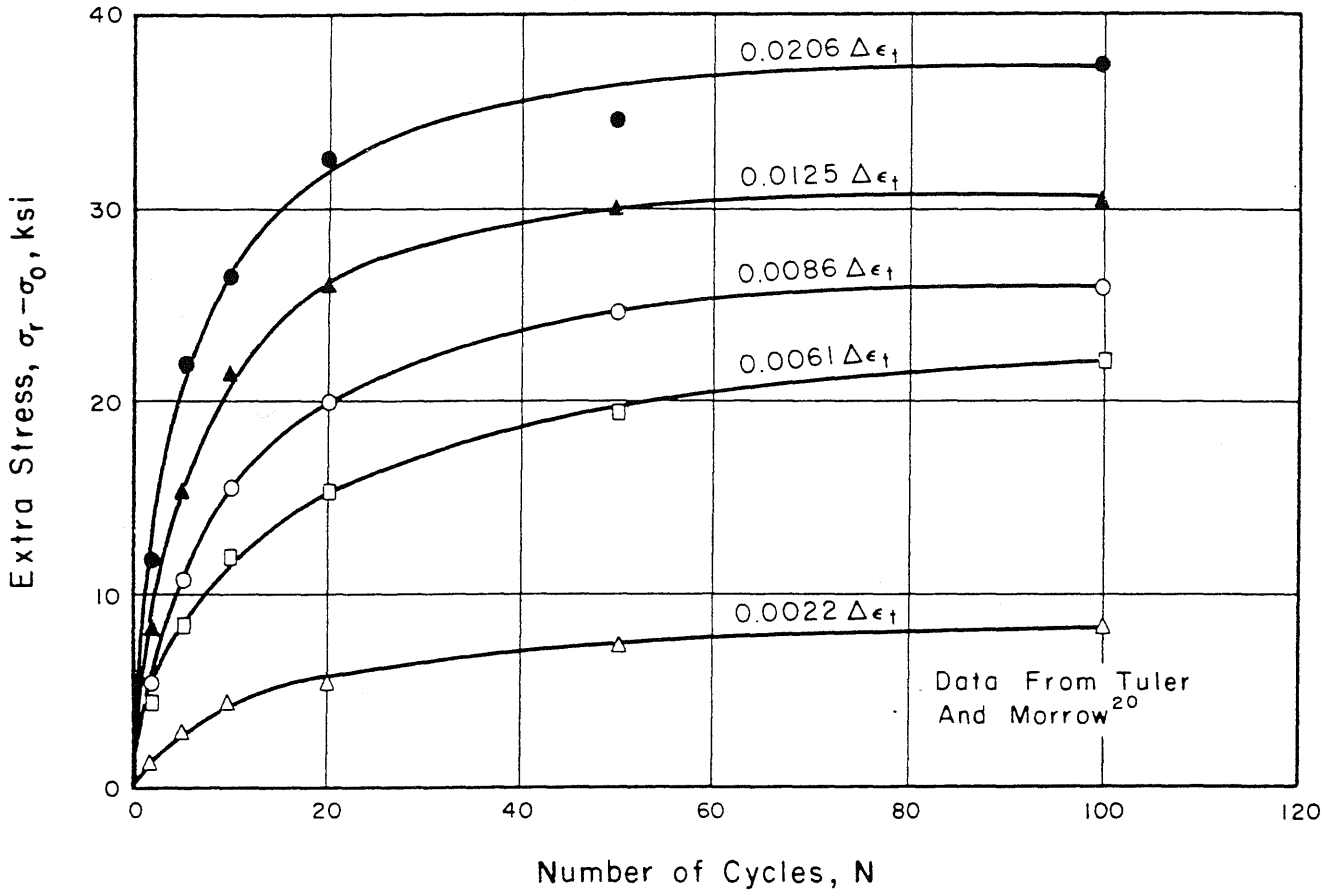

FIG. 32 CYCLIC HARDENING OF ANNEALED COPPER TESTED IN FATIGUE

ILLINOIS UNIVERSITY, URBANA. DEPARTMENT OF MINING, METALLURGY AND PETROLEUM ENGINEERING.

METALLURGICAL STUDIES OF FATIGUE DAMAGE IN MARAGING STEEL,
By R. W. Hinton and W. H. Bruckner

February, 1967, 106pp.
Structural Research Series No. 317
Contract NObs 94232

THE FATIGUE DAMAGE OF A HIGH STRENGTH 12% NICKEL MARAGING STEEL WAS OBSERVED TO ENTAIL A CHANGE IN AXIAL STRESS RANGE AND A CHANGE IN THE SUBSTRUCTURE RESULTING FROM CYCLIC DEFORMATION AT A CONSTANT STRAIN RANGE. AXIAL TESTS IN LOW CYCLE FATIGUE AND LONGER CYCLE FATIGUE WERE PERFORMED ON SAMPLES OF SOLUTION TREATED AND ON AGED 12% NICKEL MARAGING STEEL AT CONSTANT TESTING TEMPERATURES RANGING FROM 32°F TO 415°F. THE SUBSTRUCTURE OF UNTESTED SAMPLES AND SAMPLES TESTED IN STATIC DEFORMATION WAS ALSO OBSERVED BY MEANS OF THIN FILM ELECTRON MICROSCOPY. THE CHANGE IN STRESS RANGE DUE TO FATIGUE WAS RESOLVED INTO TWO COMPONENTS OF STRESS WHICH WERE FOUND TO BE DIFFERENT FUNCTIONS OF THE NUMBER OF APPLIED CYCLES OF FATIGUE. A DISLOCATION MODEL BASED ON THE ORDERING OF DISLOCATION TANGLES WAS PROPOSED AND THIS MODEL WAS SUPPORTED BY AN ACTIVATION ENERGY WHICH WAS DETERMINED FOR THE CYCLIC SOFTENING OF 12% NICKEL MARAGING STEEL. CYCLIC HARDENING WAS RELATED TO HARDENING BY THE GENERATION OF POINT DEFECTS FROM THE OBSERVATIONS MADE IN THIS INVESTIGATION AS RELATED TO A PREVIOUS INVESTIGATION OF LIF. PREDICTIONS OF FATIGUE LIFE BASED ON THE SAME AMOUNT OF CYCLIC HARDENING AT FAILURE DUPLICATED THE EXPERIMENTAL FATIGUE LIVES WITHIN 20% FROM 40 TO 20,000 CYCLES.

KEYWORDS:

Fatigue
Deformation
Substructure
Cyclic Softening
Cyclic Hardening

ILLINOIS UNIVERSITY, URBANA. DEPARTMENT OF MINING, METALLURGY AND PETROLEUM ENGINEERING.

METALLURGICAL STUDIES OF FATIGUE DAMAGE IN MARAGING STEEL,
By R. W. Hinton and W. H. Bruckner

February, 1967, 106pp.
Structural Research Series No. 317
Contract NObs 94232

THE FATIGUE DAMAGE OF A HIGH STRENGTH 12% NICKEL MARAGING STEEL WAS OBSERVED TO ENTAIL A CHANGE IN AXIAL STRESS RANGE AND A CHANGE IN THE SUBSTRUCTURE RESULTING FROM CYCLIC DEFORMATION AT A CONSTANT STRAIN RANGE. AXIAL TESTS IN LOW CYCLE FATIGUE AND LONGER CYCLE FATIGUE WERE PERFORMED ON SAMPLES OF SOLUTION TREATED AND ON AGED 12% NICKEL MARAGING STEEL AT CONSTANT TESTING TEMPERATURES RANGING FROM 32°F TO 415°F. THE SUBSTRUCTURE OF UNTESTED SAMPLES AND SAMPLES TESTED IN STATIC DEFORMATION WAS ALSO OBSERVED BY MEANS OF THIN FILM ELECTRON MICROSCOPY. THE CHANGE IN STRESS RANGE DUE TO FATIGUE WAS RESOLVED INTO TWO COMPONENTS OF STRESS WHICH WERE FOUND TO BE DIFFERENT FUNCTIONS OF THE NUMBER OF APPLIED CYCLES OF FATIGUE. A DISLOCATION MODEL BASED ON THE ORDERING OF DISLOCATION TANGLES WAS PROPOSED AND THIS MODEL WAS SUPPORTED BY AN ACTIVATION ENERGY WHICH WAS DETERMINED FOR THE CYCLIC SOFTENING OF 12% NICKEL MARAGING STEEL. CYCLIC HARDENING WAS RELATED TO HARDENING BY THE GENERATION OF POINT DEFECTS FROM THE OBSERVATIONS MADE IN THIS INVESTIGATION AS RELATED TO A PREVIOUS INVESTIGATION OF LIF. PREDICTIONS OF FATIGUE LIFE BASED ON THE SAME AMOUNT OF CYCLIC HARDENING AT FAILURE DUPLICATED THE EXPERIMENTAL FATIGUE LIVES WITHIN 20% FROM 40 TO 20,000 CYCLES.

KEYWORDS:

Fatigue
Deformation
Substructure
Cyclic Softening
Cyclic Hardening

ILLINOIS UNIVERSITY, URBANA. DEPARTMENT OF MINING, METALLURGY AND PETROLEUM ENGINEERING.

METALLURGICAL STUDIES OF FATIGUE DAMAGE IN MARAGING STEEL,
By R. W. Hinton and W. H. Bruckner

February, 1967, 106pp.
Structural Research Series No. 317
Contract NObs 94232

THE FATIGUE DAMAGE OF A HIGH STRENGTH 12% NICKEL MARAGING STEEL WAS OBSERVED TO ENTAIL A CHANGE IN AXIAL STRESS RANGE AND A CHANGE IN THE SUBSTRUCTURE RESULTING FROM CYCLIC DEFORMATION AT A CONSTANT STRAIN RANGE. AXIAL TESTS IN LOW CYCLE FATIGUE AND LONGER CYCLE FATIGUE WERE PERFORMED ON SAMPLES OF SOLUTION TREATED AND ON AGED 12% NICKEL MARAGING STEEL AT CONSTANT TESTING TEMPERATURES RANGING FROM 32°F TO 415°F. THE SUBSTRUCTURE OF UNTESTED SAMPLES AND SAMPLES TESTED IN STATIC DEFORMATION WAS ALSO OBSERVED BY MEANS OF THIN FILM ELECTRON MICROSCOPY. THE CHANGE IN STRESS RANGE DUE TO FATIGUE WAS RESOLVED INTO TWO COMPONENTS OF STRESS WHICH WERE FOUND TO BE DIFFERENT FUNCTIONS OF THE NUMBER OF APPLIED CYCLES OF FATIGUE. A DISLOCATION MODEL BASED ON THE ORDERING OF DISLOCATION TANGLES WAS PROPOSED AND THIS MODEL WAS SUPPORTED BY AN ACTIVATION ENERGY WHICH WAS DETERMINED FOR THE CYCLIC SOFTENING OF 12% NICKEL MARAGING STEEL. CYCLIC HARDENING WAS RELATED TO HARDENING BY THE GENERATION OF POINT DEFECTS FROM THE OBSERVATIONS MADE IN THIS INVESTIGATION AS RELATED TO A PREVIOUS INVESTIGATION OF LIF. PREDICTIONS OF FATIGUE LIFE BASED ON THE SAME AMOUNT OF CYCLIC HARDENING AT FAILURE DUPLICATED THE EXPERIMENTAL FATIGUE LIVES WITHIN 20% FROM 40 TO 20,000 CYCLES.

KEYWORDS:

Fatigue
Deformation
Substructure
Cyclic Softening
Cyclic Hardening

ILLINOIS UNIVERSITY, URBANA. DEPARTMENT OF MINING, METALLURGY AND PETROLEUM ENGINEERING.

METALLURGICAL STUDIES OF FATIGUE DAMAGE IN MARAGING STEEL,
By R. W. Hinton and W. H. Bruckner

February, 1967, 106pp.
Structural Research Series No. 317
Contract NObs 94232

THE FATIGUE DAMAGE OF A HIGH STRENGTH 12% NICKEL MARAGING STEEL WAS OBSERVED TO ENTAIL A CHANGE IN AXIAL STRESS RANGE AND A CHANGE IN THE SUBSTRUCTURE RESULTING FROM CYCLIC DEFORMATION AT A CONSTANT STRAIN RANGE. AXIAL TESTS IN LOW CYCLE FATIGUE AND LONGER CYCLE FATIGUE WERE PERFORMED ON SAMPLES OF SOLUTION TREATED AND ON AGED 12% NICKEL MARAGING STEEL AT CONSTANT TESTING TEMPERATURES RANGING FROM 32°F TO 415°F. THE SUBSTRUCTURE OF UNTESTED SAMPLES AND SAMPLES TESTED IN STATIC DEFORMATION WAS ALSO OBSERVED BY MEANS OF THIN FILM ELECTRON MICROSCOPY. THE CHANGE IN STRESS RANGE DUE TO FATIGUE WAS RESOLVED INTO TWO COMPONENTS OF STRESS WHICH WERE FOUND TO BE DIFFERENT FUNCTIONS OF THE NUMBER OF APPLIED CYCLES OF FATIGUE. A DISLOCATION MODEL BASED ON THE ORDERING OF DISLOCATION TANGLES WAS PROPOSED AND THIS MODEL WAS SUPPORTED BY AN ACTIVATION ENERGY WHICH WAS DETERMINED FOR THE CYCLIC SOFTENING OF 12% NICKEL MARAGING STEEL. CYCLIC HARDENING WAS RELATED TO HARDENING BY THE GENERATION OF POINT DEFECTS FROM THE OBSERVATIONS MADE IN THIS INVESTIGATION AS RELATED TO A PREVIOUS INVESTIGATION OF LIF. PREDICTIONS OF FATIGUE LIFE BASED ON THE SAME AMOUNT OF CYCLIC HARDENING AT FAILURE DUPLICATED THE EXPERIMENTAL FATIGUE LIVES WITHIN 20% FROM 40 TO 20,000 CYCLES.

KEYWORDS:

Fatigue
Deformation
Substructure
Cyclic Softening
Cyclic Hardening